# Nonlinear Finite Element Analyses for Ultimate Strength Determination of Ships under combined Loads

**Auteur :** Okpeke, Bright Ebikemefa
**Promoteur(s) :** 14956
**Faculté :** Faculté des Sciences appliquées
**Diplôme :** Master : ingénieur civil mécanicien, à finalité spécialisée en "Advanced Ship Design"
**Année académique :** 2020-2021
**URI/URL :** http://hdl.handle.net/2268.2/12879

Universität Rostock

Traditio et Innovatio

With the support of the Erasmus+ Programme of the European Union

# Nonlinear Finite Element Analyses for Ultimate Strength Determination of Ships Under Combined Loads

submitted on 02 August, 2021

by


**OKPEKE Bright Ebikemefa**

Erich_Schlesinger_Strasse, 19

18059 Rostock

bright4nky@gmail.com

Student ID No.: 220 202 366



**First Reviewer:**

Prof. Dr.Eng./Hiroshima Univ. Patrick Kaeding

University of Rostock

Chair of Ship Structures

Albert-Einstein-Str. 2

18059 Rostock

Germany

**Second Reviewer:**

Dr.-Ing. Thomas Lindemann

University of Rostock

Chair of Ship Structures

Albert-Einstein-Str. 2

18059 Rostock

Germany


EMship+ Advanced Design

Master Thesis

[This page is intentionally left blank]

## DECLARATION OF AUTHORSHIP

I, **OKPEKE Bright Ebikemefa** declare that this thesis and the work presented in it are my own and have been generated by me as the result of my own original research.

Where I have consulted the published work of others, this is always clearly attributed.

Where I have quoted from the work of others, the source is always given. With the exception of such quotations, this thesis is entirely my own work.

I have acknowledged all main sources of help.

Where the thesis is based on work done by myself jointly with others, I have made clear exactly what was done by others and what I have contributed myself.

This thesis contains no material that has been submitted previously, in whole or in part, for the award of any other academic degree or diploma.

I cede copyright of the thesis in favour of the University of Rostock.

Date: Signature:

[This page is intentionally left blank]

**ABSTRACT**

To determine the ultimate strength of a double hull VLCC under combined loads, different progressive collapse analyses were performed. Nonlinear finite element analyses using Newton-Raphson iterative scheme were performed to simulate the collapse behaviour of the double hull VLCC. This was done using ANSYS Mechanical APDL. The ultimate strength of the double hull VLCC was determined for the cases of vertical bending, horizontal bending and biaxial bending under hogging and sagging conditions.

In the case of vertical bending, the analysis performed shows that the ultimate strength under hogging condition is higher than that under sagging condition. Also, the collapse behaviour of the structure under hogging condition indicates that initial collapse starts at the central part of the deck in tension. This is followed by the collapse of the double bottom in compression. Under the sagging condition, the deck buckles in compression.

Due to symmetry, the results of the analysis carried out in the case of horizontal bending show that the ultimate strengths and collapse behaviour of the structure under hogging and sagging conditions are similar. In the biaxial case, the interaction relationship between vertical and horizontal bending is illustrated. Depending on the applied curvature ratio, the influence of one over the other dominates.

The influence of different material models on the ultimate strength was also investigated. The analysis conducted indicates that the bilinear elastic plastic material model gives a higher value of the ultimate strength when compared with the ideal elastic plastic material model. The structural components of the double hull VLCC are welded, hence, initial imperfections due to welding are introduced to the structural components. Therefore, the influence of welding residual stresses on the ultimate strength of the structure was also examined. The examination shows that welding residual stresses have little/negligible influence on the ultimate strength of the double hull VLCC.

Finally, analyses were also performed to determine the residual strength of the double hull VLCC under combined loads. Symmetric grounding damages were implemented by removing parts (elements) of the model. Expectedly, the results show that the ultimate strength of the structure decreases as the damage extent increases.

## ACKNOWLEDGEMENTS

I have been assiduous in the completion of this study. Though I really bust a gut to get this work finished on time, it would not have been possible without the support of other people.

First and foremost, I would like to thank Dr.-Ing. Thomas Lindemann. The door to his office was always open whenever my work proved to be a banana skin for me. He invariably allowed this work to be mine, but steered me in the right direction. I cannot thank you enough for your tremendous assistance during the course of this project.

I am also beholden to the team of Ship Engineering Construction, Faculty of Mechanical Engineering and Ship Technology, University of Rostock for their contributions towards the success of this work.

Also, I would like to express my sincere gratitude to Aleksashin Dimitrii for his selfless assistance and contributions in catch-22 situations. He was always ready to assist me in every difficulty that I encountered.

Furthermore, my profound gratitude goes to the coordinators of the EMSHIP+ program and all the professors that have been part of this academic journey.

My greatest thanks and praises, however, go to the Almighty God. He has been my "EVERYTHING".

**CONTENTS**

**List of Figures**

## List of Tables

# 1. INTRODUCTION

## 1.1 Background

Ship accidents/damages ineludibly occur in spite of the great technological advancements in offshore/marine engineering and the consideration of design safety margin from class societies. These accidents/damages could take the form of structural failure, grounding, collision, fire, explosion, water ingress, corrosion and/or fatigue which lead to partial loss of the structural integrity of the ship and may finally result in the hull girder collapse (Bronsart, 2017).

The hull girder failure is considered as one of the most catastrophic failure modes with severe consequences like complete damage of the ship, loss of life, environmental pollution and significant financial losses. The breaking of the hull into two parts as a result of severe vertical bending moments that surpass the ultimate hull girder strength is the most common consequence of hull girder collapse (Hughes & Paik, 2010).

There has been a considerable amount of ship failures which have resulted in the overall collapse of the ship's hull. An example is the "Energy Concentration Accident". In July 1980, the back of the ship broke at the Europort in Rotterdam during the unloading of cargo oil. It was found that the maximum load-carrying capacity of the hull structures was exceeded by the poorly executed unloading of cargo which amplified the maximum hull girder bending moment (Hughes & Paik, 2010). Similarly, an "Anonymous Capesize Bulk Carrier" broke her back during the unloading of cargo iron ore.

In November 2002, the single-hull oil tanker "Prestige" broke her back under heavy weather conditions (Figure 1.1). It was learnt that rough sea conditions can amplify hull girder loads to the extent that they reach or even exceed the corresponding design values. It was also learnt that an increase in applied hull girder loads or a decrease in hull girder strength or both can result in the collapse of the hull girder. Also, in January 2007, the bulkhead structures in between the engine room and the aft cargo hold of the British container ship M.S.C Napoli buckled when she was caught up in a storm.


*Figure 1.1: Collapse of Prestige tanker*

(source: (safety4sea, 2018))

More recently, in August 2013, MV Smart suffered structural failure amidship and broke into two parts after running aground. A similar accident to that which befell MV Smart happened to MOL Comfort some 200 nautical miles off the coast of Yemen where she broke into two (Figure 1.2).


*Figure 1.2: Structural failure of MOL Comfort*

(source: (Trust, 2013))

From the foregoing, it is imperative that the capacity of the hull girder considering extreme loads is accurately evaluated to ensure critical and safe design of a ship's hull. It is recommended that the deck or bottom panels should be designed using ultimate limit state design methods. This ensures that the hull girder is able to withstand unintended scenarios of cargo loading and unloading that cause uncertainties in the design load calculations and subsequently affect the structural design process. Hence, the ultimate limit state-based methods can better deal with the issue of hull collapse in ship structural design as opposed to the allowable working stress design approach.

## 1.2 Problem Description

In intact condition, a ship's hull can bear applied loads lesser than the design loads and under normal circumstances (weather and cargo loading), structural damages will not occur. However, the loads acting on a ship's hull are indeterminate since the nature of rough sea and possibly unusual loading/unloading of cargo cannot be exactly determine. Hence, global collapse of the ship's hull may occur when the applied loads exceed the design loads.

Buckling in compression and yielding in tension of the hull's structural members tend to occur as the applied loads gradually surpass the design loads. The structural integrity and stiffness of such members decrease. This results in the redistribution of their internal stress to adjacent intact members. Consequently, the overall hull girder stiffness slightly decreases. With continuous increase in the applied loads, progressive collapse and buckling of more structural members occur until the global hull girder finally reaches the ultimate limit state.

The determination of the ultimate hull girder strength of a ship is a challenging task that needs to be done quickly during the preliminary design stages. The ultimate strength of the ship's hull must be accurately evaluated to guarantee structural safety. In the design and safety assessment of ship structures, hull collapse prevention is the most important task, hence the need to accurately and efficiently determine the ultimate hull girder strength.

In the past, traditional working stress-based approaches were used as the standards and procedures for the structural design of ships. These were mainly based on allowable stresses and simplified buckling checks for structural components (Paik, 2018). The true ultimate limit state is not necessarily defined by these approaches. Also, the probable pattern of local failure prior to reaching the ultimate limit state cannot be understood using these approaches. It therefore implies that the determination of the true ultimate strength is of critical importance in order to obtain reliable measures of safety which can be used as a fairer basis for evaluations of vessels of different characteristics.

The ultimate limit state design approach can ease the evaluation of the actual safety margin of the ship structure. In this approach, the capacity of the ship hull girder is considered as the applicable ultimate strength, while the demand is specified with respect to the hull girder loads (Paik, 2018).

The determination of the collapse load, which defines the true ultimate strength of a ship's girder, has become a topic of increased interest to the ship research and design communities. One of the reasons behind this interest is that knowledge of the limiting conditions beyond which a hull girder will fail to perform its function will, undoubtedly, help in assessing more accurately the true margin of safety between the ultimate capacity of the hull and the maximum combined moment acting on the ship (Mansour, et al., 1998).

Unfortunately, majority of the previous works that have been carried out on the subject of ultimate strength focused on the longitudinal ultimate strength which is the ultimate strength under vertical bending moment only with little consideration given to the fact that the ultimate strength may also be affected by the horizontal bending moment. Though some past works have been carried out on the subject of ultimate strength under combined loads, further work is required.

## 1.3 Objectives

The main objective of this thesis is to systematically evaluate the ultimate strength of a double hull VLCC; investigating into the overall collapse behaviour of the cross section under vertical bending moment, horizontal bending moment and combined vertical and horizontal bending moments using static nonlinear finite element analysis techniques. Also, to investigate the effects of initial imperfections (initial deflections and welding residual stresses) on the ultimate strength. Furthermore, to examine the residual strength of the double hull VLCC due to grounding damage.

In addressing these objectives;

- An APDL script that performs numerical modeling and analysis will be developed.

- The results obtained using the developed APDL script will be validated against ISSC benchmark studies and other publications.

## 1.4 Scope of Thesis

The corresponding scope of this thesis (based on the objectives) are as follows:

- Determination of the ultimate strength of the double hull VLCC in vertical and horizontal bending.
- Examination of the effects of the interaction of combined loadings on the ultimate strength of the double hull VLCC.
- Investigation of the effects of different material models on the ultimate strength of the double hull VLCC
- Analysis of the influence of initial imperfections (initial deflection and welding residual stress) on the ultimate strength of the double hull VLCC.
- Evaluation of the residual strength of the double hull VLCC due to grounding damage.

## 1.5 Thesis Structure

The structuring of this thesis is done in a systematic manner in such a way that the procedures to determine and analyze the ultimate strength of a double hull VLCC under combined loads in intact and damaged conditions are better appreciated. Greater emphasis is however placed on the intact condition.

This report consists of five chapters. Chapter 1 presents the background of study, problem description, objectives and scope of study. In chapter 2, some theories and literatures regarding ultimate strength are reviewed. The different limit states and failure modes of ship structures are described. Also, the loads acting on a ship and the techniques of analyzing the ship's structural response to such loads are presented in this chapter. Furthermore, an overview of ultimate strength and nonlinear finite element analysis is contained in this chapter. Chapter 3 describes the modeling of the double hull VLCC. Information about element type, meshing, material model, boundary conditions, initial imperfection and damage geometry are contained in this chapter. The results obtained have been analyzed and discussed in chapter 4, where the major findings of the current study have been summarized. Based on the current thesis work, conclusions and recommendations are made and presented in chapter 5.

# 2. THEORY AND LITERATURE REVIEW

## 2.1 Limit State-Based Analysis and Failure Modes

From the viewpoint of structural design, it is necessary to be aware of the potential limit states, failure modes and methods of predicting their occurrence in order to avoid structural failure.

### *2.1.1 Limit State-Based Analysis*

A limit state is defined as a condition beyond which a structural member or an entire structure fails to perform its designed function(s) due to one or more loads and/or load effects [ (ISSC, 2015), (Hughes & Paik, 2010)]. The applicable load carrying capacity or strength of the structure is estimated for the condition and used as a limit during design. For this purpose, simplified design formulations or more refined computational analyses are usually used to assess the limit values of the structure (Paik, et al., 1996).

Four types of limit states are relevant here (Rigo & Rizzuto, 2010), namely:

i. Service or serviceability limit state

This relates to a situation typically aesthetic, functional or maintenance that hampers the proper functioning of structural elements or equipment in such a way that they can no longer perform normal operations. This might take the form of excessive vibration and noise, local cracking and unacceptable deformation. It is however noteworthy that the vessel can still remain afloat even after reaching this state.

ii. Ultimate limit state

This corresponds to the situation in which the structure or member fails in its primary load-carrying role. This is characterized by the collapse of the structure due to loss of structural capacity in terms of stiffness and strength.

iii. Fatigue limit state

This represents the occurrence of fatigue cracking of structural details due to stress concentration and damage accumulation or crack growth under repeated loading. The fatigue limit state design is carried out to ensure that the structure has an adequate fatigue life (Paik, 2018).

iv. Accident limit state

This represents excessive structural damage from accidents, such as collisions, grounding, explosion and fire, that affect the safety of the structure, the environment and personnel (Paik, 2018). In the accidental limit state design, the goal is to achieve a design in which the structure's main safety functions are not impaired during any accidental event or within a certain time after the accident.

### *2.1.2 Failure Modes*

There are many reasons or causes of ship structural failure and the extent of the failure may vary from a negligible aesthetic degradation to catastrophic failure which might lead to the loss of the ship. There are three major failure modes (Rigo & Rizzuto, 2010) namely:

i. Tensile/compressive yield of the material (plasticity)
ii. Compressive instability (buckling)
iii. Fracture (includes ductile tensile rupture, low-cycle fatigue and brittle fracture)

It is noteworthy that the basic failure modes do not always occur simultaneously, however, more than one phenomenon may in principle be involved until the structure reaches the ultimate limit state (Paik, et al., 1996).

i. Yield

Yield occurs when the stress in a structural member exceeds a level that results in a permanent plastic deformation of the material of which the member is constructed. This stress level is termed the material yield stress. At a somewhat higher stress, termed the ultimate stress, fracture of the material occurs. While many structural design criteria are based upon the prevention of any yield whatsoever, it should be observed that localized yield in some portions of a structure is acceptable (Rigo & Rizzuto, 2010).

ii. Instability and buckling

Instability and buckling failure of a structural member can occur due to load sets that result in compressive effects in the structure (Paik, 2018). This may occur at a stress level that is substantially lower than the material yield stress. The load at which instability or buckling occurs is a function of member geometry and material elasticity modulus, that is, slenderness, rather than material strength (Rigo & Rizzuto, 2010).

iii. Fracture

This failure mode occurs due to rapid extension of cracks and can be kept in check by quality control during construction and in-service inspection.

The failure modes that are of interest in this work are tensile/compressive yield of the material and compressive instability (buckling).

## 2.2 Loads On Ship

A ship encounters different loads during her lifetime. She is expected to endure and withstand the various types of loads. These loads need to be taken into consideration during structural design and analysis. Based on the ship's structural arrangement, loading effects might differ. There are different ways of classifying loads on ships and they depend on different factors like (Hughes & Paik, 2010):

### *2.2.1 Level Of Structural Influence*

Some loads influence the ship structure at one of four levels: hull girder, hull module, principal member and local. However, there are other loads that influence the ship structure at more than one level and the most fundamental is external pressure on the hull which has an influence at all four levels.

i. Hull girder level

The loads acting at this level can be classified thus: hull girder bending moment, hull girder shear loading, hull girder torsion loading and local loadings. Within the context of this work, only the hull girder bending moment is considered. The hull girder bending moment consists of three main components, viz; still water bending moment, wave induced bending moment and dynamic bending moment (i.e., whipping, slamming, springing).

ii. Hull module level

A hull module is a portion of a ship which might be one or more cargo holds/compartments, accommodation block or a funnel. The loads acting at this structural level include: hydrostatic pressure, various point/distributed loads due to weight of cargo, structure and outfitting.

iii. Principal member level

The principal structural members of a ship include: stiffened panels and pillars. The load effects acting on these principal members include: deflection, forces and stresses. In-plane normal and shear stresses, stiffener bending and plate bending stresses act on stiffened panels while axial and shear forces, twisting and bending moments and the corresponding stresses act on beam members (Hughes & Paik, 2010).

iv. Local level

Local structural elements do not appreciably affect load distribution; they only have local effect on their immediate surrounding. The local structure of a ship include: brackets, connections, fittings, reinforcements, foundations and so on. The load acting directly on the local structural level include container support point.

### *2.2.2 Variation with Time*

The loads acting on a ship can also be classified based on their variation with time, viz:

i. Static loads

The loads a ship encounter in still water condition is termed static loads. Their time duration exceeds the range of sea wave periods. Their variation during voyage is very slow/small, but during loading and unloading, a significant variation is observed.

ii. Slowly varying loads

These are loads with component periods longer than the fundamental natural period of vibration of the structure. Wave-induced dynamic pressure which results in wave-induced hull girder bending moment is the most important slowly varying load (Hughes & Paik, 2010). It results from the combination of wave encounter and the resulting ship motion.

iii. Rapidly varying loads

These are loads with component periods that are of the same order of magnitude or shorter than the longest natural period of the structure. Rapidly varying loads can take the form of slamming, forced (mechanical) vibration and other dynamic loads (Hughes & Paik, 2010).

Static loads acting on the hull girder are considered in this work. The important components of hull girder loads are vertical bending, horizontal bending, sectional shear and torsional moment as shown in figure 2.1. These arise from the distribution of local pressures, including sea and cargo loads. Simplified formulations and guidelines for calculating the design hull girder loads of merchant ships, with direct calculation of hull girder loads from first principle usually recommended in cases that involve unusual structures, pattern of loadings or operational conditions are provided by classification societies (Paik, 2018).

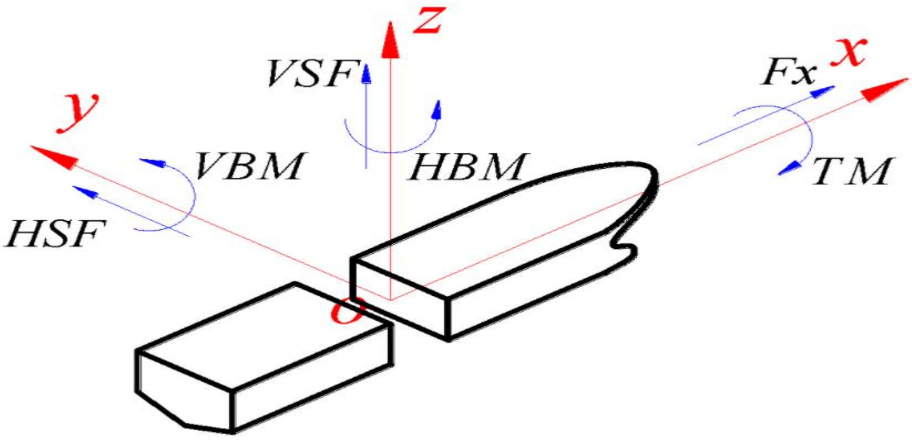


*Figure 2.1: Definition of hull girder sectional load components*
(Source: (Jiao, et al., 2017))

Where Fx is the axial force, HSF is the Horizontal Shear Force, VSF is the Vertical Shear Force, HBM is the Horizontal Bending Moment, VBM is the vertical bending moment and TM is the torsional moment. The sectional loads analyzed in this thesis are horizontal bending moment and vertical bending moment. Also, the combination of the horizontal bending moment and vertical bending moment is studied.

The horizontal bending moment arises due to the rolling of ships in an inclined condition. Also, quartering waves in which the wave crests on one side of the ship are in phase with the wave troughs on the other give rise to horizontal bending moment. The vertical bending moment occurs as a result of uneven distribution of weights and buoyancy along the length of the ship.

## 2.3 Ship's Structural Response Analysis

### *2.3.1 Static Only or Static and Dynamic*

A static analysis is carried out if the system being analyzed does not depend on time and if constant load is applied. Numerically, only the stiffness matrix of the FE model has to be solved. In dynamic analysis, the effects of time variation of loading are taken into consideration. For the dynamic analysis, the stiffness matrix, mass matrix and damping matrix (if not zero) is solved. Hence, more computational effort is required in dynamic analysis than in static analysis.

### *2.3.2 Probabilistic or Deterministic*

Probabilistic or deterministic response analysis is carried out when an explicit statistical approach is used to define loads and to calculate load effects. In the probabilistic analysis, characteristic values of load effect are calculated explicitly for the particular structure and load. It should be employed for ships whose hull girder loads are not already well established. In the deterministic analysis, the characteristic values are obtained from approximate expressions derived previously by means of a systematic series of probabilistic analyses (Hughes & Paik, 2010).

### *2.3.3 Linear or Nonlinear*

Linear structural analysis is used when the relation between applied forces and displacements is linear i.e., in the linear elastic region. The linear structural analysis is often used as a first estimate before carrying out a complete nonlinear analysis. Nonlinear structural analysis is mostly employed when buckling, ultimate strength and accidental or extreme conditions like collisions and grounding are to be analyzed (Rigo & Rizzuto, 2010). From the results of this analysis, simplified approaches and rules can be standardized.

## 2.4 Ultimate Strength

Stresses and/or deflections are used to indicate the responses of structural components of the ship hull to applied loads. Strength is the general term that is used to ascertain the structural performance criteria and the associated analyses involving stresses. Strength and/or stiffness considerations give an indication of the ability of a structure to perform its design functions. Inadequate strength of a structural member in response to applied load(s) results in loss of load-carrying capacity exhibited through one or more of the failure mechanisms already discussed.

The ultimate hull girder strength relates to the maximum load that the hull girder can support before collapse. Vertical and horizontal bending moment, torsional moment, vertical and horizontal shear forces and axial force are induced by the loads. The ultimate bending moment refers to a combined vertical and horizontal bending moments which is presently considered as a relevant design case (Rigo & Rizzuto, 2010).

When the strength of ship structures is assessed, it has been common to consider three strengths (Yao, et al., 1994): longitudinal strength, transverse strength, and local strength. Among these, longitudinal strength, which is the hull girder strength against longitudinal bending, is the most fundamental and important strength to ensure the safety of ships. Nevertheless, depending on the ship's wave encounter direction, combined loads act on the hull girder and the other 'strengths' need to be taken into consideration. This is often the case in oblique waves.

Unfortunately, majority of the works carried out in the past have only been focused on the longitudinal ultimate strength of a ship, that is the ultimate strength under vertical bending moment, with very little consideration given to the fact that the ultimate strength of a ship can be affected by horizontal bending moment. Though some previous works have been carried out on the subject of ultimate strength under combined loads, additional work is required.

Computation of ultimate bending moment depends closely on the ultimate strength of the structure's constituent panels, and particularly on the ultimate strength in compressed panels or components.

### *2.4.1 Methods for Ultimate Strength Determination*

There are basically two main approaches to evaluating the ultimate strength of ship's hull. One is to calculate the ultimate bending moment directly while the other is to perform progressive collapse analysis on the hull girder to obtain both ultimate bending moment and curvature (Rigo & Rizzuto, 2010).

#### *2.4.1.1 Direct Method*

In this approach, the stress distribution through the hull section is normally assumed. Hence, this method is applied to simple structural geometries. Also, it is assumed that post-collapse strength reduction does not occur. The direct methods of calculating ultimate strength include:

- Caldwell’s method

Caldwell was the first to theoretically attempt to predict the ultimate hull girder strength (Caldwell, 1965). He developed a direct assessment method for a simple rectangular stiffened hull section considering material yield and buckling (ISSC, 2015). The cross section composed of stiffened panels was idealized as being composed of unstiffened panels with equivalent thickness as shown in figure 2.2 (Yao & Fujikubo, 2016).

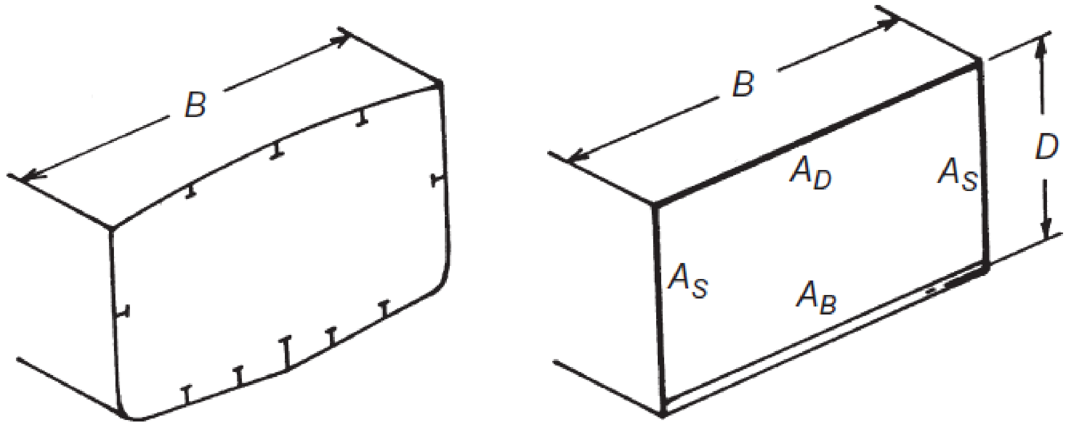


*Figure 2.2: Caldwell’s idealization of the cross-section of ship’s hull girder*

(Source: (Yao & Fujikubo, 2016))

Furthermore, Caldwell introduced the buckling induced strength reduction factor in his method. The bending stress distribution (Figure 2.3) is presumed over the simplified cross section, with the tension part reaching its yielding limit and the compression part reaching its ultimate limit in buckling. By integrating the stress over the idealized cross section, the ultimate bending moment can then be determined.

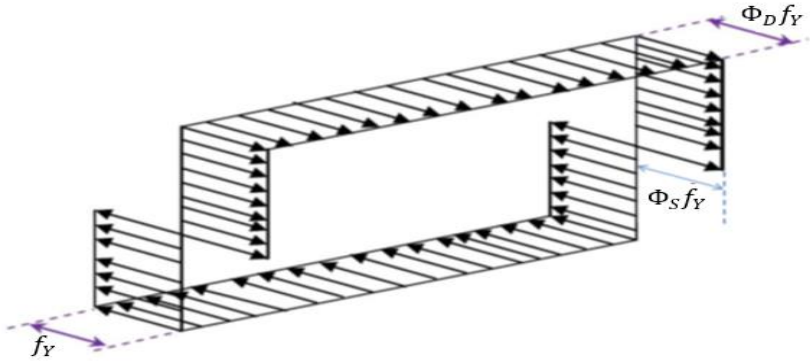


*Figure 2.3: Caldwell’s idealized stress distribution*

In the figure, $\Phi_D$ and $\Phi_S$ are buckling strength reduction factors Caldwell introduced for the deck and side shell respectively in the case of sagging and $f_Y$ is the yield stress of the material. As can be seen from figure 2.3, all structural members of the box girder reach their limit stress simultaneously. This is atypical of ship structural behaviour (especially for elements near the neutral axis) in that; structural components collapse (yield or buckle) one after the other when the applied load(s) is increased. Hence, the ultimate strength of the box girder tends to be overestimated by this approach.

- Improved methods

Sequel to the Caldwell's method, many researches were further carried out based on the Caldwell's method. The accuracy of the buckling induced strength reduction factor was improved upon by (Nishihara, 1983). Caldwell's method was also extended to the case of bi-axial bending and modified to account for the influence of grounding and/or collision damage by (Maestro & Marino, 1989). Formulations similar to that of Caldwell's were also proposed by different researchers.

These improved methods showed good correlation with measured/calculated results in many cases; negligence of the progressive collapse behaviour and strength reduction of structural elements beyond ultimate strength notwithstanding.

- Empirical formulations and interaction formulations

There are some empirical formulations that can give an initial estimation of the ultimate hull girder strength. These formulations are mostly standardized for specific vessel types (Viner, 1986). According to (Yao, 2000), a rational assessment of the ultimate bending moment in sagging and hogging conditions can be derived from the initial yielding of the deck and the initial buckling strength of the bottom plate respectively.

Empirical interaction formulations to predict the ultimate strength of hull girder under combined loads have also been studied and proposed by several authors. (Yao, et al., 1994) studied the ultimate hull girder strength interaction relation for double hull tanker under combined vertical and horizontal bending. (Paik, et al., 1996) analyzed the ultimate hull girder strength under combined vertical and horizontal bending moment for eleven vessels using the program ALPS/ISUM. Also, (Hu, et al., 2001) performed analysis on the ultimate longitudinal strength of a bulk carrier under combined vertical and horizontal bending moments by using a simplified method. (Ozguc, et al., 2007) have carried out a broad study of the hull girder ultimate strength under coupled bending moment.

Many expressions have been proposed for the ultimate strength interaction relationship between vertical and horizontal bending moments. These expressions were reviewed by (Sumi & et al., 1997) in the ISSC1997 report and are often expressed as:

$$\left(\frac{M_v}{M_{vu}}\right)^a + \alpha\left(\frac{M_h}{M_{hu}}\right)^b = 1 \qquad (2.1)$$

Where $M_v$ and $M_h$ are the vertical and horizontal bending moments respectively, $M_{vu}$ and $M_{hu}$ are the ultimate vertical and horizontal bending moments respectively. $\alpha,$ a and b are empirical constants.

There are different suggestions for the values of the empirical constants $\alpha$, a and b. (Gordo & Guedes, 1997) suggested that a = b and that their value lies between 1.50 and 1.66 and $\alpha$ = 1 for tankers. According to (Ozguc, et al., 2005), $\alpha$ = 1, a = 2.0 and b = 1.40 for hogging condition and b = 1.10 for sagging condition for bulk carriers. (Mansour, et al., 1998) proposed interaction formulations based on the calculated results for one container ship, one tanker and two cruisers with empirical constants: a = 1, b = 2 and $\alpha$ = 0.85. According to (Paik, et al., 1996), the empirical constants a and b are independent of vessel type and bending direction, and could be taken as 1.85 and 1.00 respectively where $\alpha$ = 1.

#### *2.4.1.2 Progressive Collapse Analysis*

This approach of determining the ultimate strength takes into account strength reduction (load shedding) of structural members when the ship's hull collapse behaviour is simulated. The major methods of the progressive collapse analysis include Finite Element Method (FEM), the Idealized Structural Unit Method (ISUM) and the simplified Smith's method.

- Simplified Smith's Method

Smith's method is a simplified method for performing progressive collapse analysis of ship hull girder on the basis of plane section assumption and that adjacent elements do not interact in the cross section (majorly for longitudinal bending).

In Smith's method, the ship cross section is divided into small assemblies made of stiffener and corresponding attached plating. The average stress-average strain relationships of each structural component are first obtained and analyzed considering the influences of yielding and buckling before performing a progressive collapse analysis. During the process, curvature of the cross section is applied incrementally, the corresponding incremental bending moments, individual element's incremental strain and stress are then evaluated. Failures of part of the individual elements occur due to the stress induced by the bending moment. This results in a new neutral axis position which is used for the next iterative step. By so doing, the progressive collapse behaviour is considered.

Smith's method gives a good estimation of the ultimate strength and progressive collapse behaviour. Nonetheless, its accuracy is highly dependent on the accuracy of the average stress-average strain relationships of each element.

- Finite Element Method

This is the most rational method of determining ship's hull ultimate strength through progressive collapse analysis (Rigo & Rizzuto, 2010). This method enables the consideration of both geometric and material nonlinearities. The earliest application of FEM to the hull girder collapse analysis was presented by ABS group in 1983 (Yao & Fujikubo, 2016). Special elements like orthotropic plate elements were developed and used to represent stiffened plates. This brought about the reduction of the number of degrees of freedom and elements. Yielding condition was introduced in terms of sectional force. Furthermore, special elements were developed by DNV group to perform similar progressive collapse analysis by using nonlinear FEM (Valsgard, et al., 1991).

The FEM is a powerful method for performing hull girder progressive collapse analysis. However, performing progressive collapse analysis of the complete hull girder using FEM requires large computational effort and some simplifications. Consequently, it is more convenient to perform progressive collapse analysis on a section of the hull that extends sufficiently in the longitudinal direction to model the characteristic behaviour (Rigo & Rizzuto, 2010). Nonetheless, explicit FEM can be applied to perform huge analysis using computer codes like LS-DYNA (Hallquist, 1998). Generally, a static solver with an equilibrium convergence iterator typically arc-length or Newton-Raphson method is used (Cook, et al., 2002).

- Idealized Structural Unit Method

The Idealized Structural Unit Method (ISUM) is a simplified nonlinear FEM in which modeling effort and computation time are reduced by reducing the number of nodal points and elements so that the number of unknowns in the finite element stiffness equation reduces. This is achieved by using large sized structural units to model the object structure. The large sized structural units are idealized as stiffened plate unit, stiffened panel unit, etc., while the nonlinear behaviour of the different structural members is expressed and idealized in the form of failure functions (Rigo & Rizzuto, 2010).

ISUM is not a general-purpose approach, it is limited to some particular problems. It is therefore necessary to develop ISUM elements specifically. It is noteworthy that this method is not satisfactory for linear stress analysis.

### *2.4.2 Factors Affecting Ultimate Strength Assessment*

Many factors affect the ultimate strength determination of structures. According to (ISSC, 2012) report, these factors can be categorized into three practical aspects, viz: physical aspects, modeling uncertainties and ageing effects.

a. Physical aspects

Physical aspects which affect the determination of the ultimate strength of structures include: material properties and behaviour, overall geometry and component scantlings, local variations of geometry and fabrication/initial imperfections.

Several researches have been carried out to study the influence of these physical aspects on the assessment of ultimate strength. (Khedmati, et al., 2009) carried out detailed analysis on the effects of intermittent welding on the ultimate strength of stiffened plates using the commercial software ADINA. The effects of initial geometric imperfections have also been studied by (Misirlis, et al., 2010). Furthermore, (Chaithanya, et al., 2010) studied the effect of distortion on the buckling strength of stiffened panels.

In this work, emphasis is placed on physical aspects due to material properties and behaviour as well as initial imperfections.

b. Modeling uncertainties

The uncertainties involved in ultimate strength are diverse. They include uncertainties due to geometry idealization, quantitative definition of limit state modes, approximation of analytical and numerical models, solution algorithms and interaction among components. In modelling uncertainties, numerical models are generally preferred mostly nonlinear FEM though analytical models provide good information (ISSC, 2012).

c. Ageing and in-service damage effects

The factors influencing ultimate strength determination due to ageing effects include corrosion, fractures and fatigue cracks, local buckling, mechanical damages and coating protection/environmental effects. Several investigations on the impact of ageing effects on the ultimate strength of structures have been conducted. (Wang, et al., 2008) studied the time variant hull girder strength of ageing ships. The degradation of hull girder section modulus due to corrosion was investigated by (Ivanov, 2009). (Rabiul & Sumi, 2011) analyzed the effects of corrosion pits geometry and corroded plates size in their study of the strength and deformability of steel plates. Also, (Rizzuto, et al., 2010) carried out assessment of the reliability of a tanker in damage conditions.

In this study, the effect of damage due to grounding will be investigated. An idealized symmetry damage condition is assumed and the residual strength of the double hull VLCC is assessed.

Generally, some of these factors are difficult to model hence they are implicitly taken into account by safety factors. Also, assumptions are made in some cases in order to realistically idealize the situation.

## 2.5 Nonlinear Finite Element Analysis

In many cases, the aim of a nonlinear analysis is to estimate the maximum load carrying capacity of a structure prior to structural instability or collapse. The distribution of the load on the structure is usually known in the analysis, but the magnitude of the load that the structure can support is unknown. One of the ways of determining this is by performing PCA using NLFEM. Finite element formulations of nonlinear differential equations lead to nonlinear algebraic equations for each element of the finite element mesh (Reddy, 2004). The finite element equilibrium equation for static analysis can be expressed as (Bathe, 2006):

$$[K]\{U\} = \{R\} \tag{2.2}$$

These equations correspond to a linear analysis since the displacement response {U} is a linear function of the applied load vector {R}. When this is not the case, we perform a nonlinear analysis. For a nonlinear analysis, a nonlinear relation exists between the applied load vector {R} and the displacement response {U}. Nonlinearities result in a stiffness matrix [K] that is not constant during load application, hence, the principle of superposition does not hold. This implies that displacement response {U} cannot be scaled in proportion to applied load, {R}. A separate analysis is required in each load case (Cook, et al., 2002). An iterative process is therefore required so that the product [K]{U} is in equilibrium with {R}.

The occurrence of nonlinearities in their relations among applied loads, stresses, strains, displacements and boundary conditions is illustrated in Figure 2.4 (Kim, 2015).

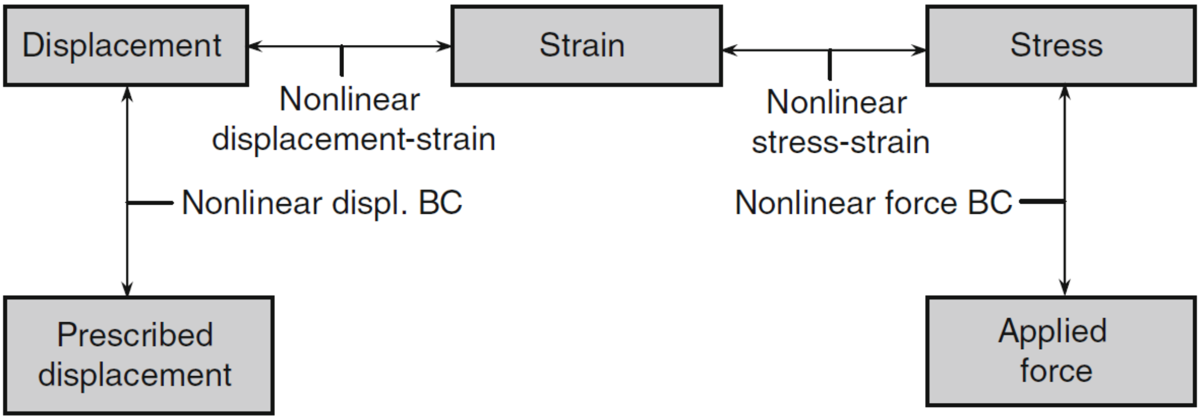


*Figure 2.4: Occurrence of nonlinearities*

(Source: (Kim, 2015))

### *2.5.1 Classification of Nonlinearities*

There are three common types of nonlinearities in structural mechanics, viz; geometric, material and contact nonlinearities. Several books are available on this subject, nevertheless, a brief overview is given here.

i. Geometric nonlinearity

Geometric nonlinearities represent situations where nonlinear relations exist among kinematic quantities (displacement, rotation and strains). They arise from the presence of large strain, small strains but finite displacements and/or rotations and loss of structural stability (Madenci & Guven, 2015), i.e., from purely geometric consideration (e.g., nonlinear displacement-strain relations) (Reddy, 2004).

In analyses involving geometric nonlinearity, the formulation of the constitutive and equilibrium equations take into account changes in geometry as the structure deforms. The structure should be in equilibrium after deformation. Hence, an additional nonlinear strain matrix $[B_u]$ is introduced into the expression of the original strain matrix. Thus:

$$[B] = [B_o] + [B_u] \qquad (2.3)$$

where $[B_o]$ is the linear part and $[B_u]$ is the nonlinear part.

ii. Material nonlinearity

Material nonlinearities occur as a result of nonlinear behaviour of the material of a structure. The constitutive relation between the stress and strain is not linear in this case. In such a material, the elastic modulus matrix is based on the current deformation, deformation history, rate of deformation, temperature, pressure, and so on.

iii. Contact nonlinearity

Contact nonlinearities result from the prescribed boundary displacements dependence on the deformation of the structure.

### 2.5.2 *Solution Techniques*

Iterative solution techniques are generally applied to nonlinear functions. The basic idea is to assume that the solution at a time t is known and that the solution at time $t + \Delta t$ is required, where dt is a well-chosen time increment. Therefore, the finite element equilibrium equation (2.2) can also be expressed as equation (2.4) assuming that the externally applied loads are described as a function of time.

*(with $[K]\{U\} = \{F\}$)*

$$^{t}\{R\} - {}^{t}\{F\} = 0 \tag{2.4}$$

where $^{t}\{\mathrm{R}\}$ is the vector of externally applied nodal point forces at time t and $^{t}\{\mathrm{F}\}$ is the vector of nodal point forces that corresponds to the element stresses at time $t$.

Hence, at time $t + \Delta t$, we have:

$$^{t+\Delta t}\{R\} - {}^{t+\Delta t}\{F\} = 0 \tag{2.5}$$

Since the solution at time t is known;

$$^{t+\Delta t}\{F\} = {}^{t}\{F\} + \{F\} \tag{2.6}$$

Where {F} is the increment in nodal point forces corresponding to the increment in element displacements and stresses from time $t$ to time $t + \Delta t$. This increment {F} can be approximated with a tangent stiffness matrix ${}^{t}[\mathrm{K}]$ which accounts for geometric and material conditions at time t:

$$\{F\} = {}^{t}[K]\{U\} \tag{2.7}$$

Where {U} is a vector of incremental nodal point displacements.

Substituting equations (2.6) and (2.7) into (2.5) gives:

$$ {}^{t}[K]\{U\} = {}^{t+\Delta t}\{R\} - {}^{t}\{F\} \tag{2.8}$$

Solving for {U}, an approximation to the displacements at time $t + \Delta t$ can be calculated thus:

$$ {}^{t+\Delta t}\{U\} = {}^{t}\{U\} + \{U\} \tag{2.9}$$

With equation (2.9), an approximation to the stresses and corresponding nodal point forces at time $t + \Delta t$ can be evaluated. From there, the next time increment can then be calculated.

It is noteworthy that the solution obtained may be subject to very significant errors due to the assumption in equation (2.5). Hence, it is required to repeat the iterative procedure until the approximate solution tends towards the actual solution equation (2.7) in some measure.

There are several iterative procedures used in nonlinear finite element analysis (see (Reddy, 2004), (Kim, 2015) and (Bathe, 2006)), however, only two would be discussed within the context of this work.

- Newton-Raphson scheme

This is a very effective and widely used iterative procedure for the solution of nonlinear finite element equations. It is an extension of the rudimentary iterative technique described above. That is, having calculated an increment in the nodal point displacements, which defines a new total displacement vector, we can repeat the incremental solution described above using the currently known total displacements instead of the displacements at time t. The Newton-Raphson scheme is illustrated in figure 2.5.

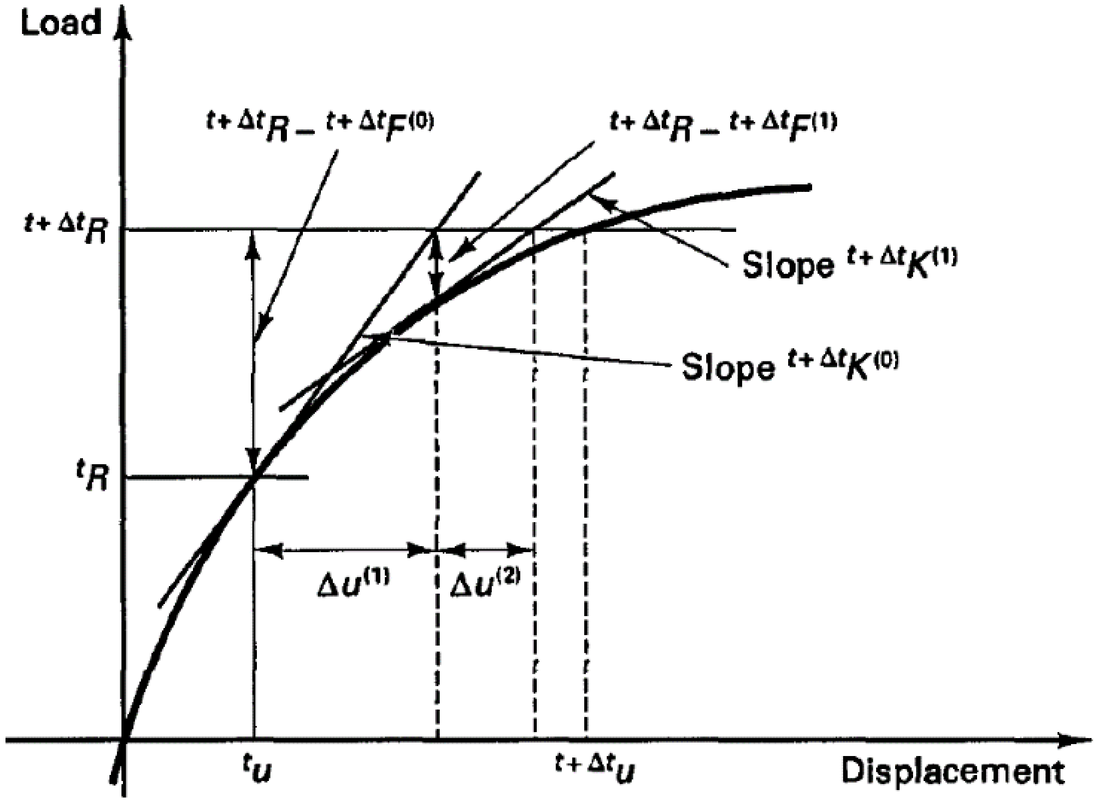


*Figure 2.5: Newton-Raphson iteration scheme*
(Source: (Bathe, 2006))

The equations used in the Newton-Raphson iterative scheme in steps of i = 1, 2, 3, …, can be expressed as:

$$^{t+\Delta t}[K]^{(i-1)}\Delta\{U\}^{(i)} = {}^{t+\Delta t}\{R\} - {}^{t+\Delta t}\{F\}^{(i-1)} \qquad \textit{(2.10)}$$

$$^{t+\Delta t}\{U\}^{(i)} = {}^{t+\Delta t}\{U\}^{(i-1)} + \Delta\{U\}^{(i)} \qquad (2.11)$$

With initial conditions:

$$^{t+\Delta t}\{U\}^{(0)} = {}^{t}\{U\};\ {}^{t+\Delta t}[K]^{(0)} = {}^{t}[K];\ {}^{t+\Delta t}\{F\}^{(0)} = {}^{t}\{F\} \qquad \textit{(2.12)}$$

It can be observed that for the first iteration, equations (2.10) and (2.11) reduce to equations (2.8) and (2.9) respectively. The iteration is continued until appropriate convergence criteria are satisfied.

The Newton-Raphson scheme is a very rapid convergent process; however, it has some negative features. It requires the calculation of a new tangent stiffness matrix in each iteration step. Consequently, it involves major computational costs due to the calculation and factorization of the tangent stiffness matrix in each iteration step. Hence, there are several other modifications of the Newton-Raphson scheme like the “modified Newton-Raphson scheme” in which case the stiffness matrix update on an accepted equilibrium configuration (see figure 2.6).

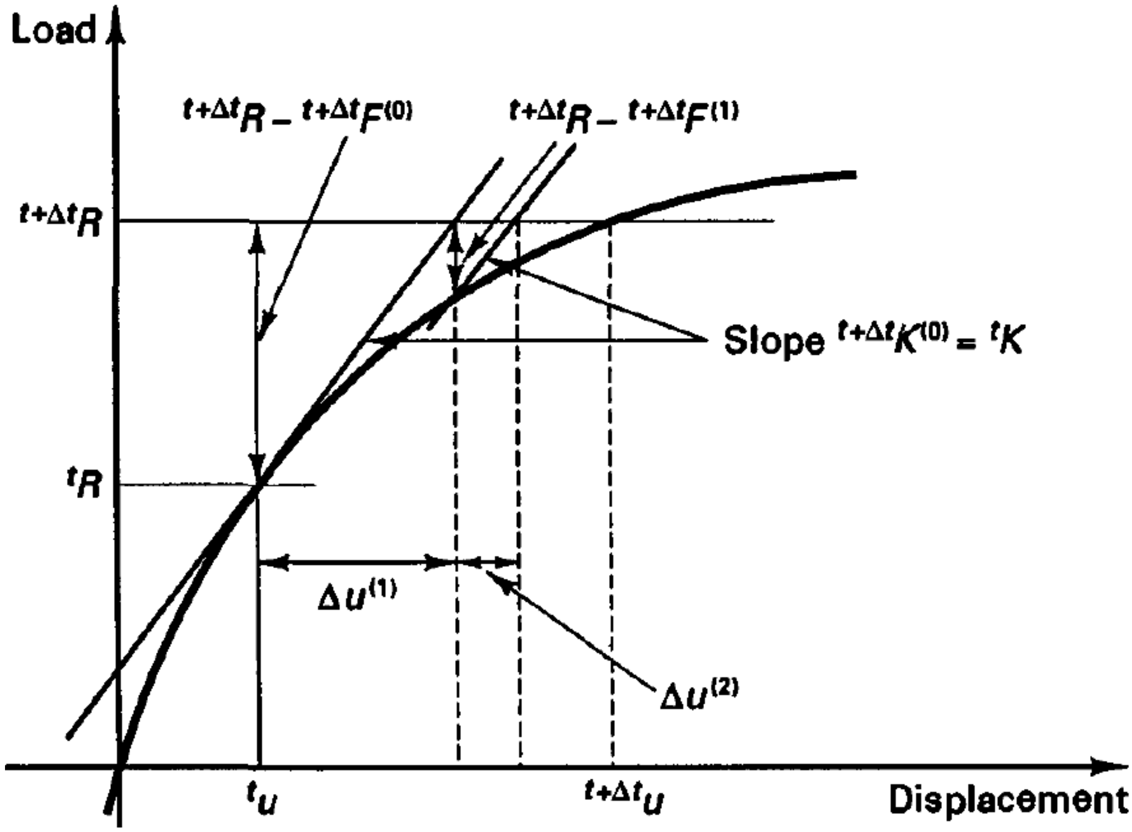


*Figure 2.6: Modified Newton-Raphson iteration scheme*

(Source: (Bathe, 2006))

- Arc-length Method

The Newton-Raphson scheme and its modifications are often used to trace nonlinear solution paths. However, the Newton-Raphson methods fail to traverse the collapse point (figure 2.7) as the tangent matrix at that point becomes singular and the iteration process diverges. Hence, a special iterative scheme that allows such changes at and beyond the collapse point must be adopted to calculate the resultant response. The Arc-length method is one of such iterative schemes.

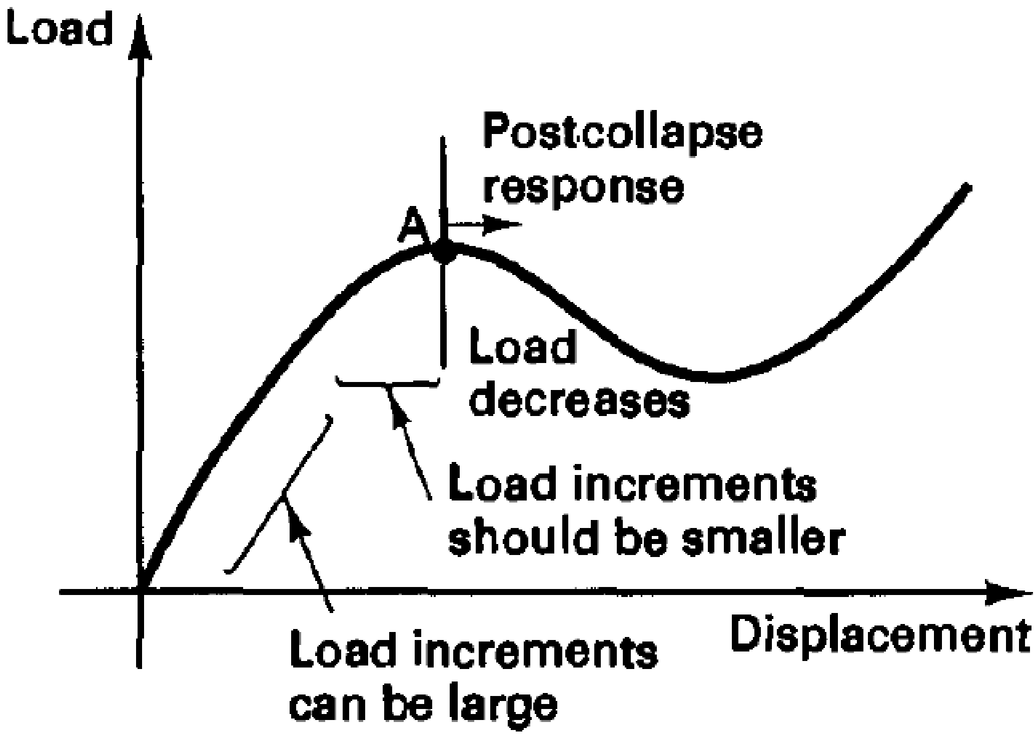


*Figure 2.7: Collapse response of a structural model*

(Source: (Bathe, 2006))

In the Arc-length method, fast convergence is obtained at each load step by introducing a load multiplier. This load multiplier either increases or decreases the intensity of the applied load so that the collapse point can be traced and the post collapse response can be evaluated (Bathe, 2006).

The analysis is based on the assumption that the load vector varies proportionally during the response calculation. The governing finite element equation is derived from equation (2.5) by introducing a load multiplier, which gives:

$$ {}^{t+\Delta t}\lambda\{R\} - {}^{t+\Delta t}\{F\} = 0 \tag{2.13}$$

where ${}^{t+\Delta t}\lambda$ is the load multiplier which is unknown and to be determined. Hence, an additional constraint equation of the form:

$$ f\left(\Delta\lambda^{(i)},\ \Delta U^{(i)}\right) = 0 \tag{2.14}$$

is needed to determine the load multiplier. Applying Taylor series and linearizing give:

$$ {}^{\tau}[K]\Delta\{U\}^{(i)} = \left({}^{t+\Delta t}\lambda^{(i-1)} + \Delta\lambda^{(i)}\right)\{R\} - {}^{t+\Delta t}\{F\}^{(i-1)} \tag{2.15}$$

There are several effective constraint equations that could be used (see (Crisfield, 1981) and (Bathe & Dvorkin, 1983). However, the spherical constant arc length criterion is used within the context of this work. It is expressed as:

$$(\lambda^{(i)})^2 + \frac{\{U\}^{(i)^T}\{U\}^{(i)}}{\beta} = (\Delta l)^2 \qquad (2.16)$$

where $\Delta l$ is the arc length for the step and $\beta$ is a normalizing factor. This criterion is described in figure 2.8.

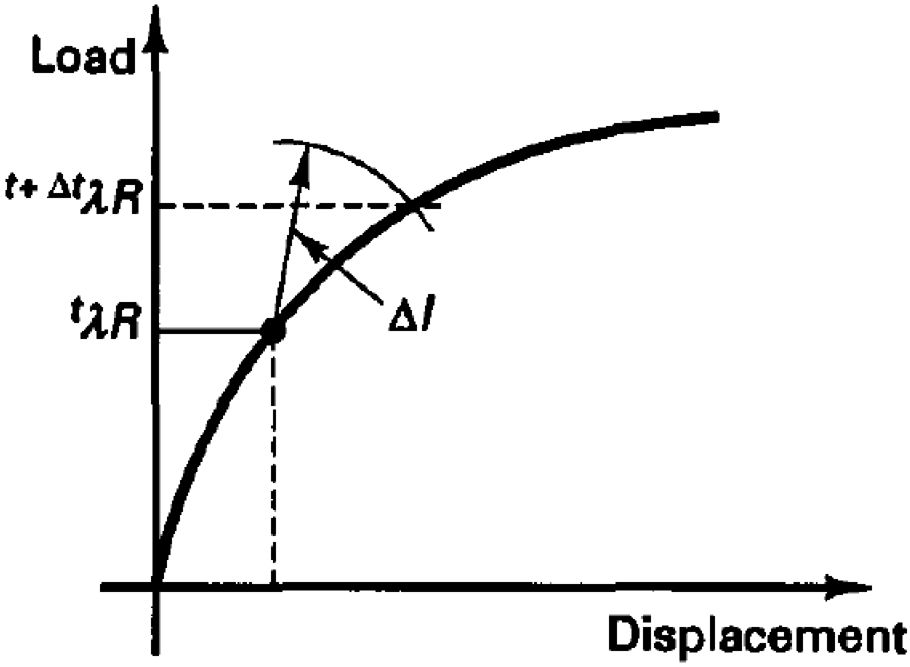


*Figure 2.8: Illustration of the spherical constant arc length criterion*

(Source: (Bathe, 2006))

# 3. MODELING

## 3.1 Ship Structural Characteristics

Currently, there is the tendency for ship structures to have double hull especially tankers. In August, 1990, the United States made the regulation that new tankers must have double hull structures (Yao, et al., 1994). Hence, a double hull VLCC is considered in this work. The main dimensions of the double hull VLCC are summarized in table 3.1 and the cross section of the double hull VLCC, extracted from ISSC2000 report, is shown in figure 3.1. The different stiffener types, properties and dimensions are attached in appendix A2.

*Table 3.1: Dimensions of Double Hull VLCC*

| Parameters | Values (m) |
|---|---|
| Length | 315 |
| Width | 58 |
| Depth | 30.4 |
| Draft | 22 |

As shown in figure 3.1, longitudinal framing system is used in the outer and inner hull plates, the standard frame spacing of the double hull VLCC is 830mm and the space between transverse frames is 4950mm. The different stiffeners used are labelled with numbers ranging from 1 to 48. For simplicity, angle-bar (stiffeners) are idealized and modelled as L-bar (stiffeners).

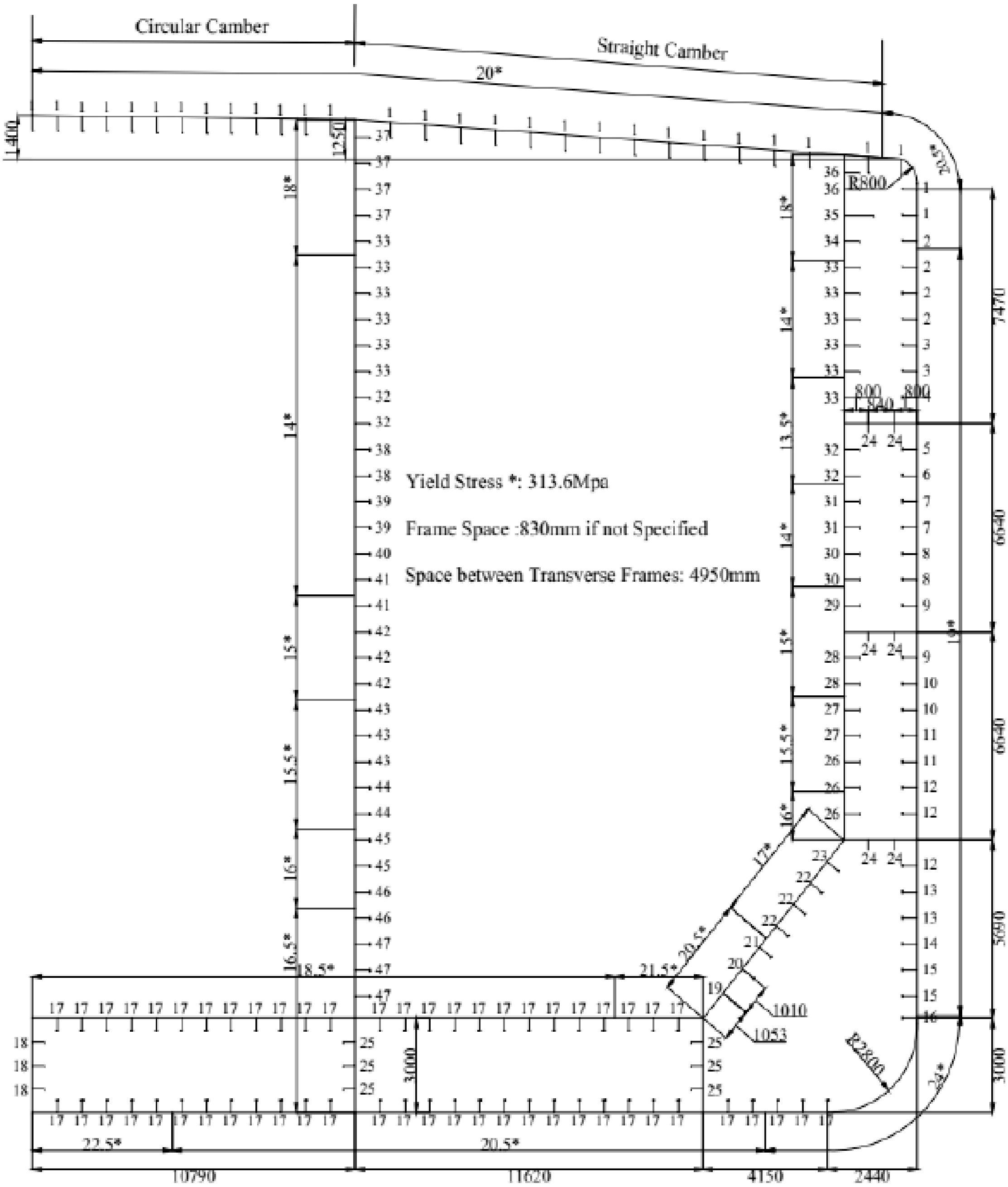


*Figure 3.1: Double hull VLCC cross section*

(source: (ISSC, 2012))

## 3.2 Procedures for Determining the Ultimate Strength

### *3.2.1 Preparation of FE Model*

One of the most crucial steps in FE analysis is FE model preparation. A poorly prepared model will invariably give bad results. The extent of the model also plays a key role for strength assessment. A 3-hold longitudinal extent is the requirement set by classification societies for strength assessment (IACS, 2020). This ensures that satisfactory results are obtained and that end effects are minimized. Nonetheless, due to computation cost, only a portion of the structure is considered. Hence, it is imperative that boundary conditions (loads, supports, etc.) are correctly idealized and applied so as to obtain satisfactory solution. In addition, appropriate element type(s) with suitable mesh sizes has to be used in the model preparation. Also, the material model has to be carefully chosen since it affects the results obtained as would be shown in this project.

In this work, a one bay-sliced hull cross-section (one transverse frame spacing) model is investigated and the element type used is 'SHELL 181'. Ideal elastic plastic and bilinear elastic plastic material models are used and their influences are investigated. The mesh size used in the ISSC 2000 report is adopted in this study.

The full depth and breadth of the VLCC are modeled. However, the dimensions of some plates of the double hull VLCC are not adequately labelled; hence some assumptions are made. The thickness of the plates which divide the compartments in the side shell plating is assumed to be equal to the thickness of the plates dividing the compartments in the double bottom. Also, to ensure compatibility of the plates with the hull dimension, plates with varied widths are used in some areas. However, to avoid using plates with decimal widths, plates of equal width with end connection plate are used. An instance is the connection from the bilge to the side shell plating (see figure 3.2). The stiffened plate field has a length of 5690mm but instead of using stiffened plate with equal width of 711.25mm or unstiffened plate with equal width of 355.65mm, the standard width of 830mm with a connection plate at the transition of the bilge to the shell plating is used. The same idealization is made for the regions surrounding the gunwales. It is however noteworthy that there may be negligible changes in the position of the stiffeners. Also, plates with widths different from the standard frame spacing are used in the deck since the stiffener spacings in the deck (circular camber and straight camber) are different (see Figure 3.1).

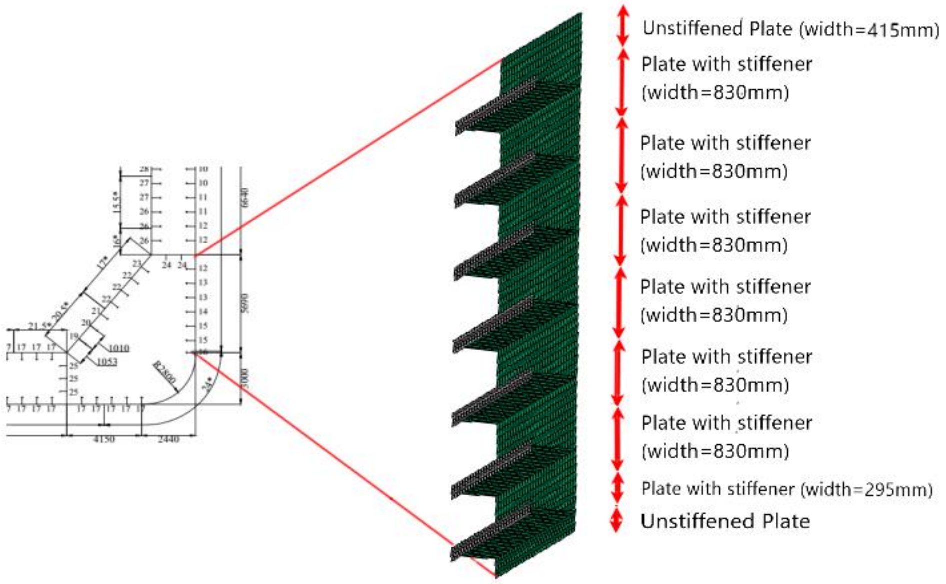


*Figure 3.2: Instance showing the use of end connection plate*

(source: (Muehmer, 2020))

### *3.2.2 Parametric Model*

The parametric modeling of the double hull VLCC was executed using ANSYS mechanical APDL. This is a scripting language in which parameters (variables) are used to automate common tasks or build models. With this tool, the dimensions, shape and properties of the model is defined. For easy scripting, half of the double hull VLCC is modeled. This modeled part is discretized into five parts: double bottom, double bottom tank, side shell, longitudinal bulkhead and deck as shown in figure 3.3. The other half is then modelled using symmetry condition. The centre line longitudinal is modeled separately.

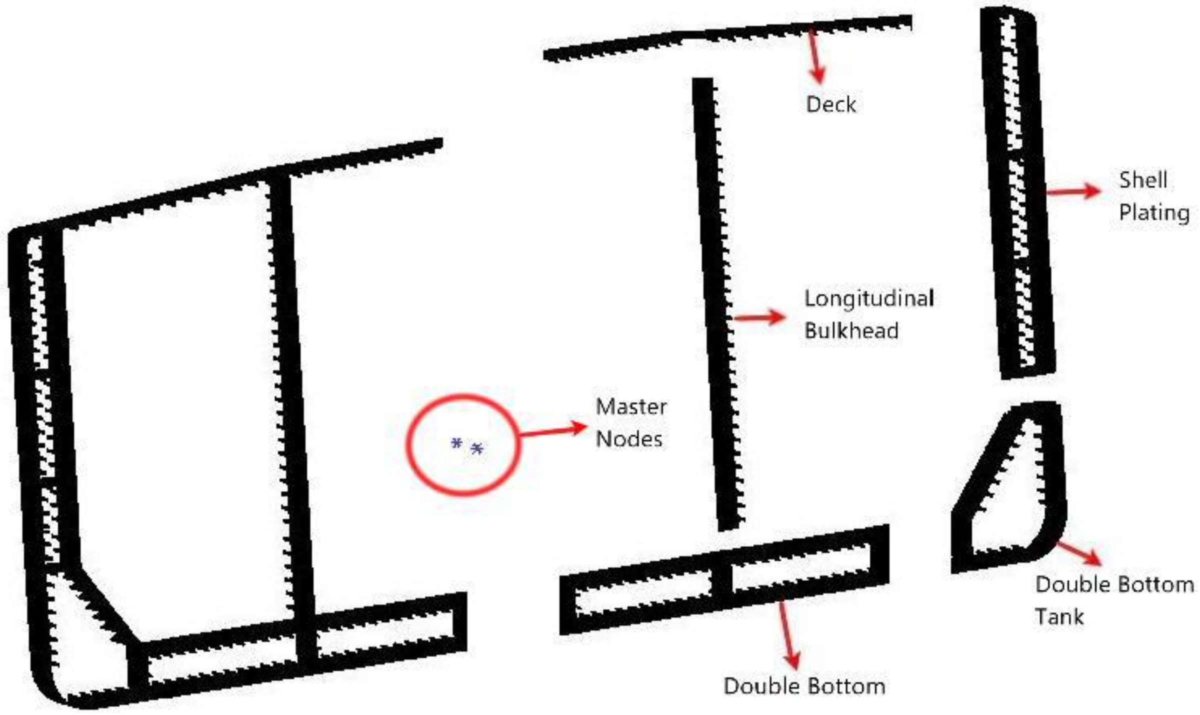


*Figure 3.3: Exploded diagram of the parametric FE model*

(source: (Muehmer, 2020))

The sequence of processes followed to finally obtain the required model and results is shown in the flowchart below (figure 3.4). This is done in a very condensed manner. Text files are enmeshed into other text files and are called up when the script is run. Five main text files are scripted namely; material, parameter, modeling, boundary conditions and postprocessing files. The material file houses the two materials models (elastoplastic and bilinear elastoplastic material models) used in this work. The user has the option to choose between the two material models. The parameter file contains the parameters of the model which include; the dimensions of the model, plates and stiffeners. It also contains information regarding mesh discretization, element type and applied loads. The modeling file contains sub-files used for model building. These sub-files give information about the definition of coordinate systems (global and local) and element connectivity. The boundary condition file contains information about master nodes, applied constraints, coupling equations and loads application. This file also provides the user with the option to choose between the two solution schemes employed in this work. In the postprocessing script, further processing is carried out and the final results can be inspected. Based on the solution scheme chosen in the boundary condition file, the user also has to choose the same solution scheme for the postprocessing file. The “tanker” file houses and calls the main files in the sequence shown in the flowchart.

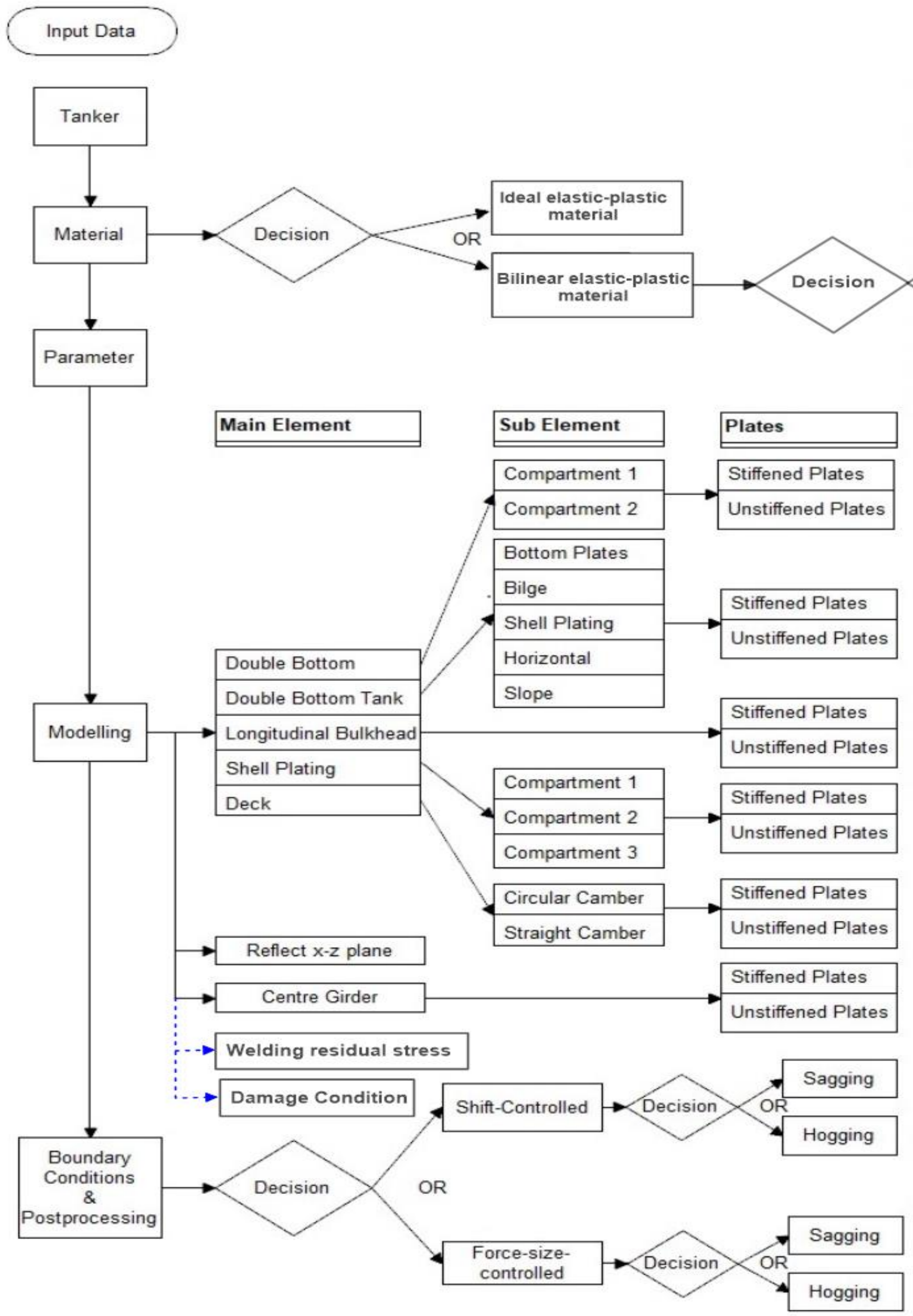


*Figure 3.4: Process flowchart*

Generally, three stages are involved in the finite element solution (Madenci & Guven, 2015):

- Preprocessing: this entails defining the problem in terms of keypoints/lines/areas/volumes, element type, material/geometric properties and meshing.
- Solution: this has to do with loads and constraints specification and solving of the resulting set of equations.
- Postprocessing: this involves additional processing and inspecting of the results.

### *3.2.3 Element Type*

The vital parts of a finite element model are the nodes and elements. In the discretization of the model into finite elements, it is important that an element that properly captures the physical behaviour of the structure is used. Since large deflection behavior is involved in the post-buckling strength analysis of the model, an element that is suitable for this structural behaviour is required. In this study, the 4-node structural shell element "SHELL 181" is used.

"SHELL 181" is a four-node element with six degrees of freedom at each node: translations in the x, y, and z directions, and rotations about the x, y, and z-axes, suitable for analyzing thin to moderately thick shell structures. Its formulation is based on logarithmic strain and true stress measures. It is well-suited for linear, large rotation and large strain nonlinear applications (ANSYS, Inc.). The element geometry is shown in figure 3.5.

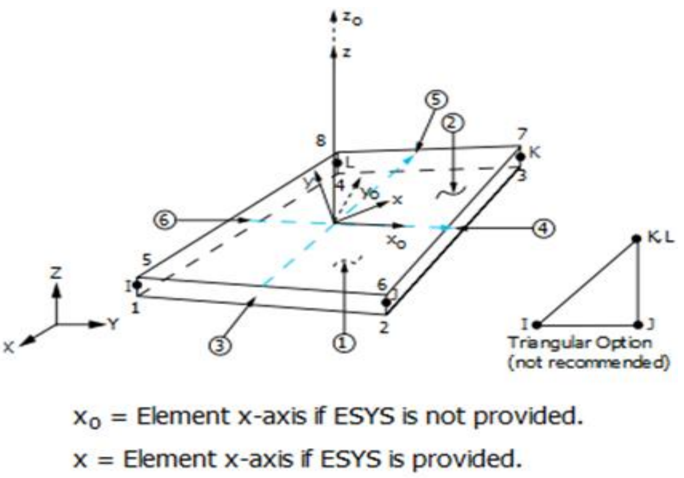


*Figure 3.5: Geometry of SHELL '181' element*

(source: (ANSYS, Inc.)

### 3.2.4 *Meshing/Element Size*

Mesh size is a very vital issue in finite element analysis. The complexity level of finite element analysis determined by the accuracy, computing time and efforts needed for meshing of finite element models is influenced by the mesh density. There exists a close relation between mesh density and solution convergence. According to FEA theory, finely meshed FE models give very accurate results but at the expense of computing time and vice versa. Hence, balances involving modeling time, accuracy, computation time and cost must be made.

Generally, the right mesh size is one that exhibits no major variances in the results when mesh refinement is introduced. In this study, the mesh size was decided on the basis of previous experience. Figure 3.6 gives an insight into the number of elements in-between stiffener spacing, stiffener web, stiffener flange and the longitudinal extent of the model.

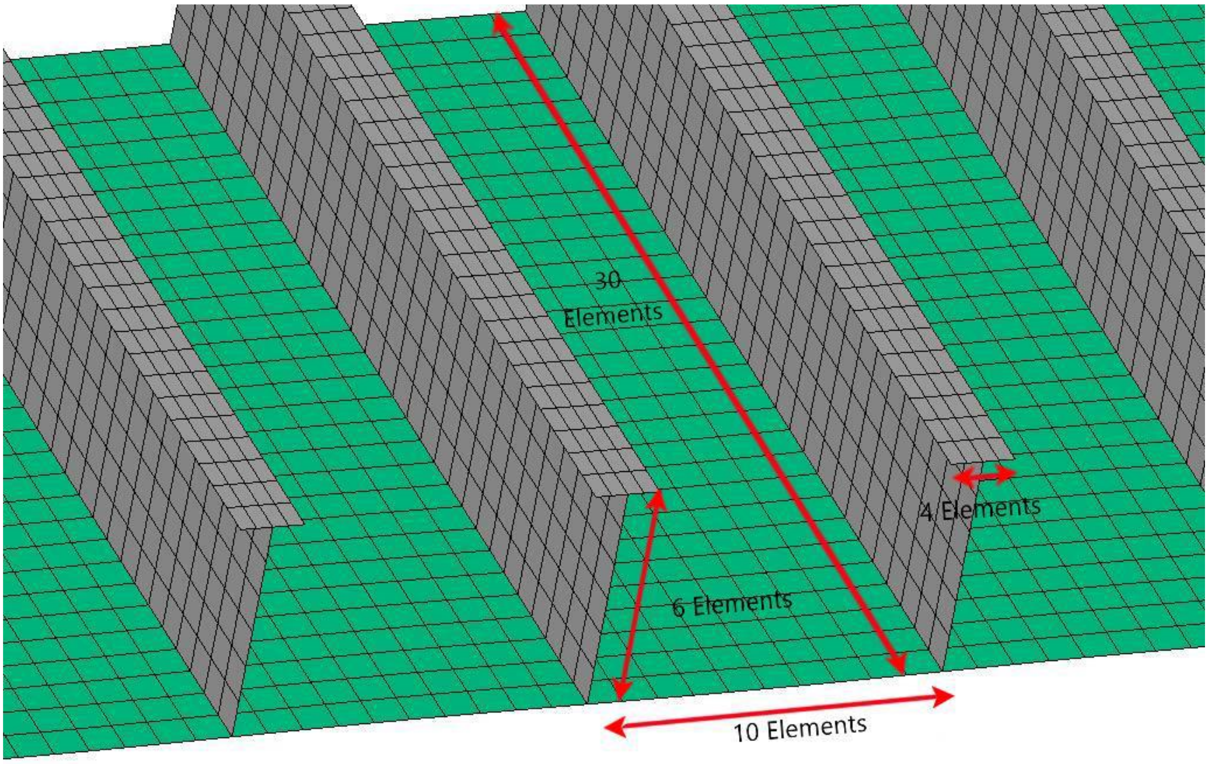


*Figure 3.6: Mesh discretization*

From figure 3.6, it can be seen that:

- The longitudinal expanse of the model is divided into 30 elements
- The stiffener spacing is divided into 10 elements

- The stiffener web height is divided into 6 elements
- The stiffener flange is divided into 4 elements

### *3.2.5 Material Modeling*

The double hull VLCC is built mainly with two different types of steel; one with a yield strength of 313.6MPa and the other with a yield strength of 352.8MPa. The detailed material data is shown in table 3.2. The distribution of the two different kinds of steel is not clearly shown in figure 3.1, however, all plates are built with steel of yield strength 313.6MPa. In addition to that, the deck, outer shell plating and the double bottom stiffeners are built with the same steel. Also, the double bottom tank stiffeners are built with the same steel except for the slope of the double bottom tank which is made of steel with yield strength of 352.8MPa. The other stiffeners of the VLCC are all built with steel of yield strength 352.8MPa.

*Table 3.2: Properties of Double Hull VLCC Steels*

| Steel type | $Re_H$ (N/mm$^2$) | E (N/mm$^2$) | $\upsilon$ (-) |
|---|---|---|---|
| 1(*) | 313.6 | 206000 | 0.3 |
| 2(**) | 352.8 | 206000 | 0.3 |

In this work, the influence of the material behaviour is modeled/studied using two material models: elastic-perfectly plastic model and bilinear elastic plastic model. The elastic-perfectly plastic model is a simplified model in which the effects of strain hardening and necking are not taken into consideration. The reverse is the case for the bilinear elastic plastic model. For the analysis with bilinear elastic plastic model, two tangent moduli ($E_{t1}$ and $E_{t2}$) are considered. They are expressed as:

$$E_{t1} = \frac{E}{100} \tag{3.1}$$

$$E_{t2} = \frac{E}{50} \tag{3.2}$$

where E is Young's modulus.

### *3.2.6 Boundary Conditions*

Since the model being considered is a cut-out from a larger structure, boundary conditions need to be properly applied. Appropriate boundary conditions are very vital in obtaining the right solutions and must be realistically idealized. Boundary conditions enmesh constraints and loads application.

#### *3.2.6.1 Constraints*

Constraints are simulated using symmetry boundary conditions and Multi-Point Constraint (MPC). At the aft and fore ends of the model cross section, symmetry boundary conditions are simulated in a way that out of plane rotations are suppressed (figure 3.7) i.e., rotations about the Y- and Z- axes are equal to zero. Furthermore, an imaginary transverse frame is assumed at the centre of the model (at X = 0) and symmetry boundary conditions are also simulated depending on the orientation of the elements. Vertical translation and rotation about longitudinal direction are suppressed for horizontally oriented components ($U_z = \theta_x = 0$), while horizontal translation and rotation about longitudinal direction are suppressed for vertically oriented elements ($U_y = \theta_x = 0$) (see Figure 3.8).

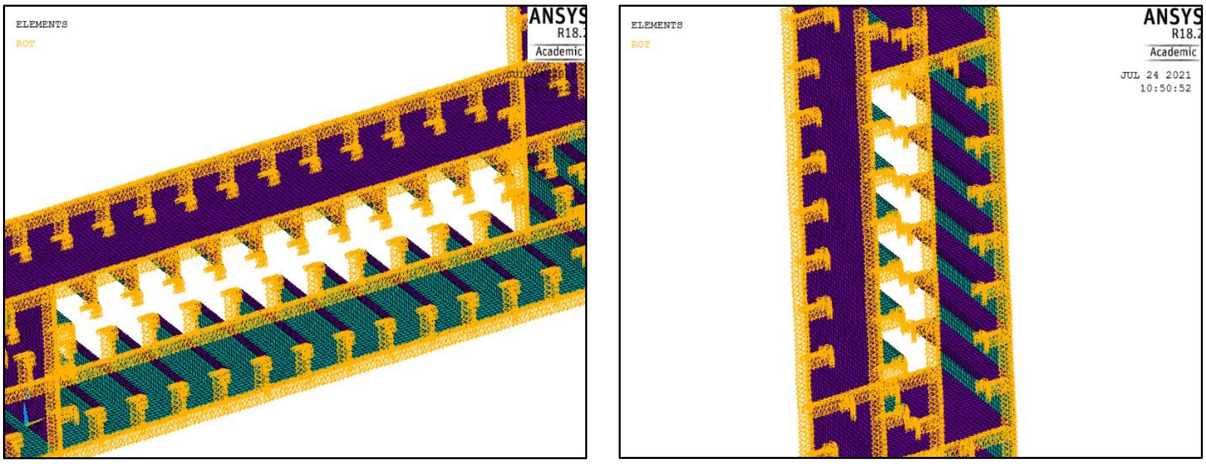


*Figure 3.7: Symmetry boundary condition for aft and fore ends: double bottom (left)and side shell (right)*

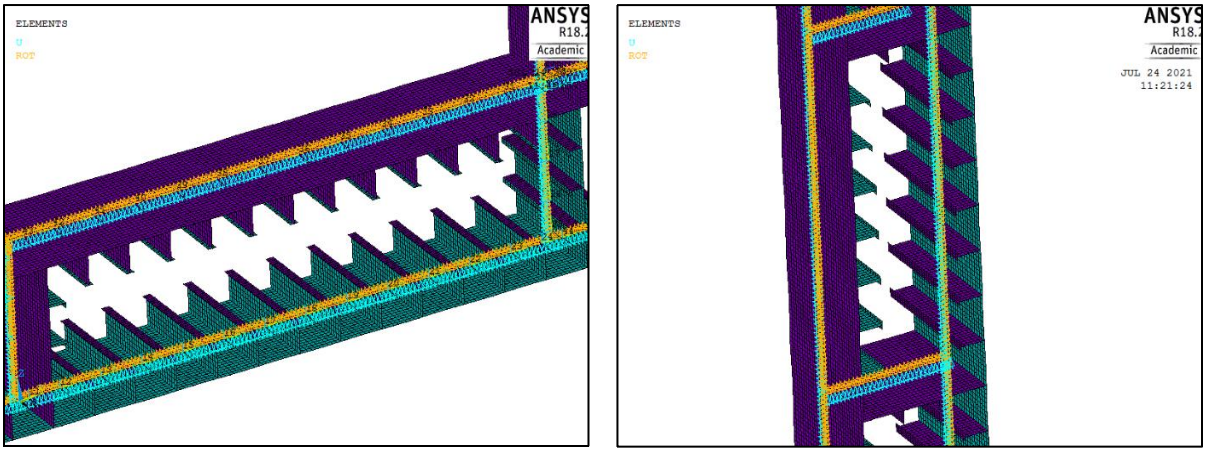


*Figure 3.8: Symmetry boundary condition for frame: horizontally oriented elements (left) and vertically oriented elements (right)*

However, some assumptions were made in the double bottom tank and gunwale. These parts are composed of elements that are neither vertical nor horizontal. The slope of the double bottom tank is assumed to be horizontally and vertically oriented and hence vertical and horizontal translations as well as rotation about the longitudinal direction are suppressed ($U_y = U_z = \theta_x = 0$). Also, the bilge and gunwale are assumed to be partly horizontal (from 0 to 45 degrees) and partly vertical (from 45 to 90 degrees) (Figure 3.9 and Figure 3.10).

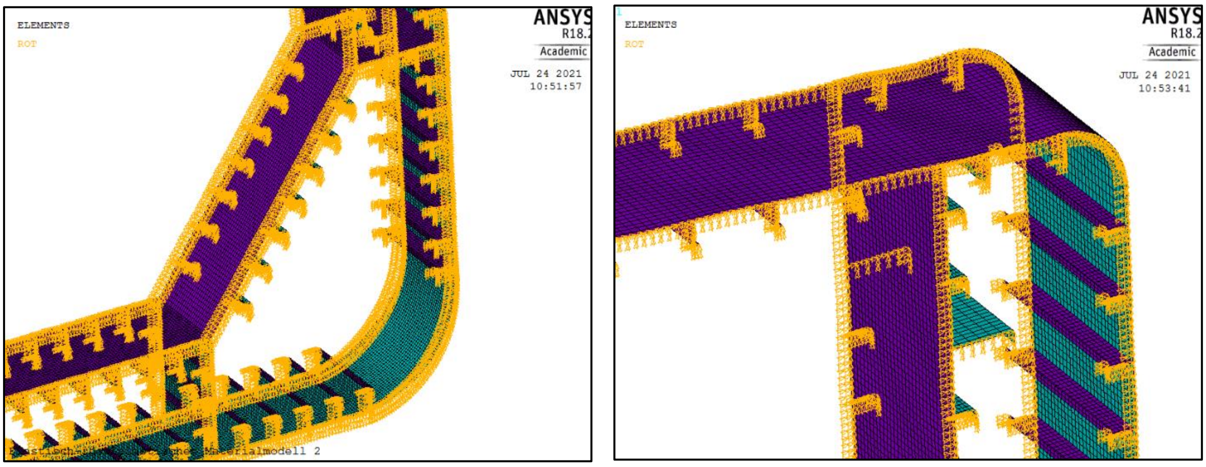


*Figure 3.9: Symmetry boundary condition for aft and fore ends: double bottom tank (left) and right gunwale (right)*

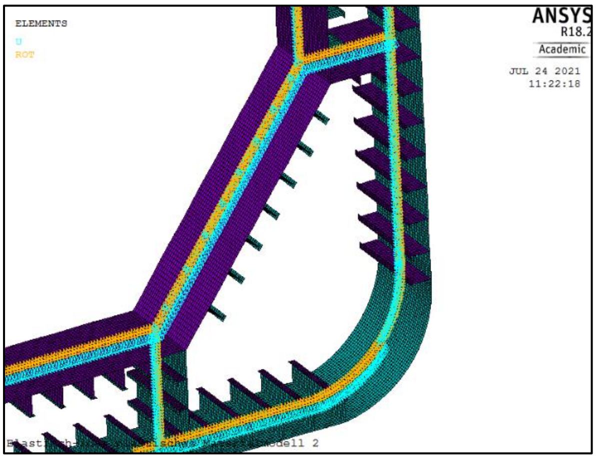


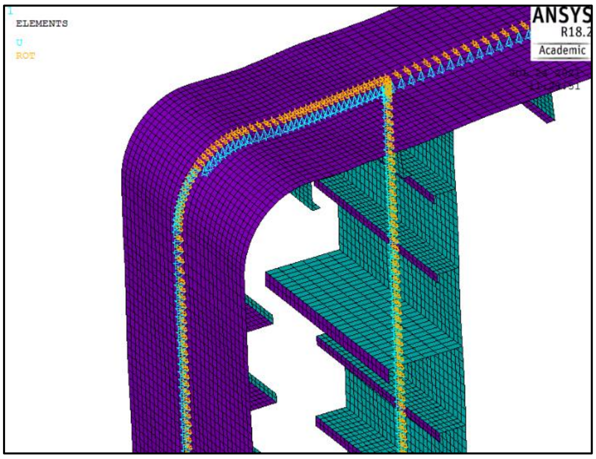


*Figure 3.10: Symmetry boundary condition for frame: double bottom tank (left) and left gunwale (right)*

#### *3.2.6.2 Load Application*

Loads are applied to the model by means of two master nodes (reference nodes) at the aft and fore ends of the model. These master nodes are set at the intersection between the centerline and the centroid of the model cross section. The master nodes are modelled using "MASS21" element type. "MASS21" is a point element having up to six degrees of freedom: translations in the nodal x, y, and z directions and rotations about the nodal x, y, and z axes (ANSYS, Inc.). These master nodes are used to constrain all nodes at the aft and fore ends of the model cross-section using Multi-Point Constraint (this entails the coupling of the applied load on the master nodes or rotation of the master nodes at the aft and fore ends to the displacement of the aft and fore ends of the model cross-section). Load or rotation is then incrementally applied through the master nodes and the resultant bending moment and curvature results can be obtained directly from the master nodes (see Figure 3.11).

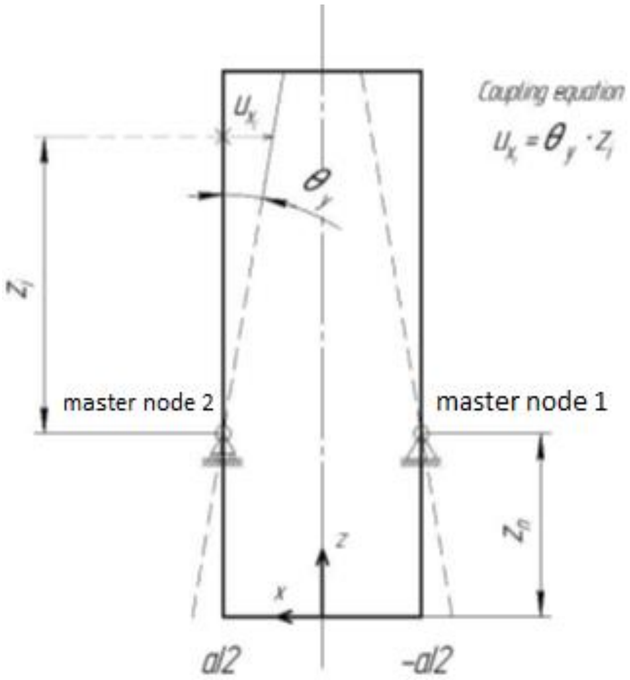


*Figure 3.11: Sample of Multi-Point Constraint for Vertical Bending load case*

Constraints are also applied on the degrees of freedom of the master nodes depending on the load case being considered/analyzed. Three load cases are analyzed in this study: vertical bending, horizontal bending and combined vertical and horizontal bending load cases.

- Load case 1: vertical bending

In the case of vertical bending, all the degrees of freedom of master node 1 are suppressed except rotation about the nodal y-axis. For master node 2, rotation about the nodal y-axis and translation in the nodal x-direction are allowed but the other degrees of freedom are suppressed. A summary of the boundary condition for the load case of vertical bending is shown in table 3.3. Consequently, the input for the Multi-Point Constraint can be expressed in the form of the constraint (coupling) equation:

$$U_{xi} = \theta_y * Z_i \qquad (3.3)$$

*Table 3.3: Applied Boundary Conditions for Vertical Bending Load Case*

| Location | Translation | | | Rotation | | |
|---|---|---|---|---|---|---|
| | $U_x$ | $U_y$ | $U_z$ | $\theta_x$ | $\theta_y$ | $\theta_z$ |
| Aft end | | | | | | |
| Cross section | Coupling equation | - | - | - | Fixed | fixed |
| Master node 1 | Fixed | Fixed | Fixed | Fixed | - | Fixed |
| Fore end | | | | | | |
| Cross section | Coupling equation | - | - | - | Fixed | Fixed |
| Master node 2 | - | Fixed | Fixed | Fixed | - | fixed |

- Load case 2: horizontal bending

In the case of horizontal bending, all the degrees of freedom of master node 1 are suppressed except rotation about the nodal z-axis. For master node 2, rotation about the nodal z-axis and translation in the nodal x-direction are allowed but the other degrees of freedom are suppressed. Consequently, the input for the Multi-Point Constraint can be expressed in the form of the constraint (coupling) equation:

$$U_{xi} = \theta_z * Y_i \quad (3.4)$$

A summary of the boundary condition for this load case is shown in table 3.4.

*Table 3.4: Applied Boundary Conditions for Horizontal Bending Load Case*

| Location | Translation | | | Rotation | | |
|---|---|---|---|---|---|---|
| | $U_x$ | $U_y$ | $U_z$ | $\theta_x$ | $\theta_y$ | $\theta_z$ |
| Aft end | | | | | | |
| Cross section | Coupling equation | - | - | - | Fixed | Fixed |
| Master node 1 | Fixed | Fixed | Fixed | Fixed | Fixed | - |
| Fore end | | | | | | |
| Cross section | Coupling equation | - | - | - | Fixed | Fixed |
| Master node 2 | - | Fixed | Fixed | Fixed | Fixed | - |

- Load case 3: combined vertical and horizontal bending

In the biaxial bending case, all the degrees of freedom of master node 1 are suppressed except rotations about the nodal y- and z- axes ($\theta_y$ and $\theta_z$). For master node 2, rotations about the nodal y- and z-axes and translation in the nodal x-direction are allowed but the other degrees of freedom are suppressed. Consequently, the input for the Multi-Point Constraint can be expressed in the form of the constraint (coupling) equation:

$$U_{xi} = \theta_y * Z_i + \theta_z * Y_i \tag{3.5}$$

A summary of the boundary conditions for the load case of bi-axial bending moment is presented in table 3.5.

*Table 3.5: Applied Boundary Conditions for Biaxial Bending Load Case*

| Location | Translation | | | Rotation | | |
|---|---|---|---|---|---|---|
| | $U_x$ | $U_y$ | $U_z$ | $\theta_x$ | $\theta_y$ | $\theta_z$ |
| Aft end | | | | | | |
| Cross section | Coupling equation | - | - | - | Fixed | Fixed |
| Master node 1 | Fixed | Fixed | Fixed | Fixed | - | - |
| Fore end | | | | | | |
| Cross section | Coupling equation | - | - | - | Fixed | Fixed |
| Master node 2 | - | Fixed | Fixed | Fixed | - | - |

Note: the '-' in table 3.3, table 3.4 and table 3.5 means no constraint applied (free).

The interaction relationship for the case of biaxial bending according to (Paik, et al., 1996) is used in this study. It can be expressed as:

$$\left(\frac{M_v}{M_{vu}}\right)^{1.85} + \left(\frac{M_h}{M_{hu}}\right) = 1 \tag{3.6}$$

The simulation of the biaxial loading condition was done by simultaneously applying rotations about the y- and z- nodal axes of the master nodes. Four different curvature ratios were considered ($\theta_y/\theta_z$ = 5, 2, 1 and 0.3) for both hogging and sagging conditions.

In general, the configurations adopted for vertical bending, horizontal bending and bi-axial bending allow plastic deformations due to changes in the neutral axis positions to be realistically simulated.

## 3.3 Modeling of Initial Imperfections

One of the most important factors influencing ultimate strength is imperfection. Imperfections in the form of initial deflection and welding residual stresses are always present in ship structures due to the welding of the structural components. The welding process often involves uneven rapid heating and cooling which brings about the expansion and contraction of structural members thereby resulting in the deformation of the structural components and the creation of residual stresses.

Initial distortions and welding residual stresses can considerably reduce the load carrying capacity (ultimate strength) of ship structures and hence should be taken into account during the determination of the ultimate strength of ship structures and welded components in general. Consequently, initial imperfections must be properly modeled to ensure accurate determination of the ultimate strength.

### *3.3.1 Initial Deflection Modeling*

Several researches have been carried out to realistically model the initial distortion of welded structures and so many literatures on the subject are available. The likes of (Faulkner, 1975), (Carlsen, 1980), (Grondin, et al., 1999) and many more have made efforts to model the initial deformation of welded structures using different approaches. In addition, class societies have regulations regarding the maximum initial deformation of plates after fabrication.

In order to validate the results of this work using the ISSC2000 benchmark studies, the initial distortion mode shapes have been modeled to be consistent with those of ISSC2000 report in that an “average” level of imperfection is represented with the imperfection magnitudes and shapes. The mode shapes are based on the assumption of elastic buckling. Three mode shapes of welding induced initial deflection are relevant in this case (Figure 3.12):

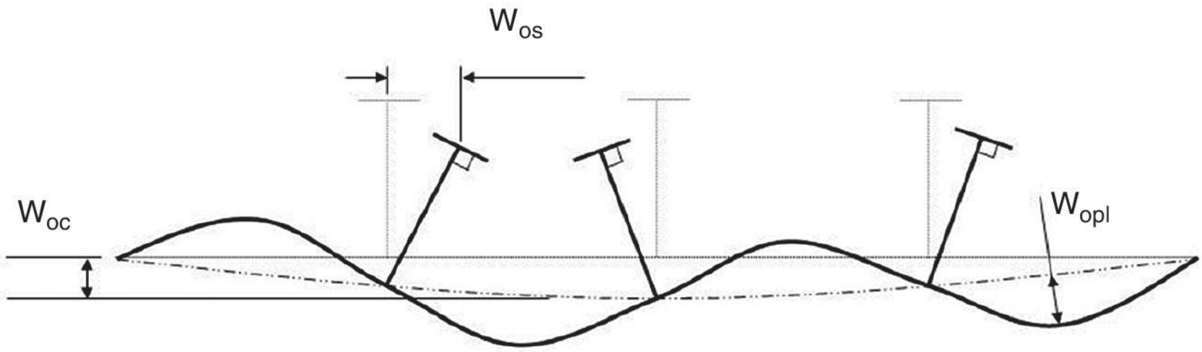


*Figure 3.12: Mode shapes of initial deflection*

(source: (Paik, 2018))

- Plate initial deformation

A relatively conservative approach is adopted in that the plate deflections are modeled to alternate direction. The initial plate deformation, considering the aspect ratio of the model plating, has been chosen to be three half-waves in the longitudinal direction and one in the transverse direction (figure 3.13). The plate initial deformation can be mathematically expressed using a two mode Fourier series given as:

$$W_{Opl} = A_O \, sin\frac{k\pi x}{a} sin\frac{\pi y}{b} + B_O \, sin\frac{\pi x}{a} \qquad (3.7)$$

where:

$A_O$ = amplitude of initial deflection of plate panel

$a$ = length of plate

$b$ = breadth of plate

$k$ = aspect ratio

The amplitude of plate panel initial deflection, $A_O$ can be determined using the formulation:

$$A_O = 0.1\beta^2 t \qquad (3.8)$$

where:

$\beta$ = slenderness ratio

$t$ = thickness of plate

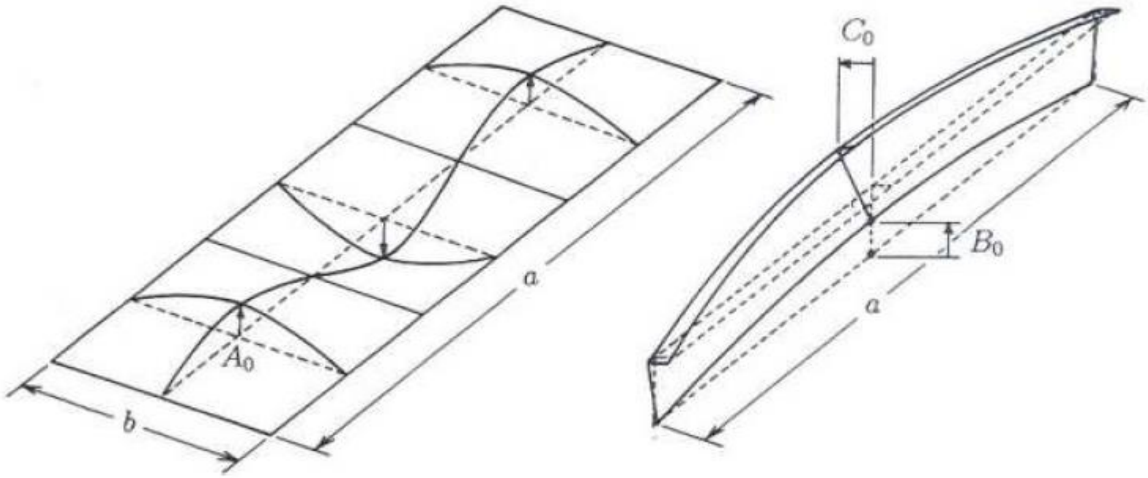


*Figure 3.13: Assumed stiffened plate initial deformation*

(source: (ISSC, 2012))

The slenderness ratio, $\beta$ can be expressed as:

$$\beta = \frac{b}{t}\sqrt{\frac{R_{eH}}{E}} \tag{3.9}$$

where:

$R_{eH}$ = yield strength of plate

From equation (3.8), it can be seen that the amplitude of plate initial deflection depends on slenderness ratio and plate thickness. This is very crucial in the modeling of the initial deformation of the VLCC since it is built with plates of different thicknesses. Varying amplitudes, due to different plate thicknesses, brings about gaps in the model which results in solutions that do not converge. In order to be relatively conservative, average values of the amplitudes are used. A table showing the average values of the amplitudes used in this study is attached in appendix A3.

With these modifications, gaps were observed at the unstiffened transition plates. Therefore, equation (3.7) was modified for the case of unstiffened plates since the distortion of stiffened and unstiffened plates is different (figure 3.14). The sinusoidal wave at the edge is thus brought to zero. Hence, the formulation for unstiffened plates initial deformation can be expressed as:

$$W_{Opl} = A_O \sin\frac{n\pi x}{a} \sin\frac{\pi y}{b} \tag{3.10}$$

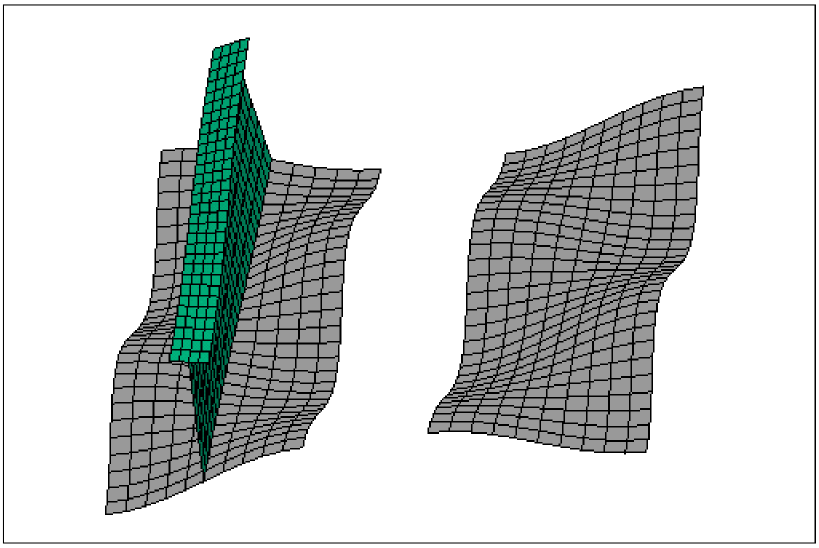

*Figure 3.14: Initial deflection of stiffened and unstiffened plates*

- Stiffener lateral deformation

Stiffener deformation is of two categories (Smith, et al., 1992). The first involves the side-ways deflection of the stiffener from its supposed position. This may occur together with the plate (figure 3.12) or column (figure 3.15). Nonetheless, there is negligible difference between the two configurations. The second category of stiffener deformation involves the distortion of the stiffener web (figure 3.16).

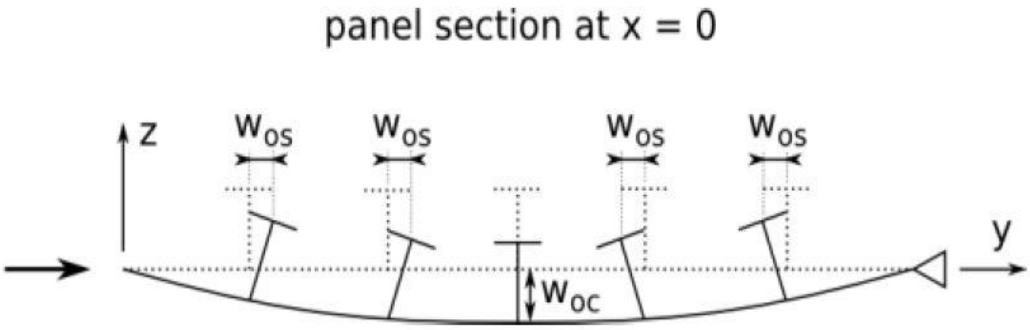


*Figure 3.15: Side deflection of stiffener coupled with column*

(source: (ISSC, 2015))

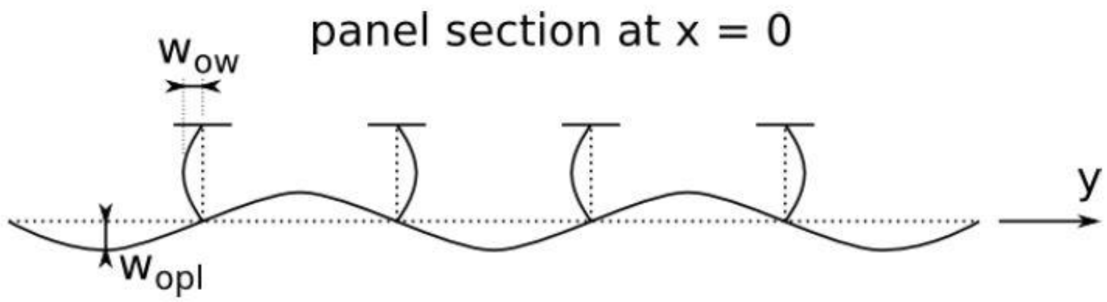


*Figure 3.16: Stiffener web distortion*

(source: (ISSC, 2015))

The side-ways deflection of the stiffener attached with the plating is assumed in this work. This can be mathematically expressed as:

$$W_{Os} = B_O \sin \frac{\pi x}{a} \tag{3.11}$$

where:

$B_O$ = amplitude of initial deflection of stiffener in vertical direction. It can be obtained using the formulation:

$$B_o = 0.0015a \tag{3.12}$$

Furthermore, in order to guarantee smooth transition of the stiffener initial deflection to the transition plates, an exponential function of the stiffener initial deflection is required at the unstiffened plates. This can be expressed as:

$$W_{Os} = e^{y-b/2} B_O \sin \frac{\pi x}{a} \tag{3.13}$$

- Column initial deformation

This is a global mode shape that describes the distortion of the plate and stiffeners as a single unit (ISSC, 2015). The column type initial deformation of the support members is modeled using the formulation:

$$W_{Oc} = C_O \sin \frac{\pi x}{a} \tag{3.14}$$

where:

$C_O$ = amplitude of stiffener initial deflection in horizontal direction. It can be obtained using the formulation:

$$C_O = 0.0015a \tag{3.15}$$

A sample of the initial deformation applied to the double bottom of the model is shown in figure 3.17.

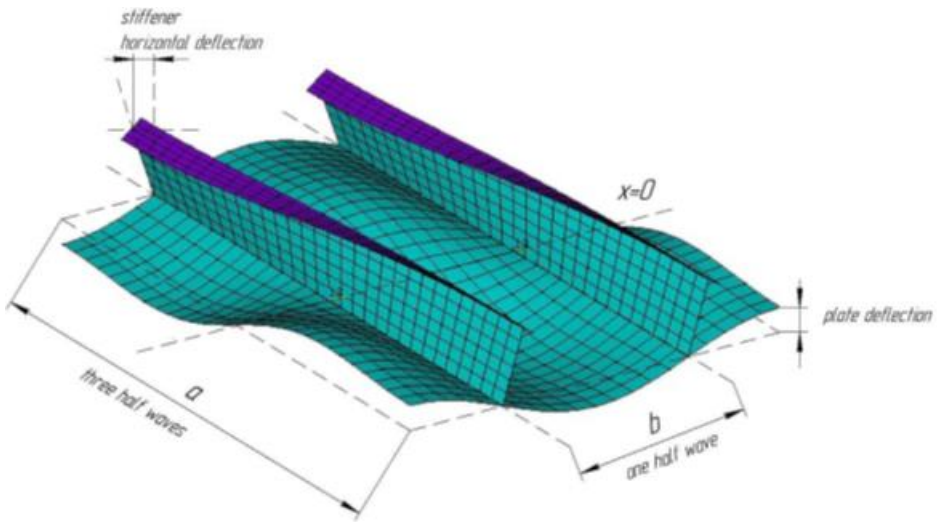


*Figure 3.17: Parametric model showing initial deformation*

### 3.3.2 Welding Residual Stress Modeling

In the modeling of welding residual stress, the model is divided into stiffened panels and the distributions of welding residual stress is idealized as being composed of tensile and compressive stress blocks. Figure 3.18 and figure 3.19 show the idealizations adopted in this study for a portion of the double bottom. The magnitude of the welding residual stress is dependent upon the weld heat input (Fujikubo & Yao, 1999) which can be expressed as:

$$\Delta Q = 78.8 \cdot f^2 \tag{3.16}$$

Where $f$ [mm] denotes the leg length of the fillet weld. According to (Yao & Fujikubo, 2016), $f$ can be taken as 7.0mm.

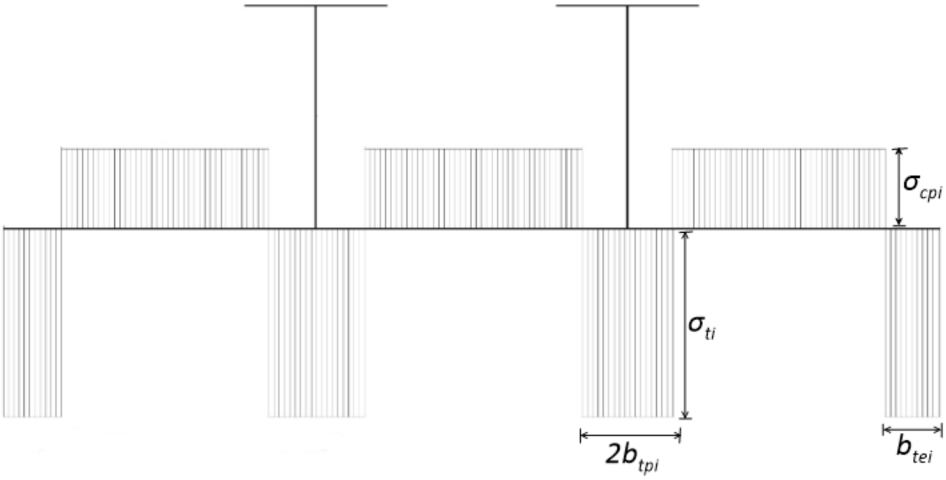


*Figure 3.18: Assumed welding residual stresses for stiffened plates*

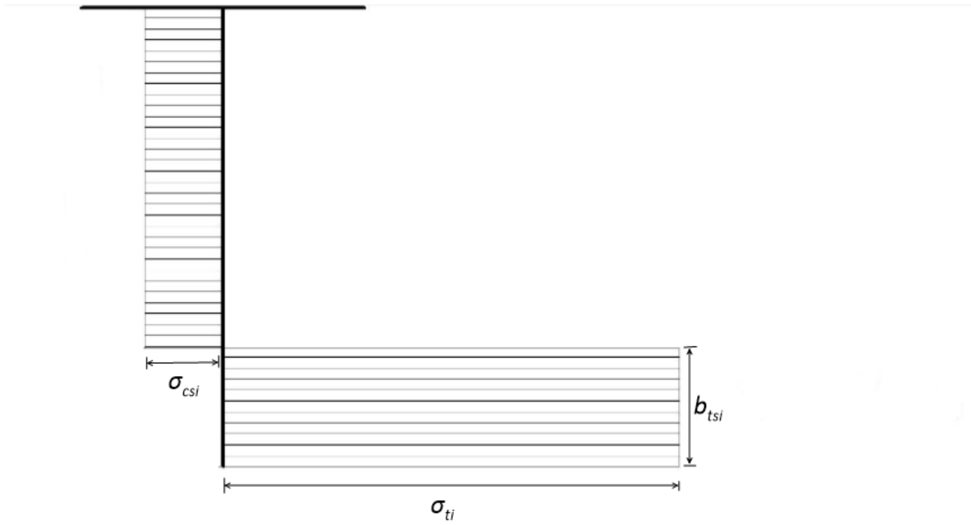


*Figure 3.19: Assumed welding residual stresses for stiffeners*

The breadths of the tensile residual stress area of the plating $b_{tp}$ and stiffener $b_{ts}$ can be expressed as

$$b_{tp} = \frac{t_w}{2} + 0.26\frac{\Delta Q}{(t_w+2t_p)} \tag{3.17}$$

and

$$b_{ts} = \frac{t_w}{t_p} + 0.26\frac{\Delta Q}{(t_w+2t_p)} \tag{3.18}$$

The breadth of the tensile residual stress area at the corners, $b_{te}$ of the panel can be expressed as:

$$b_{te} = \frac{t_p}{2} + 0.13\frac{\Delta Q}{t_p} \tag{3.19}$$

Welding residual stress is self-equilibrating (Yao & Fujikubo, 2016), hence, the tensile residual stresses developed along the weld line and the compressive residual stresses developed in the middle of the plate element are in equilibrium. Therefore, considering self-equilibrating condition for the combination of plates and stiffeners and assuming that the compressive residual stresses of the plate panel and stiffener are the same, the compressive residual stress can therefore be expressed as:

$$\sigma_c = \frac{b_{te1}t_{p1}\sigma_{tp} + b_{te2}t_{p2}\sigma_{tp} + \sum 2b_{ti}t_{pi}\sigma_{tpi} + \sum b_{tsi}t_{wi}\sigma_{tsi}}{\sum B_i t_{pi} - \left(b_{te1}t_{p1} + b_{te2}t_{p2} + \sum 2b_{tpi}t_{pi}\right) + \sum A_{si} - \sum b_{tsi}t_{wi}} \tag{3.20}$$

where:

$A_{si}$ = cross section area of stiffener web

$\sigma_{tp}$ = tensile residual stress

The magnitude of the tensile residual stress, $\sigma_{tp}$ depends on the material (Yao & Fujikubo, 2016). It is usually taken as the yield stress of the material (Paik, 2018). It should be noted that the welding of the stiffener flange is not taken into consideration in this work.

Two different configurations of welding residual stresses are adopted in this thesis:

- wrs: in this configuration, the tensile stresses are modified and applied to the element breadth along the weld lines (Figure 3.20).
- awrs: in this configuration, the tensile stresses are artificially applied to the element breadth along the weld lines without any modifications (Figure 3.21).

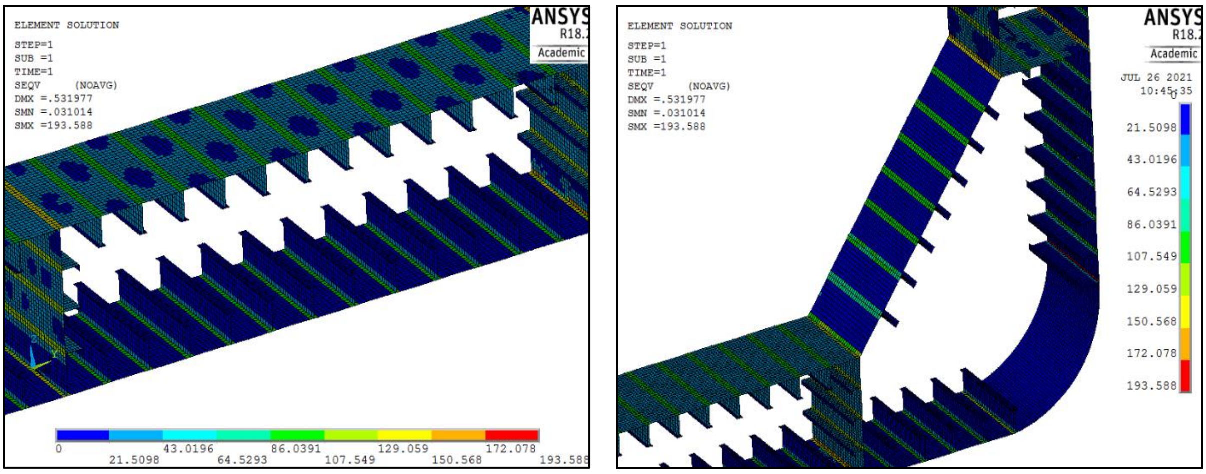


*Figure 3.20: "wrs" configuration: double bottom (left) and double bottom tank (right)*

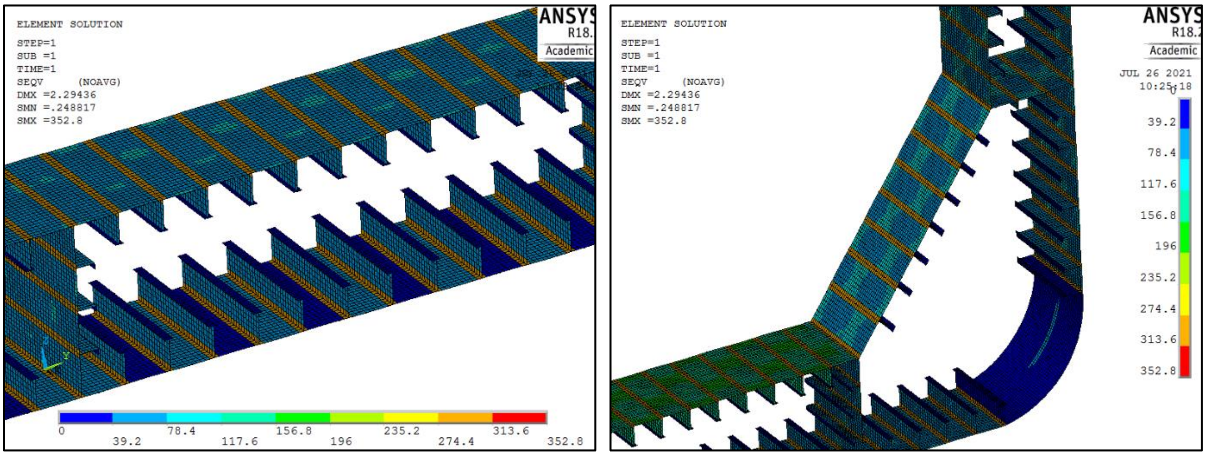


*Figure 3.21: "awrs" configuration: double bottom (left) and double bottom tank (right)*

### 3.4 Modeling of Damage Condition

Symmetric damage due to grounding is considered in this work. The residual strength of the grounded double hull VLCC is evaluated by removing the damaged part of the model cross section. The damaged part is idealized in such a way that the damage starts and ends in the middle of stiffener spacing. This enables consistency with the adopted mesh size. It is however noteworthy that the position of the neutral axis changes in the damage cases. Hence, this must be taken into account in the determination of the residual strength. The location and dimensions of the damages as well as the position of the neutral axis is presented in table 3.6 and the geometry of the damage conditions are shown from figure 3.22 to figure 3.24.

*Table 3.6: Locations and Dimensions of Damages*

| Damage case | Location | Vertical extent (mm) | Horizontal extent (mm) | Neutral axis (mm) |
|---|---|---|---|---|
| Dam_1 | Double bottom | 325 | 3735 | 13252 |
| Dam_2 | Double bottom | 1065 | 8715 | 13749 |
| Dam_3 | Double bottom | 1895 | 16185 | 14649 |
| Dam_4 | Double bottom | 1895 | 20335 | 15129 |
| Dam_5 | Double bottom | 3000 | 20335 | 17431 |

Five damage cases are considered in this work. The damage regions are shaded in red as shown from Figure 3.22 to figure 3.24. A sample of a damaged model (dam_1) built in ANSYS is shown in the appendix.

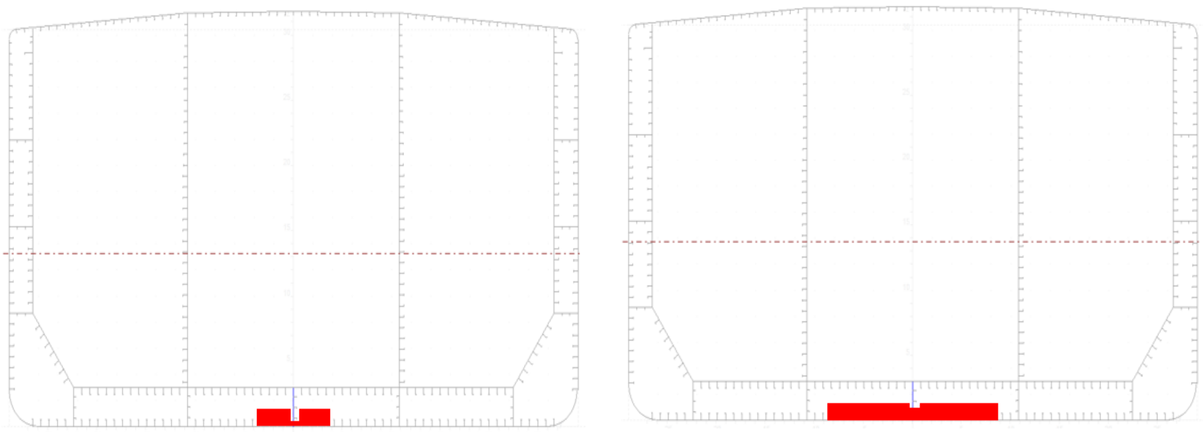

*Figure 3.22: location and dimension of damage: dam_1 (left) and dam_2 (right)*

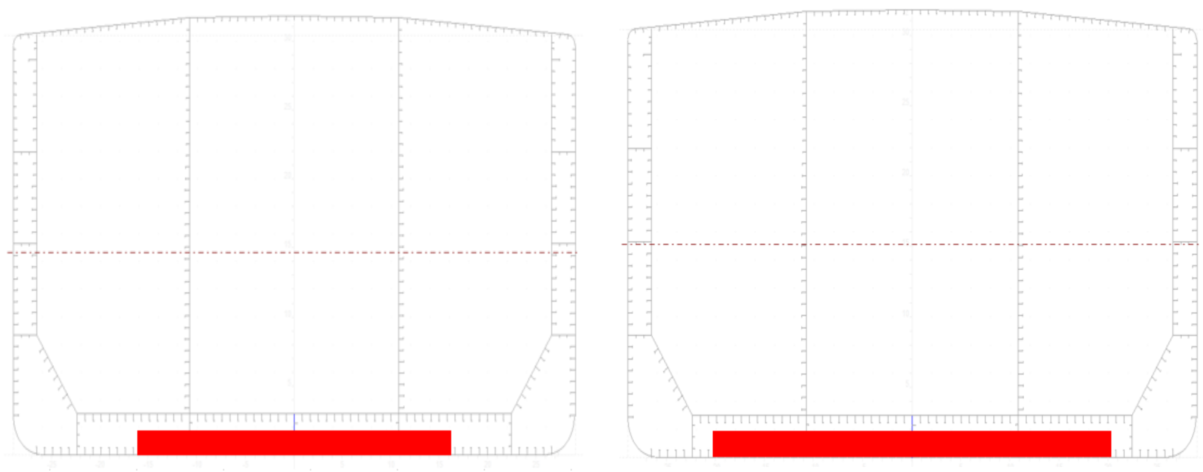

*Figure 3.23: location and dimension of damage: dam_3 (left) and dam_4 (right)*

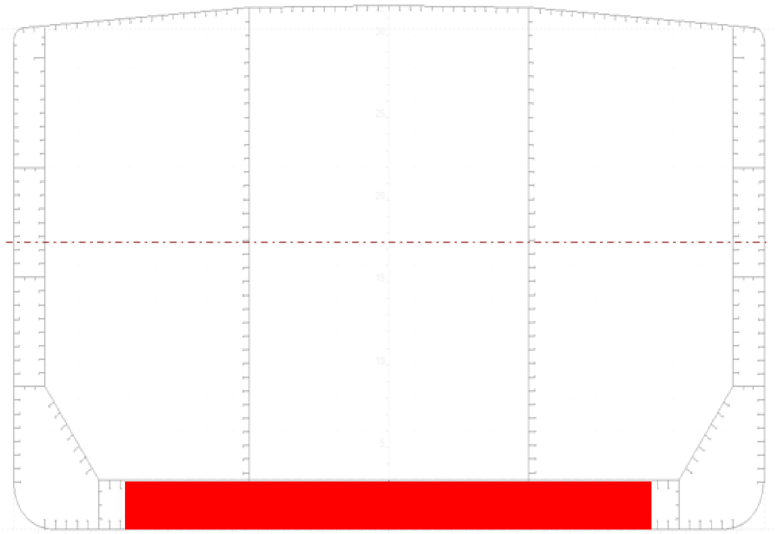

*Figure 3.24: location and dimension of damage for dam_5*

### *3.4.1 Residual Strength Determination*

The procedures for the determination of the ultimate strength of the model in intact condition are adopted for the determination of the residual strength of the different damage cases. The same element type, mesh size and load application routines are used for the damage cases. Constraints and coupling equations are applied only on the intact part of the damaged model. The residual strength of the damaged model is evaluated for the conditions of vertical bending, horizontal bending and bi-axial bending.

# 4. RESULTS AND ANALYSES

The results and analyses of the ultimate and residual strengths of the double hull VLCC for the considered loading conditions are described in this chapter. These results are validated against ISSC2000 and ISSC2012 benchmark studies and other publications. Newton-Raphson and Arc-length iterative schemes are applied in the solution of the nonlinear finite element analyses for the determination of ultimate strength through either displacement-controlled or force-controlled procedure. The displacement-controlled approach involves the application of a predefined rotation about the y-axis (vertical bending moment), z-axis (horizontal bending moment) and y- and z-axes (bi-axial bending) of the master nodes. The force-controlled method involves the application of moment. There is the option of choosing between displacement-controlled analysis using the Newton-Raphson iterative scheme and force-controlled procedure using either the Newton-Raphson or Arc-length control iterative scheme. The influence of the different solution schemes on the results are examined.

The ideal elastic plastic material model is used for the analysis of the results obtained within the context of this work. Nevertheless, the influence of the bilinear elastic plastic material model is also investigated. Special attention is also paid to the effects of welding residual stresses on the ultimate strength as described in section 3.3.2.

Furthermore, the residual strength of the double hull VLCC due to grounding damage is investigated. The influence of the extent of the considered damage cases are also considered.

## 4.1 Load Case 1: Vertical Bending

The boundary conditions and coupling equation specific to the case of vertical bending as described in section 3.2.5 are adopted. Also, load application routine as described in section 3.2.5 is used.

### *4.1.1 Hogging Condition*

The results obtained for the case of vertical bending moment in hogging is presented in figure 4.1. The different solution approaches (displacement-controlled analysis using Newton-Raphson iterative scheme and force-controlled calculation using Newton-Raphson and Arc-length iterative scheme) are shown. As can be seen from the figure, the different solution approaches follow the same curve path delivering approximately the same values for the maximum bending capacity and curvature (table 4.1). However, the force-controlled calculation using the Newton-Raphson iterative scheme terminates the fastest. This is followed by the force-controlled calculation using Arc-length iterative scheme and then displacement-controlled analysis using Newton-Raphson iterative scheme.

On further investigation, it was observed that the results obtained with the force-controlled calculation using the Newton-Raphson iterative scheme do not exceed the ultimate strength. This solution approach terminates immediately the maximum bending capacity is attained. Consequently, the behaviour of the curve/double hull VLCC beyond the ultimate strength cannot be analyzed using this solution approach. Strength reduction beyond the ultimate strength can be studied using either the displacement-controlled analysis (with Newton-Raphson iterative scheme) or force-controlled calculation (with Arc-length iterative scheme). Nevertheless, the displacement-controlled analysis using the Newton-Raphson iterative scheme gives the best convergence and is thus used for further analysis in this study.

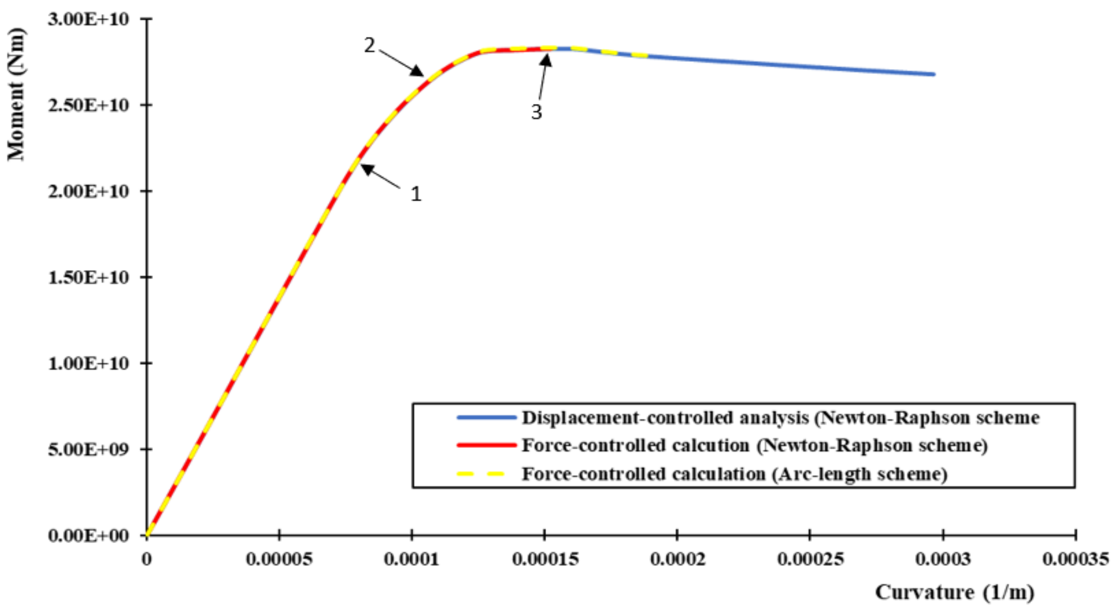


*Figure 4.1: moment-curvature relationship for vertical bending in hogging condition*

From figure 4.1, some important structural behaviours are noteworthy as the moment-curvature curve changes from the linear to nonlinear region under hogging condition. At point 1, the elements at the central part of the deck undergoes plastic deformation by yielding in tension. This then spreads to the side shells and the longitudinal bulkheads close to the deck. It is also observed that some localized plate yielding in compression occurs in the double bottom at this point (figure 4.2). This is because the bending strain at the deck is higher than the bending strain at the double bottom and also due to the fact that the neutral axis of the double hull VLCC is located below mid-height of the cross section. As can be seen in figure 4.1, there is no reduction in strength of the members after initial collapse by yielding has occurred in the deck. Consequently, the moment-curvature curve still increases though the deck has yielded. Nonetheless, the relative stiffness reduces as the yielded region spreads through the side shells and the longitudinal bulkheads.

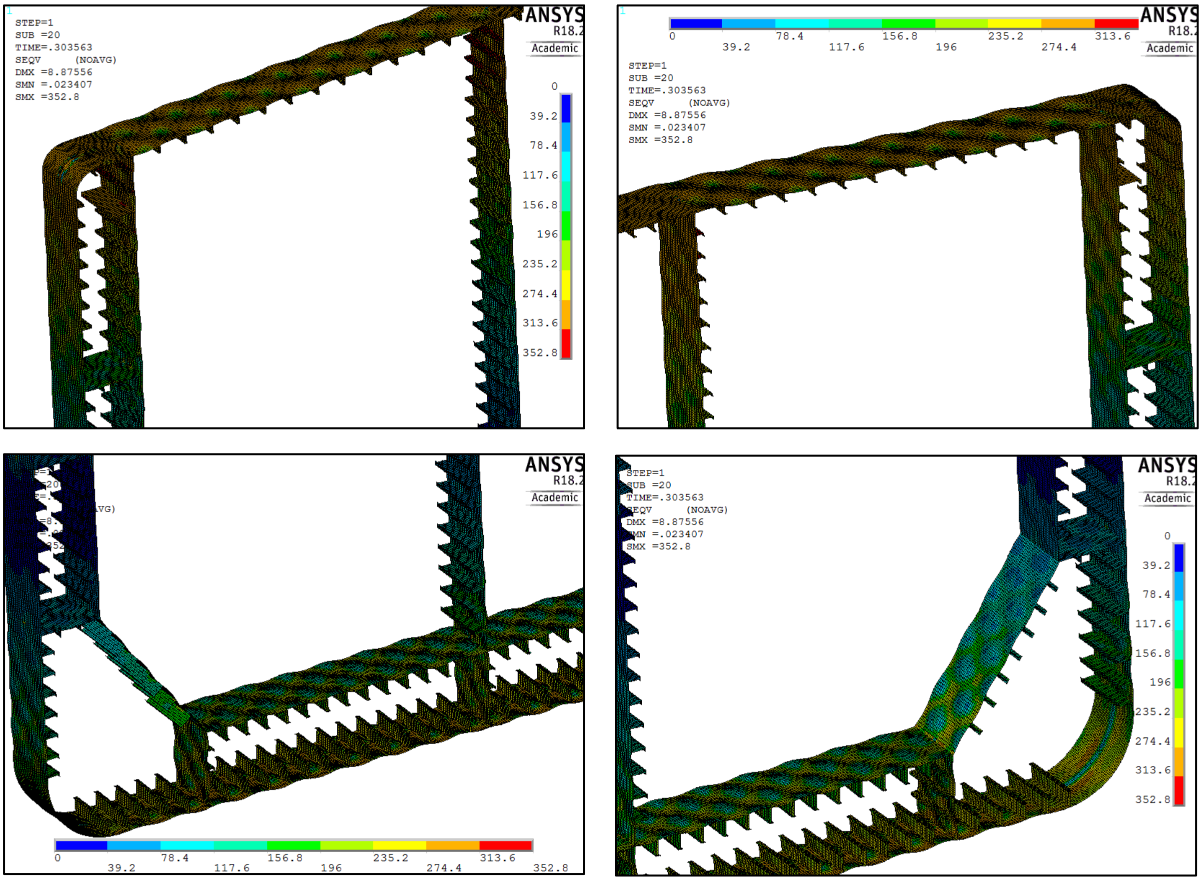


*Figure 4.2: von Mises stress distribution for VBM under hogging (point 1)*

Further up the curve at point 2, the deck yields almost completely. The side shells and longitudinal bulkheads close to the deck completely deform plastically. The stiffeners of the longitudinal bulkheads and those of the inner side shells close to the deck region which happen to have higher material yield strength also yields completely. Buckling of the double bottom becomes more visible as shown in figure 4.3. Buckling collapse also extend to part of the double bottom tank at this point. It can also be observed from figure 4.1 that there is no strength reduction at this point.

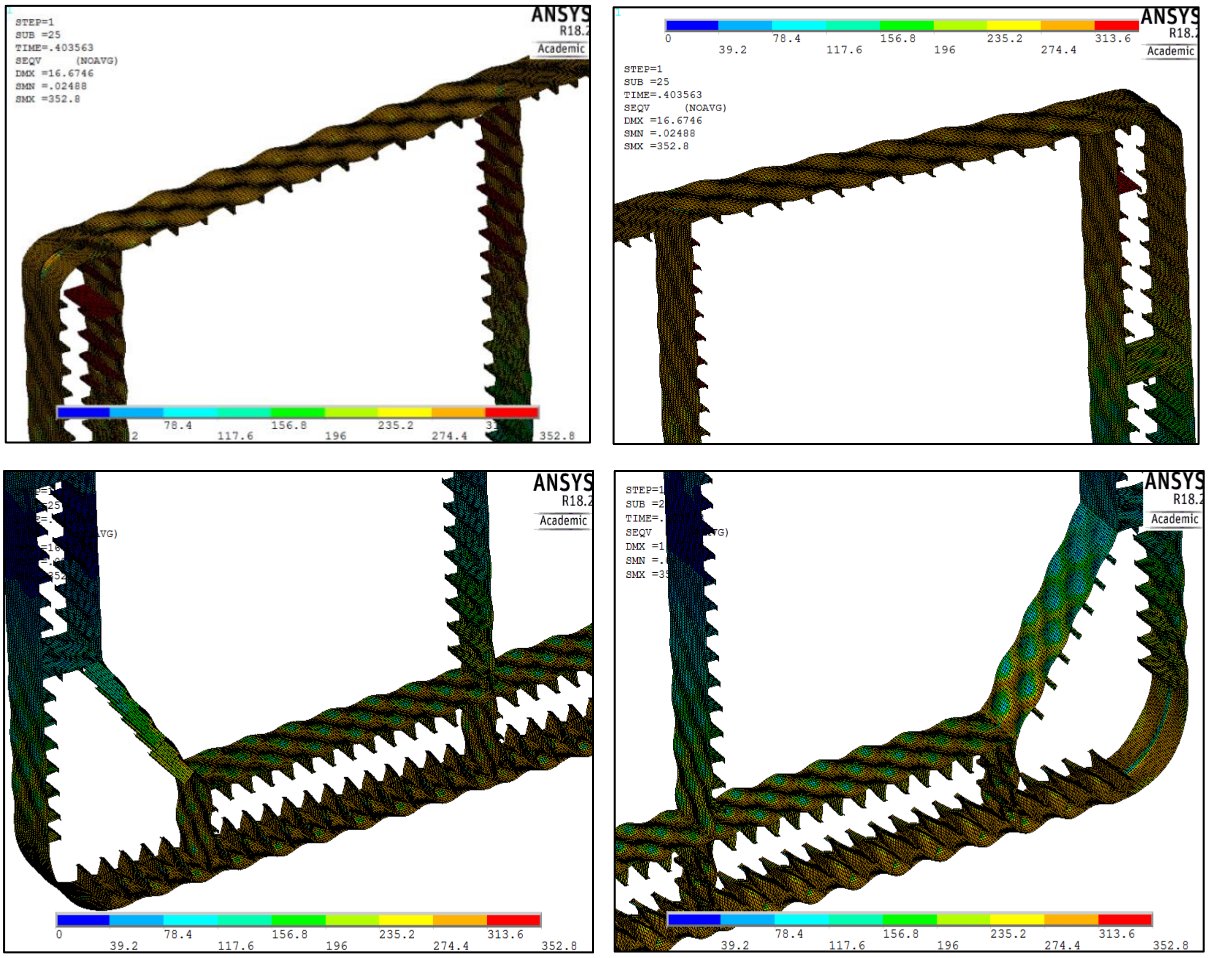


*Figure 4.3: von Mises stress distribution for VBM under hogging (point 2)*

Finally, as the applied curvature at the master nodes is further increased to point 3, the ultimate vertical bending capacity in hogging is attained and the double bottom structure collapses (figure 4.4). Also, the deck region becomes fully yielded at this point. Beyond this point, the strength of the structure begins to decrease (see figure 4.1).

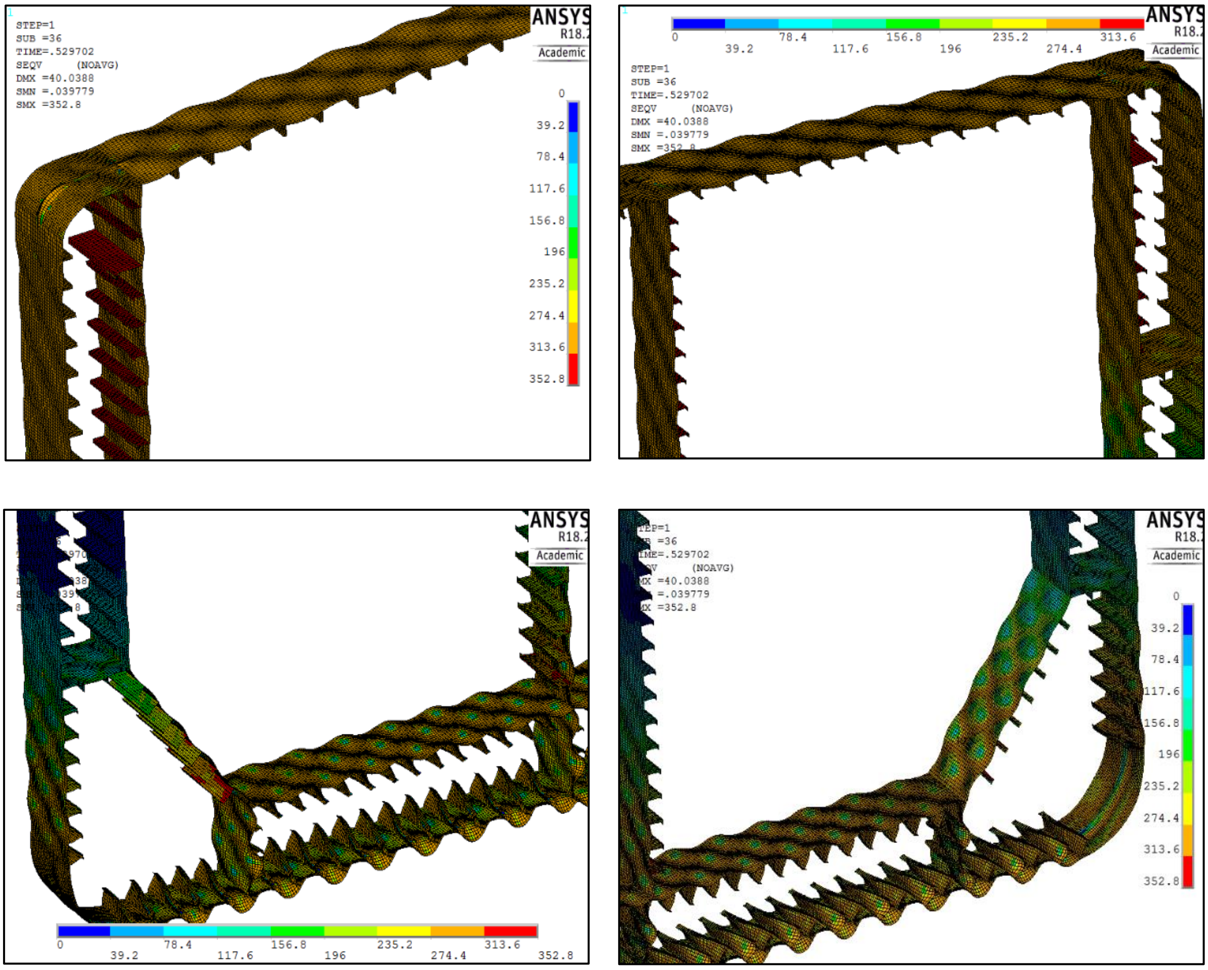


*Figure 4.4: von Mises stress distribution for VBM under hogging (point 3)*

The ultimate capacities for pure hogging moment found by the present investigation are listed in table 4.1.

*Table 4.1: Results of Ultimate Strength Analysis in Hogging Using Different Solution Approaches*

| Load Application Technique | Solver | Ultimate Strength (GNm) | Curvature (1/m) |
|---|---|---|---|
| Displacement control | Newton-Raphson | 28.27 | 0.00015 |
| Force control | Newton-Raphson | 28.25 | 0.00015 |
| Force control | Arc-length | 28.29 | 0.00016 |

As can be seen in the table above, negligible differences exist among the three approaches. Thus, the displacement-controlled analysis using the Newton-Raphson iterative scheme is adopted for further analyses in this study.

**Note**: a scaling factor of 10 is used in displaying the von Mises stress distributions in this study.

### *4.1.2 Sagging condition*

In the case of sagging, the moment curvature curve did not converge properly. Some measures were then taken to improve the convergence of the curve. First, the number of sub-steps were increased and the convergence of the curve greatly improved. However, this measure involves longer computation time. Furthermore, the convergence of the curve was analyzed using bilinear elastic plastic material model. It was observed that this material model convergences in shorter sub-steps.

The results obtained for the case of vertical bending in sagging is presented in figure 4.5. The ultimate strength of the double hull VLCC for vertical bending load case in sagging condition was found to be 26 GNm.

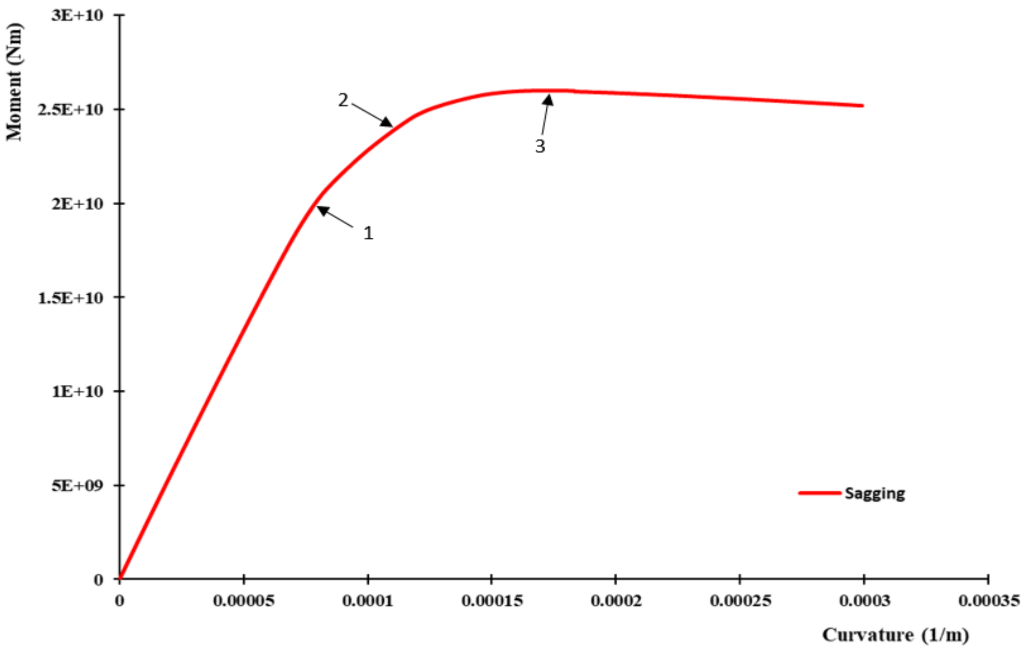


*Figure 4.5: Moment-curvature relationship for vertical bending in sagging condition*

From figure 4.5, it can be seen that the behaviour of the curve changes along the curve path from linear to nonlinear. These changes are as a result of structural failure/collapse as the applied load is continually increased. At the point where the linear elastic behaviour ends (point

1 of figure 4.5), the applied load is 19.33 GNm. At this point, the plates of the central deck region start to buckle in compression. This then extends to the longitudinal bulkheads and the side shells close to the deck. It is also observed that at this point, there is the initiation of some localized yielding in the double bottom of the structure (figure 4.6).

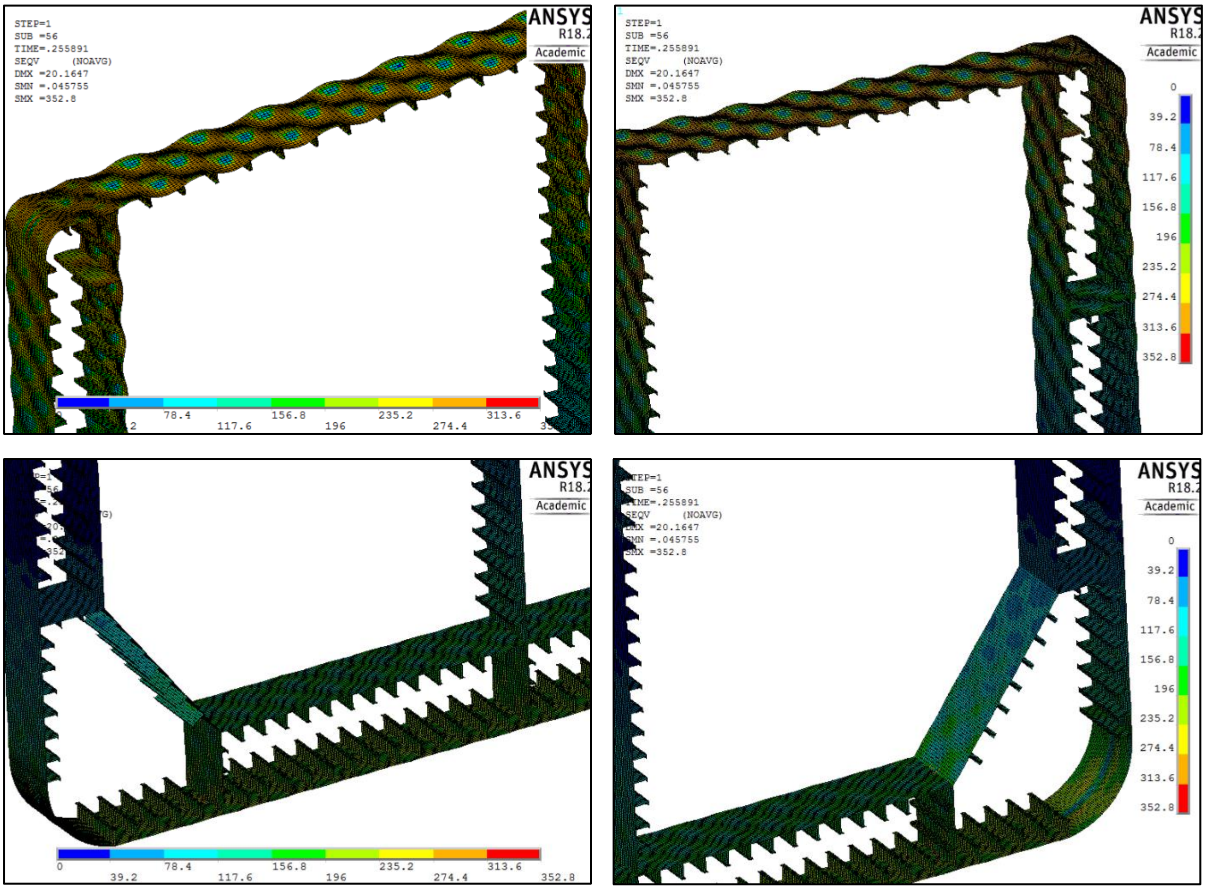


*Figure 4.6: Von Mises stress distribution for VBM under sagging condition (point 1)*

Further up the curve, at the point where the applied load is gradually increased to 23.88 GNm (point 2 of figure 4.5), buckling collapse of the central part of the deck region takes place. This extends to the longitudinal bulkheads and side shells close to the deck of the structure. Furthermore, the stiffeners of the double bottom and some of the stiffeners in the double bottom tank become completely yielded in tension at this point. Additionally, some localized plate yielding begins to propagate in the double bottom and at the intersection point between the inner bottom and the longitudinal bulkheads (figure 4.7).

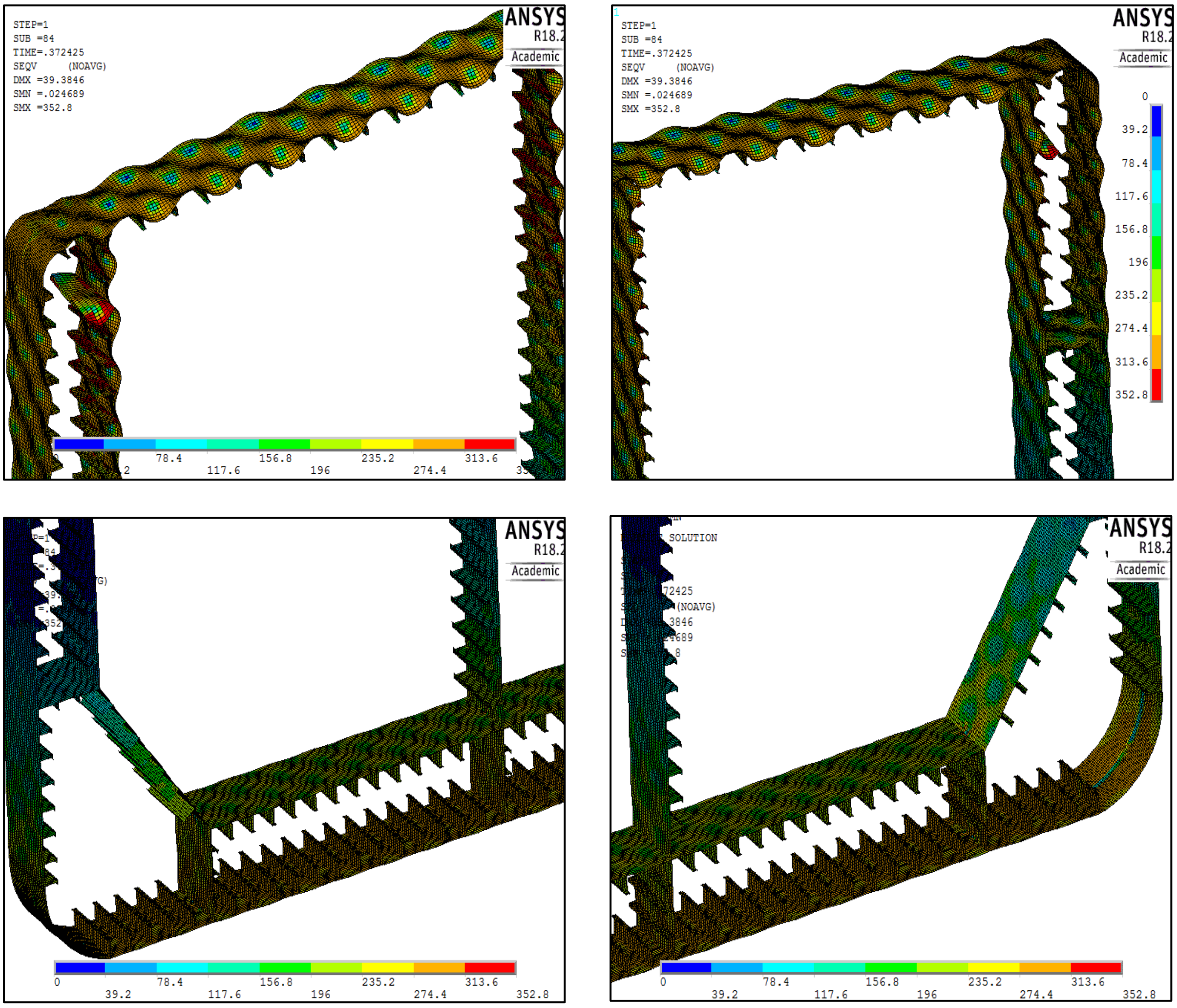


*Figure 4.7: Von Mises stress distribution for VBM under sagging condition (point 2)*

Finally, at the point where the applied load is 26.00 GNm (point 3 of figure 4.5), the ultimate bending capacity of the structure under sagging condition is attained. At this point, the deck region buckles completely in compression and this extends to the longitudinal bulkheads and side shells. Also, the double bottom of the structure yields completely in tension at this point. Furthermore, the stiffeners and plate field of the longitudinal bulkheads close to the double bottom also yields in tension at this point. The yielding collapse also extends to some parts of the double bottom tank as can be seen in figure 4.8.

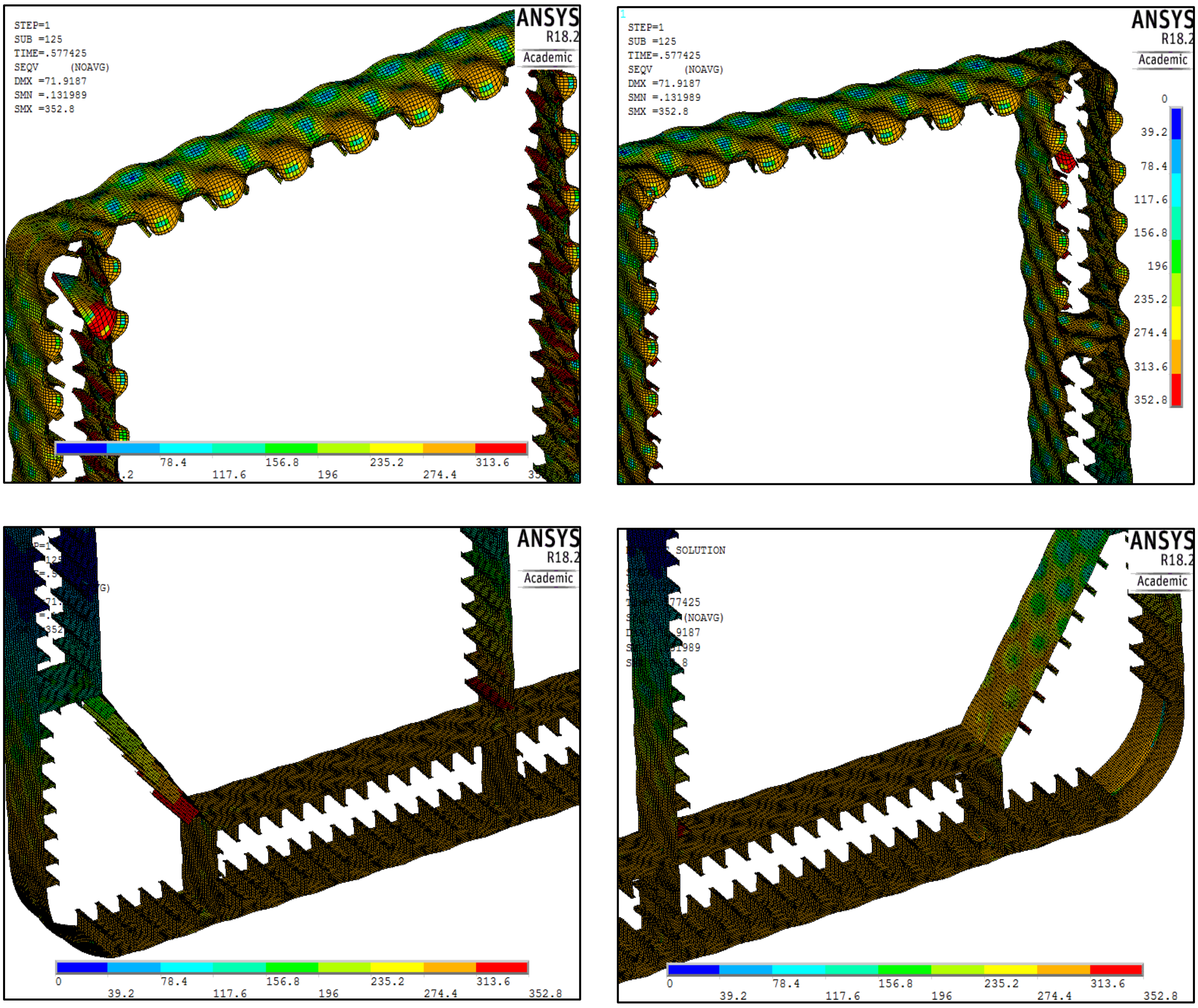


*Figure 4.8: Von Mises stress distribution for VBM under sagging condition (point 3)*

### *4.1.3 Influence of Material Model*

The material model implemented influences the value of the ultimate strength obtained. Figure 4.9 shows the moment-curvature curves in hogging and sagging conditions for the different material models considered in this work. Similar behaviour is observed in the linear elastic region for the different curves, however, as the applied load increases beyond this region, differences in material behaviour can be observed as a result of the different stiffness values of the materials. In the case of the bilinear elastic material model, it can be seen that the tangent modulus is directly proportional to the load-carrying capacity of the structure. Thus, as the tangent modulus increases, the load-carrying capacity of the structure also increases as shown in figure 4.9.

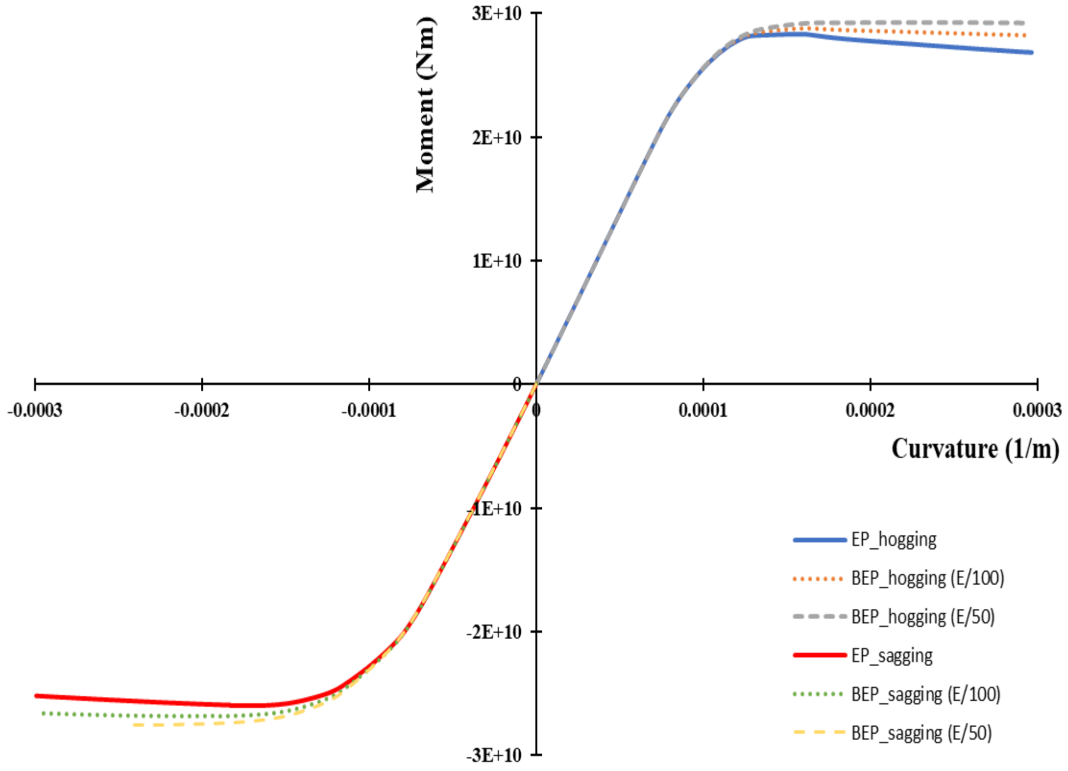


*Figure 4.9: moment-curvature curves showing the influence of material model on ultimate strength*

It can also be seen from the figure that the bilinear elastic plastic material models give a higher value of the ultimate strength when compared with the ideal elastic-plastic material model. It is also noteworthy that the strain hardening parameter influences the obtained result in the case of bilinear elastic plastic material. The higher the strain hardening parameter (a function of the stiffness of the material), the higher the obtained result. The ultimate strength for the different material models is summarized in table 4.2.

*Table 4.2: Results of The Influence of Material Models Used*

| Material Model | Ultimate Strength (GNm) | |
|---|---|---|
| | Hogging Condition | Sagging Condition |
| Ideal Elastic Plastic | 28.27 | 26.00 |
| Bilinear Elastic Plastic, $\left(\frac{E}{100}\right)$ | 28.76 | 26.83 |
| Bilinear Elastic Plastic, $\left(\frac{E}{50}\right)$ | 29.25 | 27.59 |

### *4.1.4 Influence of Welding Residual Stress*

The effects of welding residual stresses on the ultimate strength are shown in figure 4.10. The two welding residual stress configurations described in section 3.3.2 were adopted. In the case of 'wrs', there is negligible influence/impact of welding residual stresses on the ultimate strength. However, the influence of welding residual stress is more pronounced in the case of 'awrs' where the breadth of the mesh size is taken as the breadth of the tensile residual stress area.

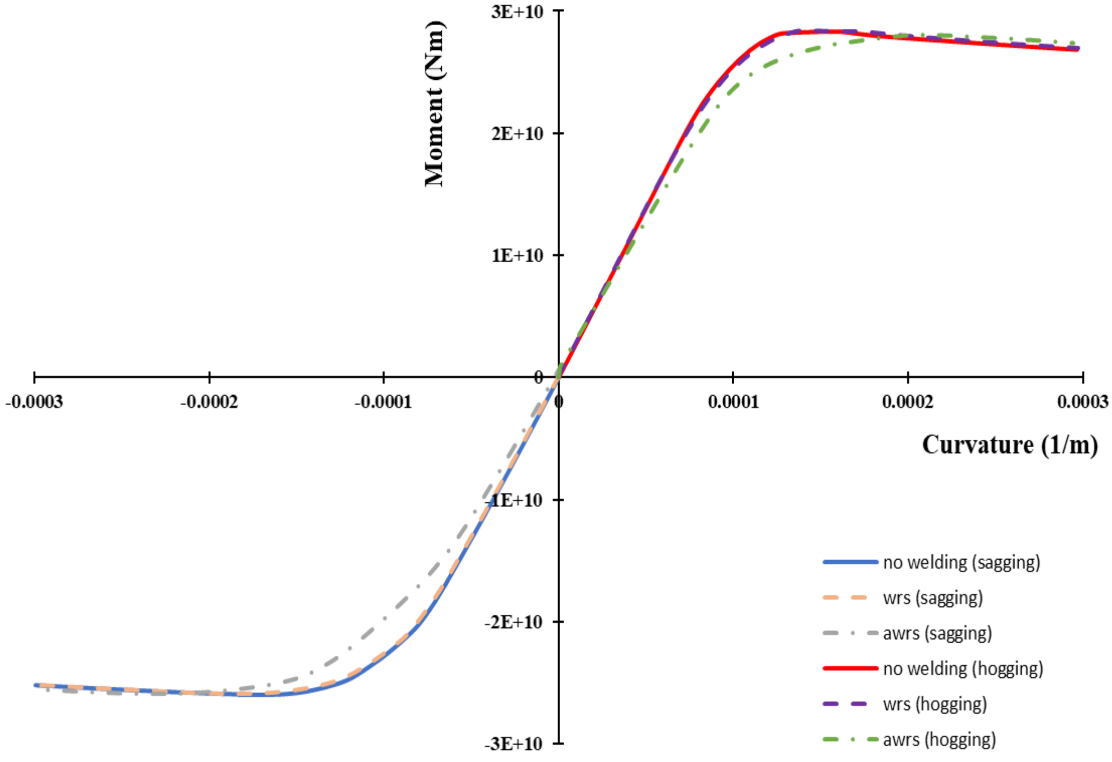


*Figure 4.10: Moment-curvature curves showing effects of welding residual stresses on ultimate strength*

From figure 4.10, it can be seen that the curve path showing the influence of the welding residual stress configuration 'awrs' deviates from the path of the other curves. This is as a result of the assumption made in the modeling of this welding residual stress configuration. Hence, the 'awrs' configuration undergoes largest curvature to attain approximately the same stress values as those without welding residual stress and the 'wrs' configuration. Nevertheless, there are negligible differences in the ultimate bending capacities for the three cases. The results of the ultimate vertical bending capacity and their related curvature for the three different cases are shown in table 4.3. From the results, it can therefore be said that welding residual stresses have negligible influence on the ultimate strength of ships.

*Table 4.3: Results of The Influence of Welding Residual Stresses*

| Welding Residual Stress Model | Hogging | | Sagging | |
|---|---|---|---|---|
| | Ultimate Strength | Curvature | Ultimate Strength | Curvature |
| No Weld | 28.27 | 0.00015 | 26.00 | 0.00017 |
| Wrs Model | 28.36 | 0.00014 | 25.95 | 0.00019 |
| Awrs Model | 28.01 | 0.00021 | 25.90 | 0.00023 |

### *4.1.5 Result Validation*

The results of this investigation are validated against the ISSC2000 and ISSC2012 reports. The results are presented in table 4.4.

*Table 4.4: Comparison of Longitudinal Ultimate Strength Obtained by Different Researchers*

| Source | Contributor | Methodology | Ultimate Strength (GNm) | |
|---|---|---|---|---|
| | | | Hogging | Sagging |
| ISSC 2000 Report | Chen | ISUM | 27.40 | 24.33 |
| | Cho | Smith method | 28.66 | 20.80 |
| | Yao | Smith method | 28.88 | 20.42 |
| | Rigo (1) | Smith method | 28.31 | 19.57 |
| | Rigo (2) | Modified P-M | 25.61 | 24.07 |
| | Masaoka | ISUM | 30.59 | 26.59 |
| ISSC 2012 Report | Paik | NLFEM | 27.34 | 22.50 |
| | | ISUM | 25.59 | 21.97 |
| | | Modified P-M | 25.67 | 22.39 |
| | | Smith | 28.42 | 22.13 |
| | Wang | NLFEM | 31.00 | 25.00 |
| | | Smith | 29.85 | 25.01 |
| | UoG | RINA rules | 28.20 | 21.70 |
| Current Investigation | | NLFEM | 28.27 | 26.00 |

As can be seen from the table, there are slight differences in the results obtained by the different researchers and the current investigation. These slight differences could be attributed to the different idealizations and assumptions made by the different researchers. For instance, there are slight differences in the position of the neutral axis adopted by the different contributors in ISSC2000 report (see (ISSC, 2000)). This could lead to slight differences in the attained ultimate strength results. Nevertheless, it can be seen that the ultimate strength value obtained in this study is in good correlation with the results obtained by the different contributors.

## 4.2 Load Case 2: Horizontal Bending

The boundary conditions and coupling equation specific to the case of horizontal bending as described in section 3.2.5 are adopted. Also, load application routine as described in the same section is used.

### *4.2.1 Hogging and Sagging Conditions*

The results for the horizontal bending load case in hogging (positive moment) and sagging (negative moment) conditions are shown in figure 4.11. Due to symmetry with respect to the centre plane, the results obtained for both hogging and sagging conditions are similar. The results for the maximum bending capacity and corresponding curvature values for both hogging and sagging conditions are shown table 4.5.

*Table 4.5: Ultimate strength obtained for horizontal bending load case*

| Condition | Ultimate Strength (GNm) | Curvature (1/m) |
|---|---|---|
| Hogging | 44.38 | 0.00014 |
| Sagging | 44.38 | 0.00014 |

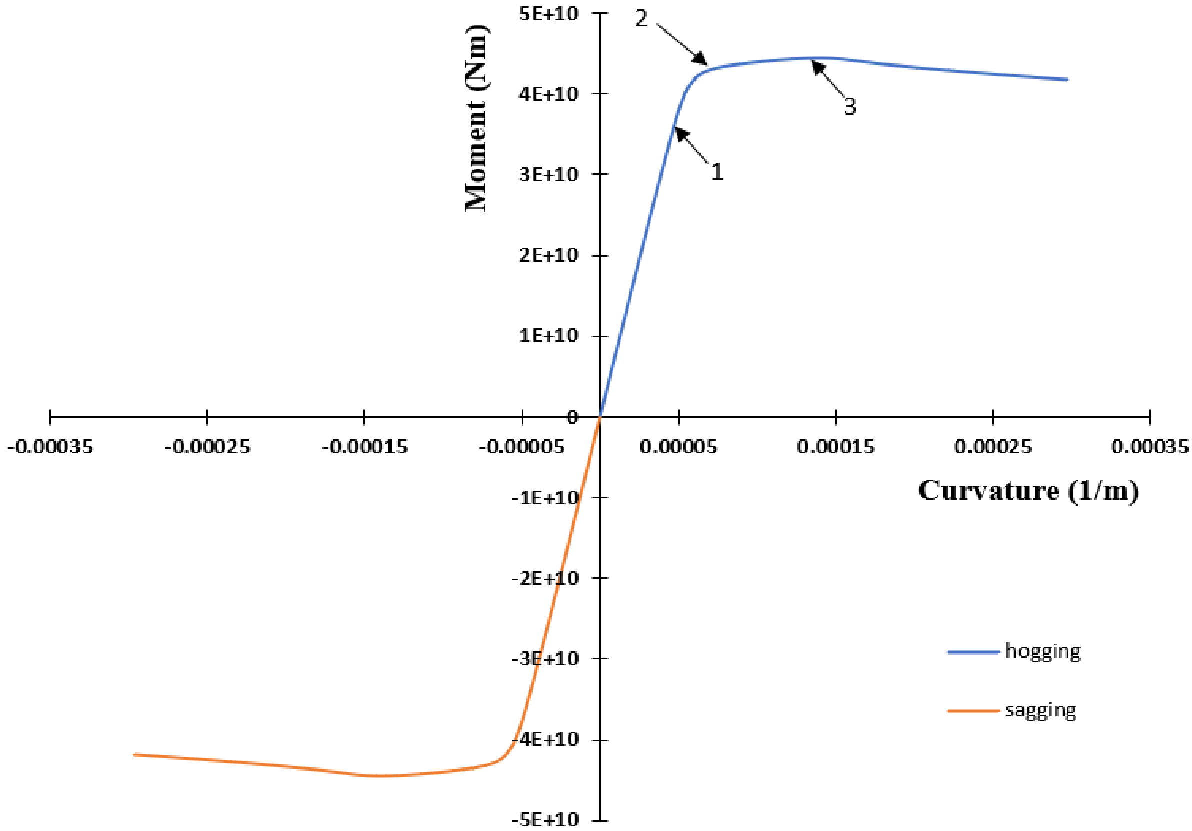


*Figure 4.11: Moment-curvature relationship for horizontal bending in hogging and sagging conditions*

From figure 4.11, the behaviour of the double hull VLCC at some critical points is worth considering. At point 1, the side shell at the starboard side begins to yield in tension extending to the deck and double bottom tank (figure 4.12). Also, initial collapse of the side shell in compression commences at the port side simultaneously, spreading through the deck and double bottom tank.

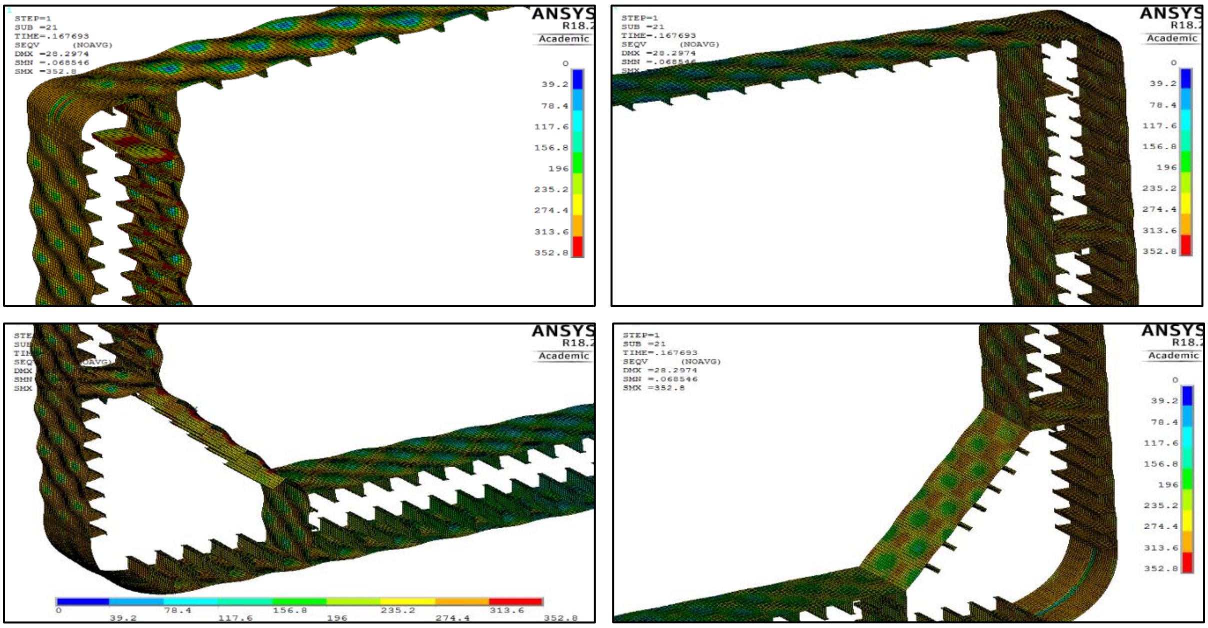


*Figure 4.12: von Mises stress distribution for horizontal bending under hogging condition (point 1)*

On further increase of the applied curvature to point 2 (see figure 4.11), the side shell and double bottom tank at the starboard side yields completely in tension. The plastic deformation then extends to the deck and double bottom of the structure (figure 4.13). At the same time, the side shell and double bottom tank at the port side continues to buckle in compression spreading to the deck and double bottom.

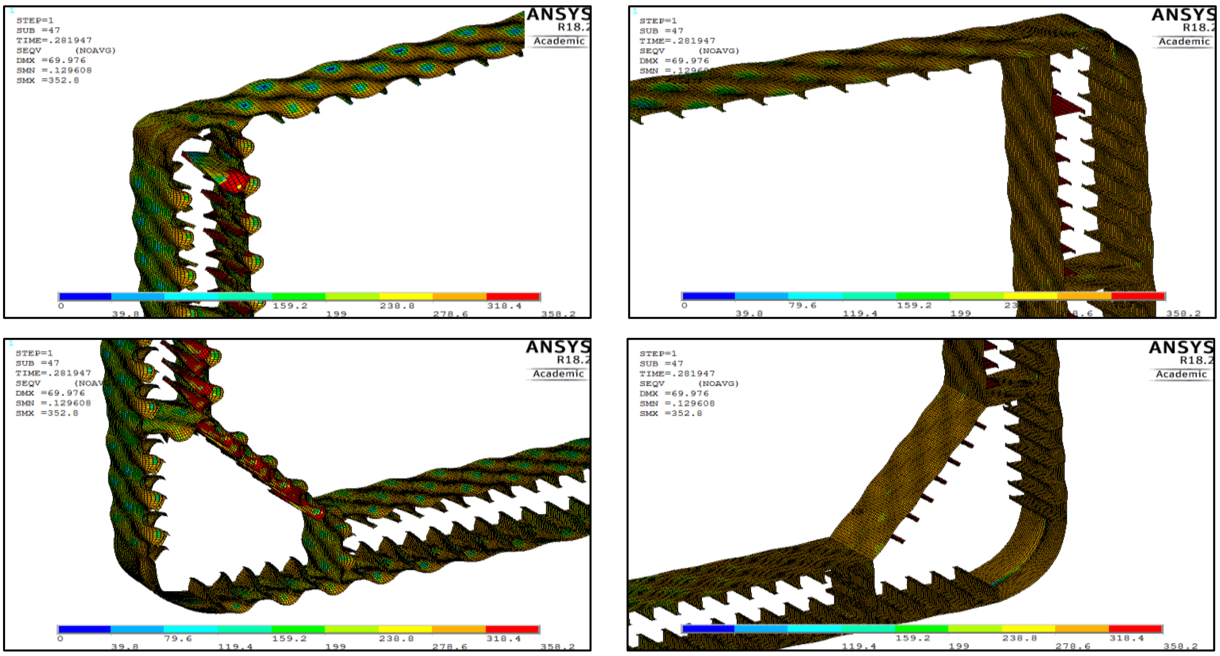


*Figure 4.13: von Mises stress distribution for horizontal bending under hogging condition (point 2)*

Finally, the ultimate capacity of the double hull VLCC is attained at point 3. At this point, the side shell, deck and double bottom tank at the right side of the VLCC is fully yielded in tension (see Figure 4.14). Simultaneously, the left side of the deck, side shell and double bottom tank collapses due to buckling in compression.

It can be observed that tensile yielding and compressive instability (buckling) occur simultaneously in the case of horizontal bending. This is as a result of the magnitude of the bending strain in the side shells being equal since the neutral axis lies at the centre line of the cross section. Furthermore, due to symmetry with respect to the centre plane, only the collapse behaviour under hogging (positive moment) condition is illustrated here since that for the sagging (negative moment) condition will just be a mirror reflection of the hogging case.

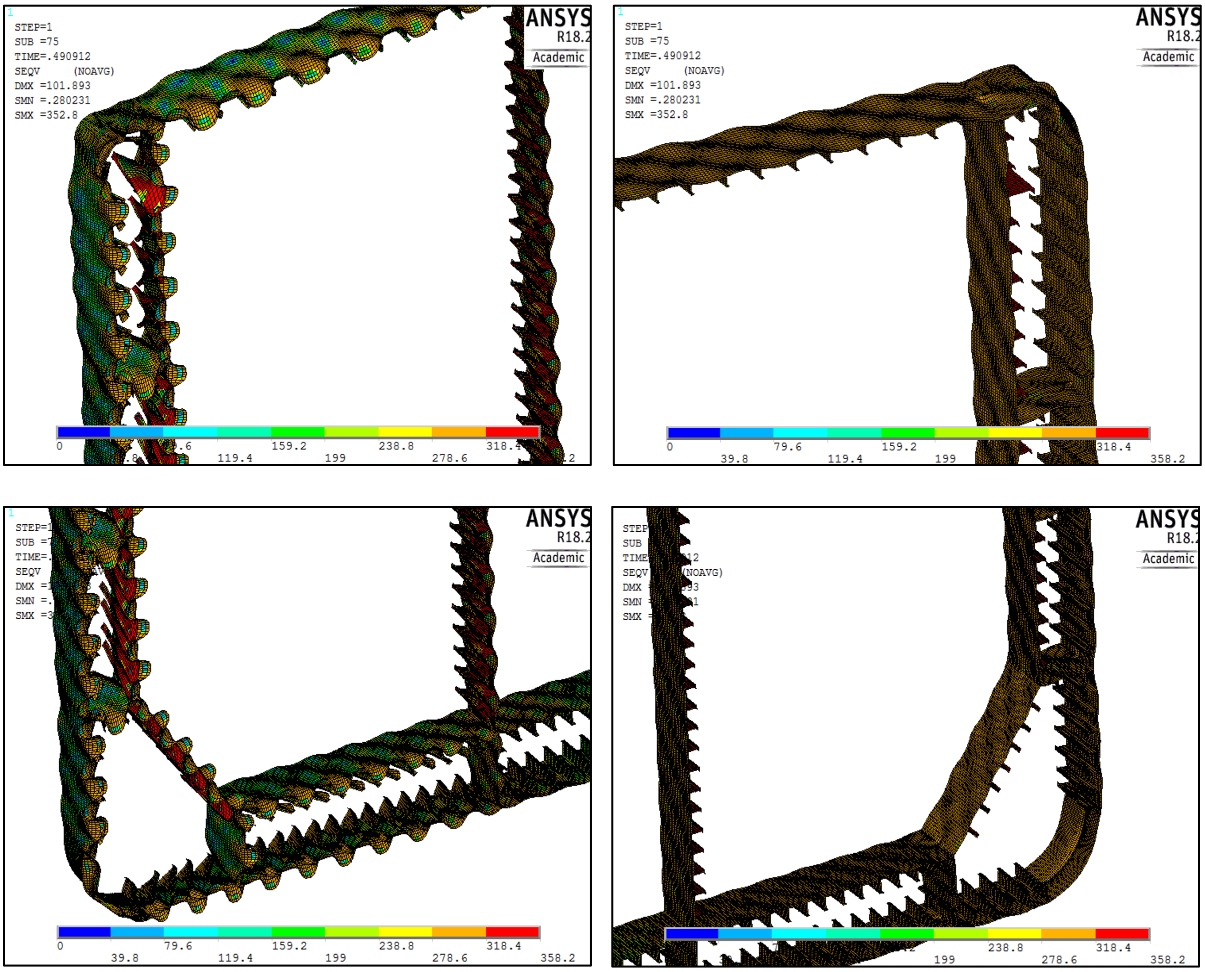

*Figure 4.14: von Mises stress distribution for horizontal bending under hogging condition (point 3)*

### *4.2.2 Influence of Material Model*

The material model implemented influences the value of the ultimate strength. Figure 4.15 shows the curves for the different material models considered in the case of horizontal bending. Similar behaviour is observed in the elastic region for the different curves, however, as the applied load increases, differences in material behaviour can be observed as a result of the different stiffness values of the different material models.

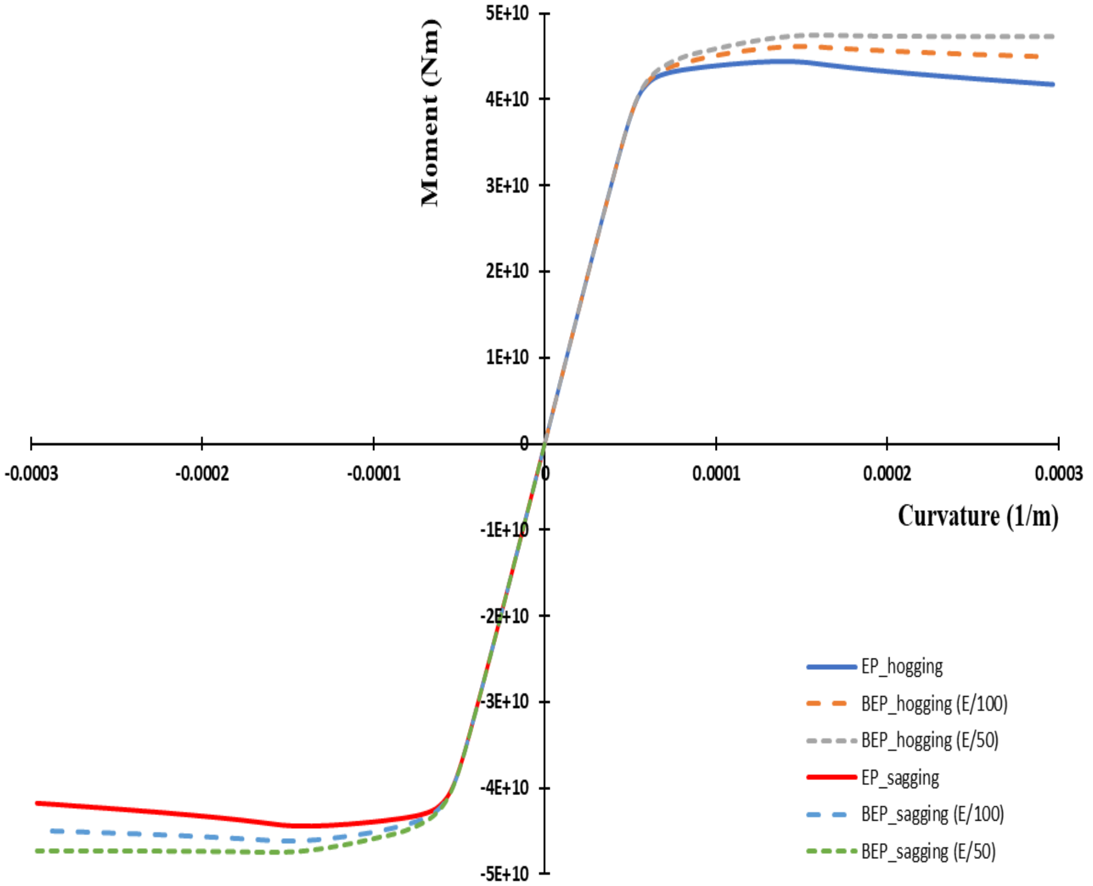


*Figure 4.15: moment-curvature curves showing the influence of material model on ultimate strength for horizontal bending load case*

It can be seen from the figure that the bilinear elastic plastic material models give a higher value of the ultimate strength when compared with the ideal elastic-plastic material model. It is also noteworthy that the strain hardening parameter influences the obtained result in the case of bilinear elastic plastic material. The higher the strain hardening parameter (a function of the stiffness of the material), the higher the obtained result. The ultimate strength for the different material models is summarized in table 4.6.

*Table 4.6: Results of the influence of material model on ultimate strength for horizontal bending load case*

| Material Model | Ultimate Strength (GNm) | |
|---|---|---|
| | Hogging Condition | Sagging Condition |
| Ideal Elastic Plastic | 44.38 | 44.38 |
| Bilinear Elastic Plastic, $\left(\frac{E}{100}\right)$ | 46.12 | 46.11 |
| Bilinear Elastic Plastic, $\left(\frac{E}{50}\right)$ | 47.39 | 47.40 |

### *4.2.3 Influence of Welding Residual Stress*

The effects of welding residual stresses on the ultimate strength are shown in figure 4.16. For the 'wrs' configuration, there is negligible influence of welding residual stresses. However, the influence of welding residual stress is more pronounced in 'awrs' configuration where the breadth of the element size is taken as the breadth of the tensile residual stress area.

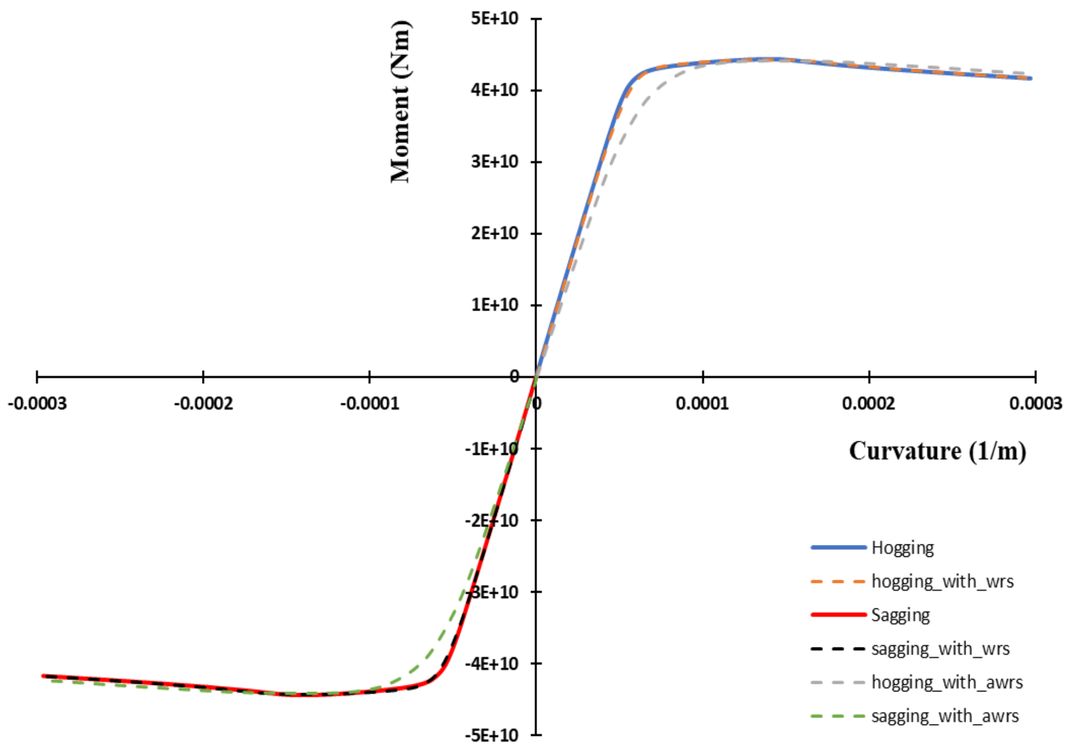


*Figure 4.16: moment-curvature curves showing the effects of welding residual stresses on ultimate strength for horizontal bending load case*

The results of the ultimate horizontal bending capacity and their related curvature are shown in table 4.7. From the table, it can be seen that there are negligible differences in the ultimate horizontal bending capacity for the three cases.

*Table 4.7: Results of The Influence of Welding Residual Stresses on Ultimate Strength for Horizontal Bending Load Case*

| Welding Residual Stress Model | Hogging | | Sagging | |
|---|---|---|---|---|
| | Ultimate Strength (GNm) | Curvature (1/m) | Ultimate Strength (GNm) | Curvature (1/m) |
| No weld | 44.38 | 0.00014 | 44.38 | 0.00014 |
| wrs model | 44.30 | 0.00014 | 44.30 | 0.00014 |
| awrs model | 44.12 | 0.00014 | 44.12 | 0.00014 |

### *4.2.4 Result Validation*

The results obtained for the case of horizontal bending is validated against other literatures. This is presented in table 4.8.

*Table 4.8: Comparison of transverse ultimate strength with other publications*

| Source | Ultimate Strength (GNm) | |
|---|---|---|
| | Hogging | Sagging |
| (Yao, et al., 1993) | 39.22 | 39.22 |
| (Zhu, et al., 2020) | 43 | 43 |
| Current Investigation | 44.38 | 44.38 |

From the table, it can be seen that there is a good correlation between the results of (Zhu, et al., 2020) and those of the current study. However, the results tend to be a little higher than those of (Yao, et al., 1993).

## 4.3 Load Case 3: Bi-Axial Bending

The boundary conditions and coupling equation specific to the case of bi-axial bending as described in section 3.5.2 are adopted. Also, load application routine as described in the same section is used.

### *4.3.1 Hogging and Sagging Conditions*

The results obtained for biaxial bending in hogging and sagging conditions are shown in figure 4.17. The curvature ratios are increased from 0.3, 1, 2 and 5. From the figure, the interaction relationship between combined vertical and horizontal bending and the influence of one on the other can be analyzed depending on the inclined position of the ship during rolling. It can be seen from the figure that the results obtained are not too far from the suggestions of Paik in his formulation of the interaction relationship for the case of combined vertical and horizontal bending. In general, the results obtained in this study fit perfectly in an ellipse. This corresponds to the case where the empirical constants $\alpha$, a and b are 1, 2 and 2 respectively.

On further examination, it is observed that as the applied curvature ratio increases, the vertical bending load case dominates and the structure tends to behaviour like the case of pure vertical bending. The reverse is the case when the applied curvature ratio decreases.

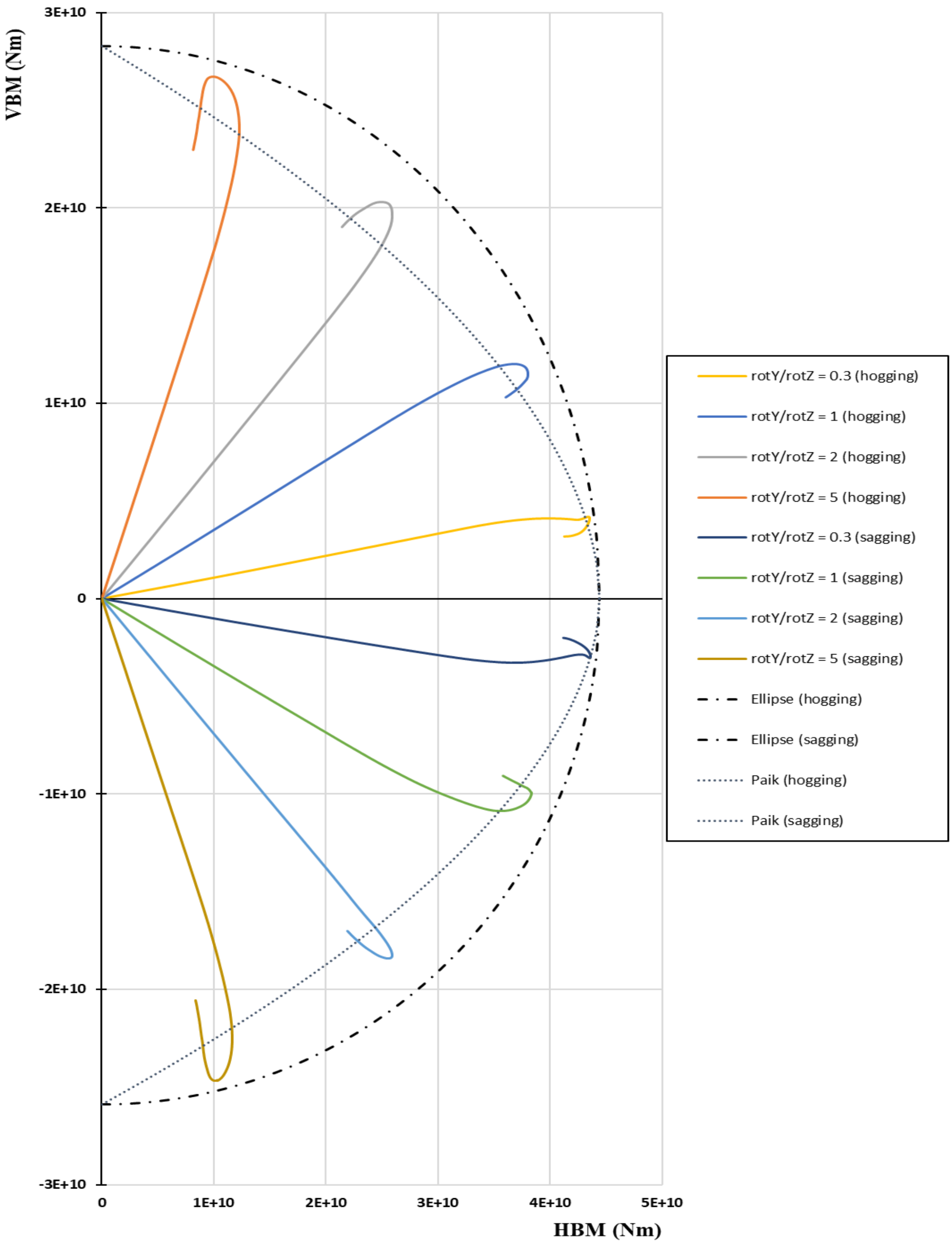


*Figure 4.17: diagram showing the interaction relationship between vertical and horizontal bending for different curvature ratio*

A summary of the results obtained for the maximum bending capacity of the double hull VLCC in the biaxial case is presented in table 4.9.

*Table 4.9: Results of maximum bending capacities for biaxial bending load case*

| Curvature Ratio (rotY/rotZ) | Maximum Bending Capacity (GNm) | | | |
|---|---|---|---|---|
| | Hogging | | Sagging | |
| | Mz | My | Mz | My |
| 0.3 | 43.56 | 4.18 | 43.62 | 3.30 |
| 1 | 38.04 | 12.00 | 38.34 | 10.86 |
| 2 | 25.92 | 20.32 | 25.90 | 18.43 |
| 5 | 12.31 | 26.72 | 11.69 | 24.67 |

From the table, it is clear that the maximum bending capacities of the combined load case in hogging and sagging conditions are less than those obtained for pure vertical bending and pure horizontal bending. This is due to the interaction of one on the other. To analyze the structural behaviour of the double hull VLCC in the biaxial case, the instance where the applied curvature ratio is unity will be used. This implies a condition where the same rotation is applied to both vertical and horizontal bending.

Under the hogging condition, three points are analyzed. The first point is at the end of the linear elastic region which is at the point Mz = 30.15 GNm and My = 10.55 GNm. The second point is where maximum vertical bending capacity occur which is at My = 12.00 GNm. Finally, the third point is where maximum horizontal bending capacity occur which is at Mz = 38.04 GNm (see figure 4.18).

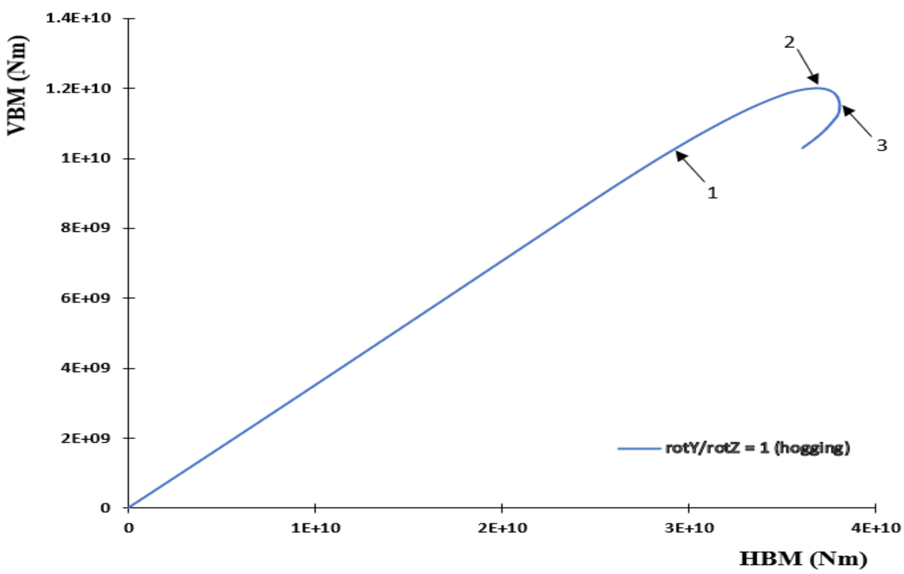


*Figure 4.18: biaxial interaction relationship diagram for curvature ratio of one in hogging condition*

At point 1, the starboard gunwale yields in tension. Also, yielding of the side shell and deck plating close to the starboard gunwale occurs at this point. However, the plastic deformations are more pronounced in the side shell while those of the deck are just some localized yielding. In addition, initial collapse in compression of the port side double bottom tank occurs concurrently (figure 4.19).

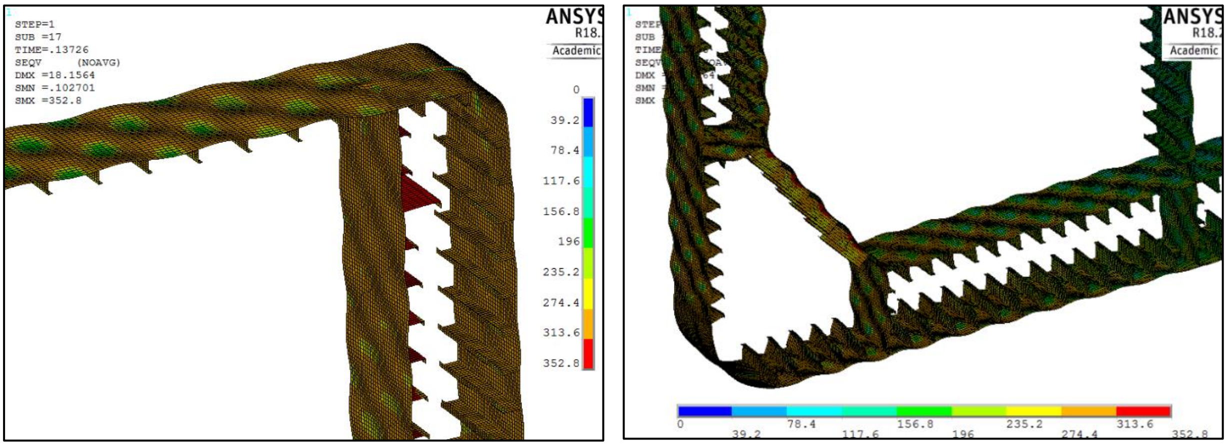


*Figure 4.19: Von Mises stress distribution for biaxial load case with curvature ratio of one under hogging*

As the applied curvature is gradually increased to point 2, the side shell plating and deck plating at the starboard gunwale become completely yielded. This then spreads through the starboard side shell and extends further along the deck plating. Also, the port side double bottom tank buckles at this point (figure 4.20); spreading along the side shell and double bottom of the structure.

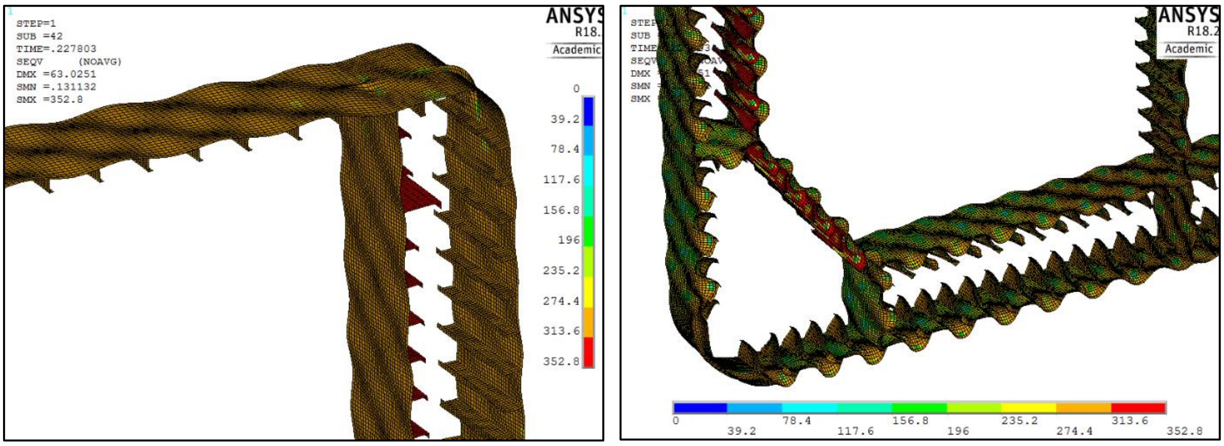


*Figure 4.20: Von Mises stress distribution for biaxial load case with curvature ratio of one under hogging (point 2)*

Finally at point 3, yielding collapse spreads to the starboard double bottom tank and through the longitudinal bulkhead close to the starboard side shell. At this point, the port side double bottom tank collapses completely in compression. The buckling collapse spreads through the side shell, the double bottom and the port side longitudinal bulkhead (Figure 4.21).

From the above observations, the effects of the interaction of vertical bending and horizontal bending under hogging condition become clearer. Unlike in the pure vertical bending load case in hogging condition (section 4.1), the whole deck region does not yield in tension and the whole double bottom does not buckle in compression in the case of biaxial bending. Also, unlike in the case of pure horizontal bending in hogging (section 4.2), the port side gunwale and the surrounding region does not buckle completely in compression and the starboard double bottom tank region does not yield completely in the case of biaxial bending.

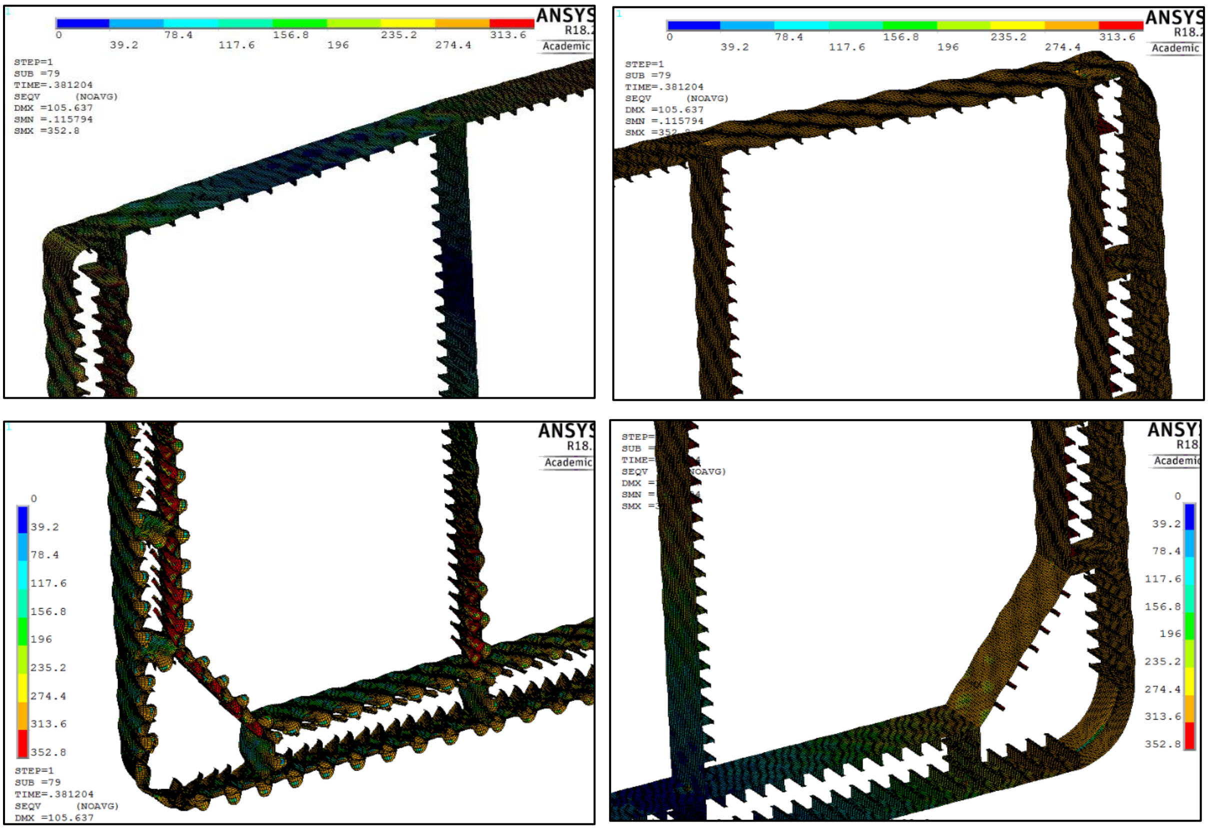


*Figure 4.21: Von Mises stress distribution for biaxial load case with curvature ratio of one under hogging (point 3)*

Under the sagging condition, three points are also analyzed. The first point is at the end of the linear elastic region which is at the point Mz = 25.78 GNm and My = 8.74 GNm. The second point is where maximum vertical bending capacity occur which is at My = 10.86 GNm. Finally, the third point is where maximum horizontal bending capacity occur which is at Mz = 38.34 GNm (see Figure 4.22).

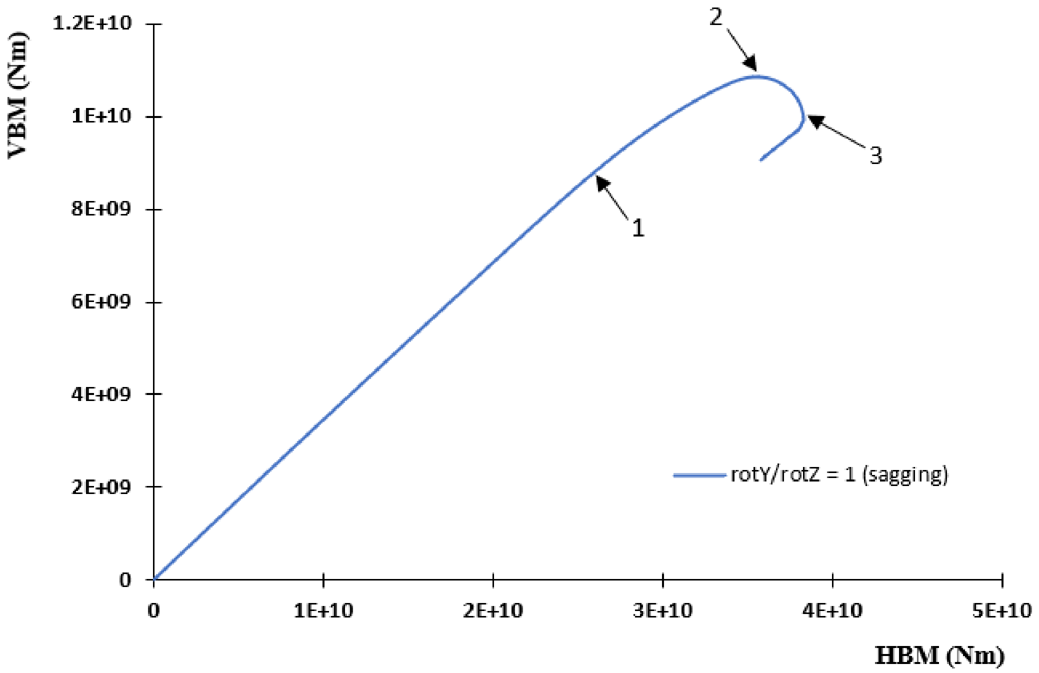


*Figure 4.22: biaxial interaction relationship diagram for curvature ratio of one in sagging condition*

At point 1, initial collapse starts at the right gunwale. This creeps through the deck and side shell as some localized plastic deformation. As shown in figure 4.23, the deformation also extends to the right longitudinal bulkhead. Simultaneously, some localized yielding in tension commences at the left double bottom tank (see figure 4.24).

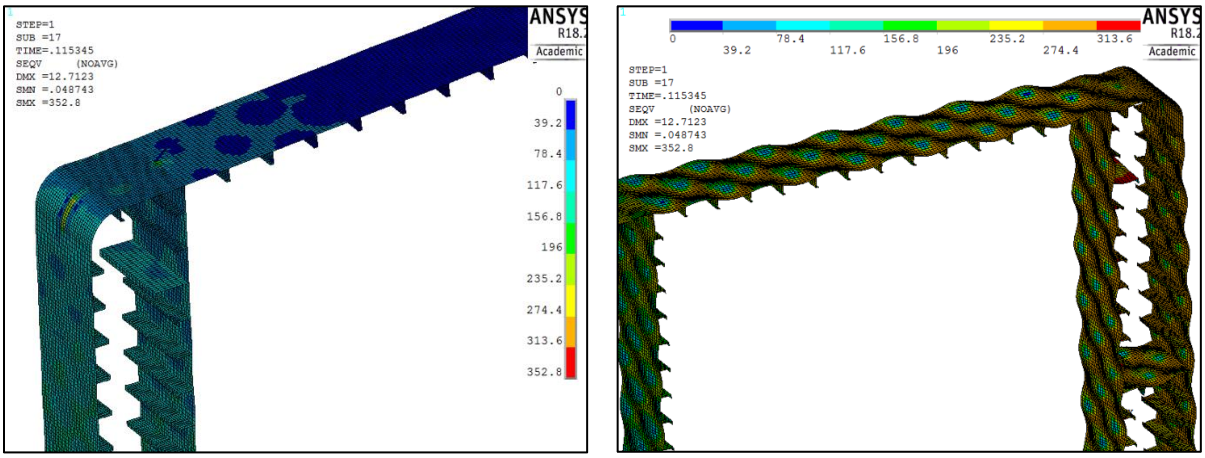


*Figure 4.23: von Mises stress distribution of the deck region for biaxial load case of deck region with curvature ratio of one under sagging (point 1)*

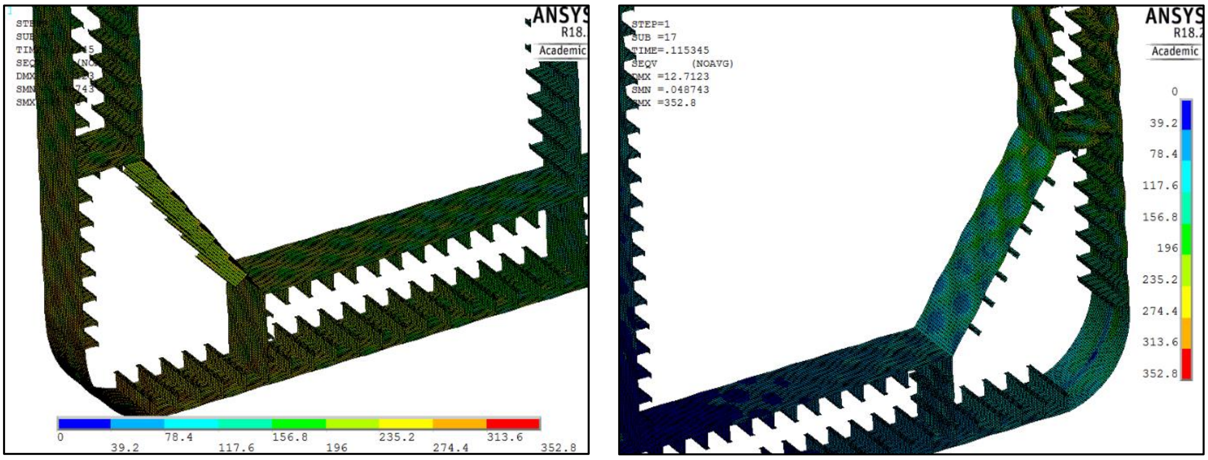


*Figure 4.24: von Mises stress distribution of the bottom region for biaxial load case of bottom region with curvature ratio of one under sagging (point 1)*

At point 2, the maximum vertical bending capacity is reached. At this point, the right gunwale buckles in compression. This extends through the side shell down to the double bottom tank as can be seen in figure 4.25. Concurrently, the port side double bottom tank yields completely in tension. This spreads through the double bottom and the side shell close to the double bottom tank.

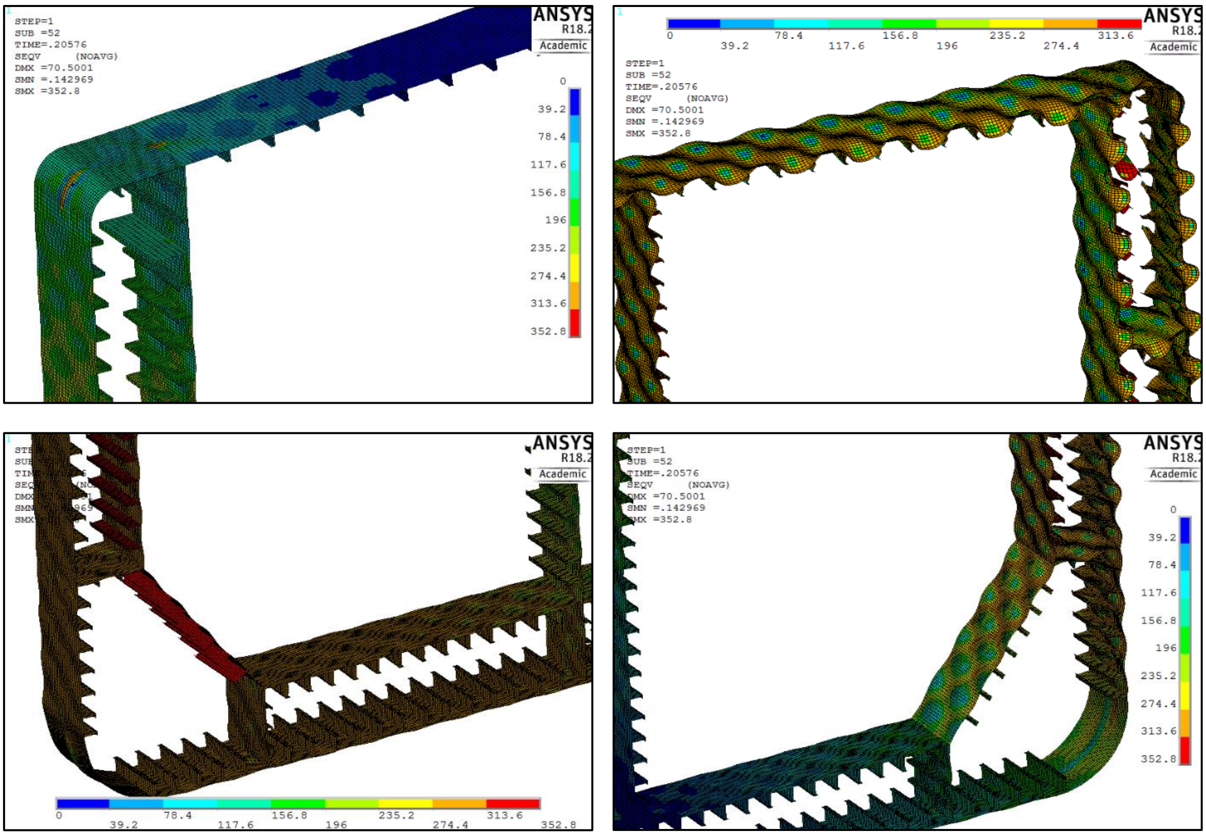


*Figure 4.25: von Mises stress distribution for biaxial load case with curvature ratio of one under sagging (point 2)*

Finally at point 3, the maximum horizontal bending capacity is attained. At this point, the right-side double bottom tank buckles fully. The right-side longitudinal bulkhead close to the deck also buckles completely at this point. At the same time, the yielding of the left side double bottom tank extends further along the double bottom and the side shell (see figure 4.26).

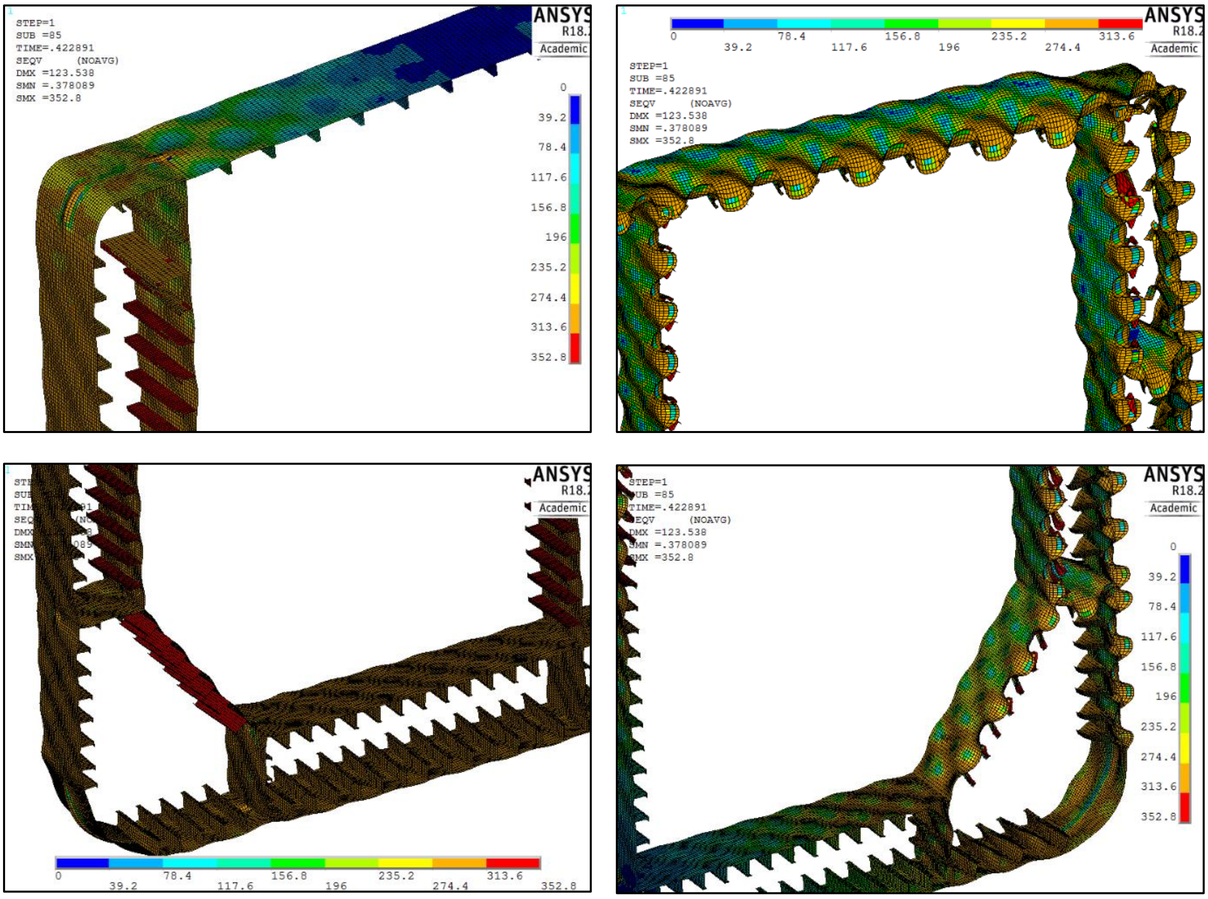

*Figure 4.26: Von Mises stress distribution for biaxial load case with curvature ratio of one under sagging (point 3)*

### *4.3.2 Influence of Welding Residual Stress*

The effects of welding residual stresses on the ultimate strength in the case of combined vertical and horizontal bending are shown in figure 4.27. In this case, only the 'wrs' configuration is investigated. In the figure, the dash curves represent the case where welding residual stresses are taken into account. As can be seen from the figure, welding residual stresses have negligible influence on the obtained results.

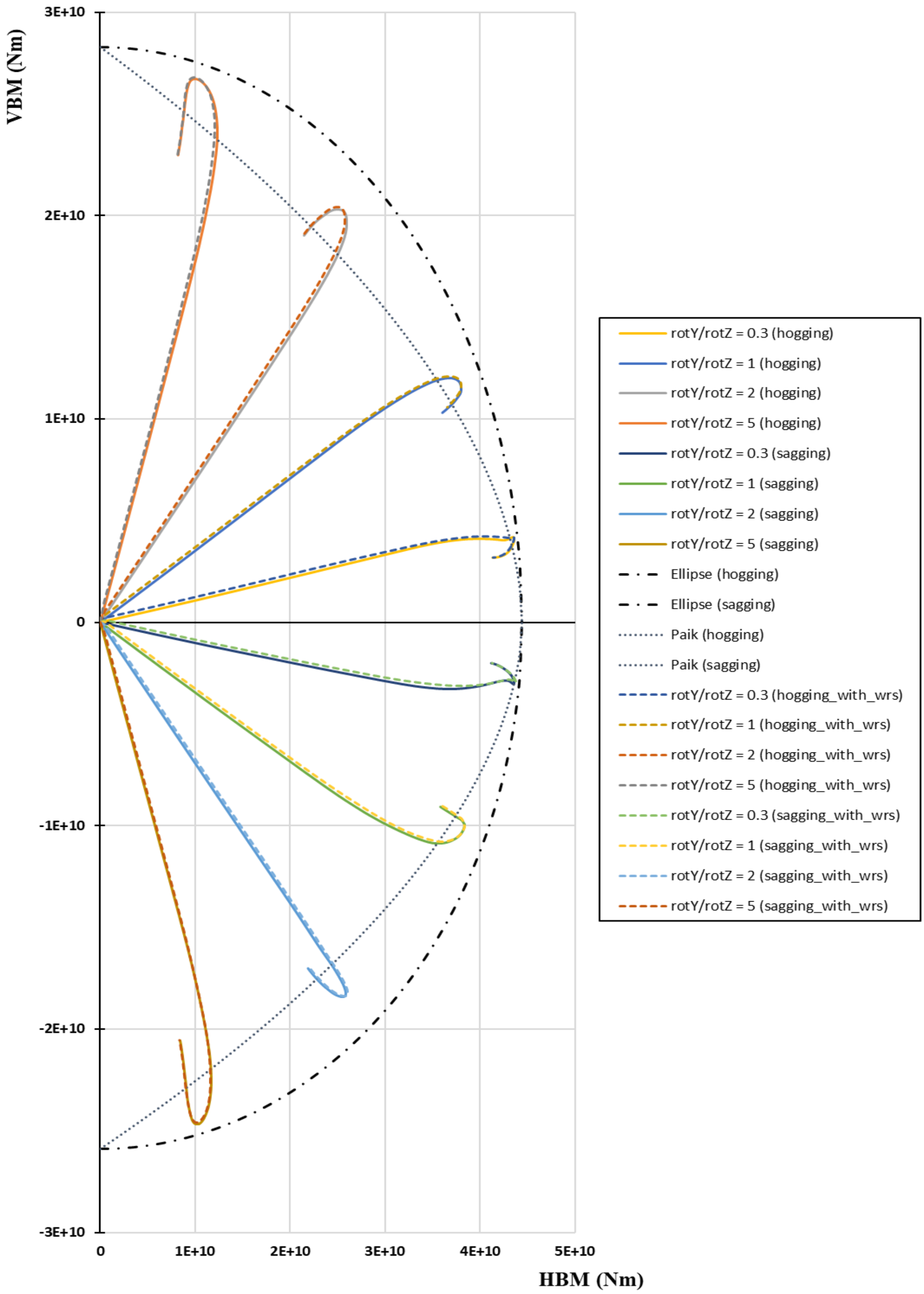


*Figure 4.27: biaxial interaction curves showing the effects of welding residual stresses*

## 4.4 Results and Analysis of Residual Strength

The residual strength of the damaged double hull VLCC is analyzed for vertical, horizontal and biaxial bending load cases under hogging and sagging conditions. The modeling of the damage cases is described in section 3.4. The results obtained for the considered damage cases are presented and analyzed in the following sections.

### *4.4.1 Vertical Bending Load Case*

The boundary conditions, coupling equations and load application routines are as described in section 3.2.5.

- Hogging and sagging conditions

Figure 4.28 shows the results of the residual strength of the different damage cases considered in comparison with that of the intact condition.

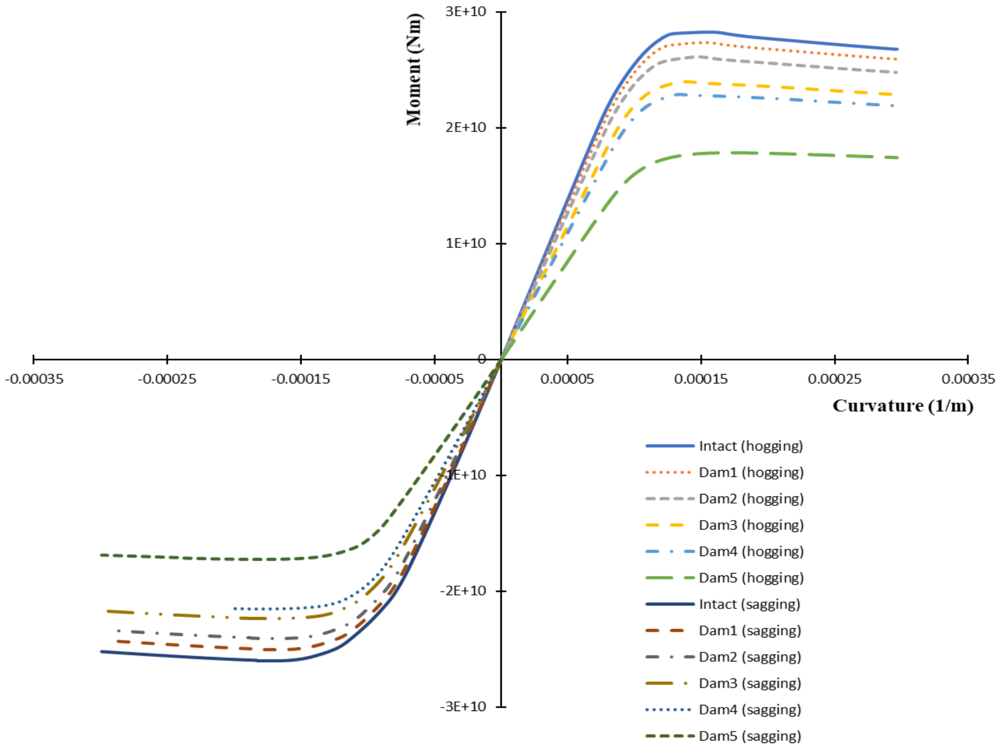


*Figure 4.28: Results of ultimate strength in intact and damaged conditions for vertical bending load case*

As expected, there is a gradual reduction in the value of the ultimate strength as the extent of the damage increases. The results obtained for this investigation are summarized in table 4.10.

*Table 4.10: Results of US in intact and damaged conditions for vertical bending load case*

| Model | Ultimate Strength (GNm) | |
|---|---|---|
| | Hogging | Sagging |
| Intact | 28.27 | 26.00 |
| Dam1 | 27.40 | 25.04 |
| Dam2 | 26.16 | 24.11 |
| Dam3 | 24.00 | 22.36 |
| Dam4 | 22.87 | 21.52 |
| Dam5 | 17.85 | 17.30 |

The collapse behaviour of the damaged double hull VLCC in the worst-case scenario (Dam5) is investigated under hogging and sagging conditions. Three critical points are chosen for each condition as shown in figure 4.29 below.

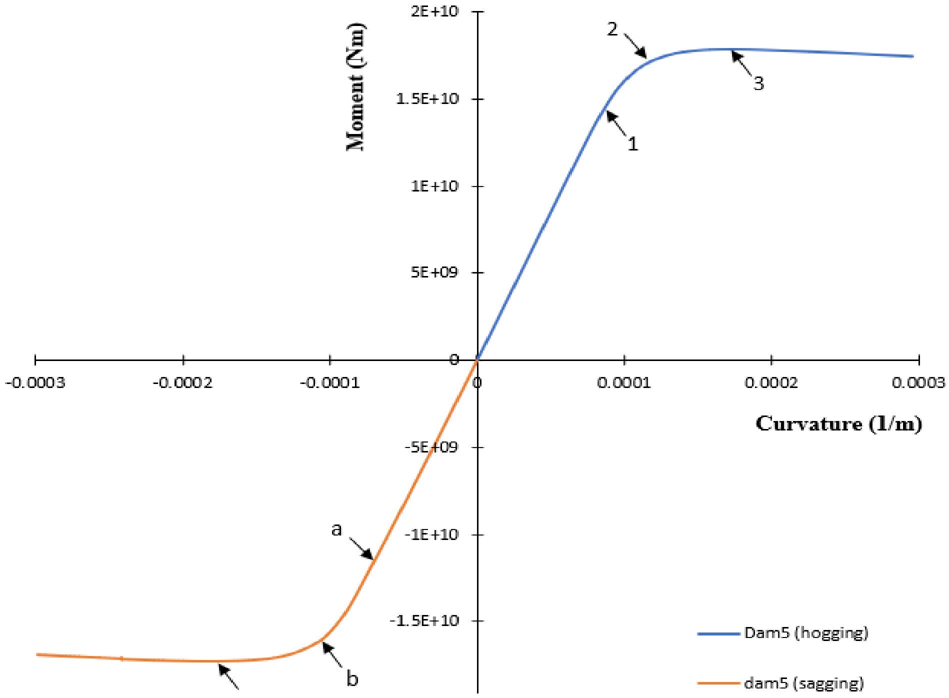


*Figure 4.29: moment curvature curve for vertical bending load case of 'dam5' in hogging and sagging*

Under the hogging condition, at point 1, it is observed that localized yielding in tension begins at the deck and spreads through the side shells and the longitudinal bulkheads. Simultaneously, buckling in compression of the double bottom tank, the remaining parts of the double bottom, and the longitudinal bulkheads close to the damage region commences (figure 4.30).

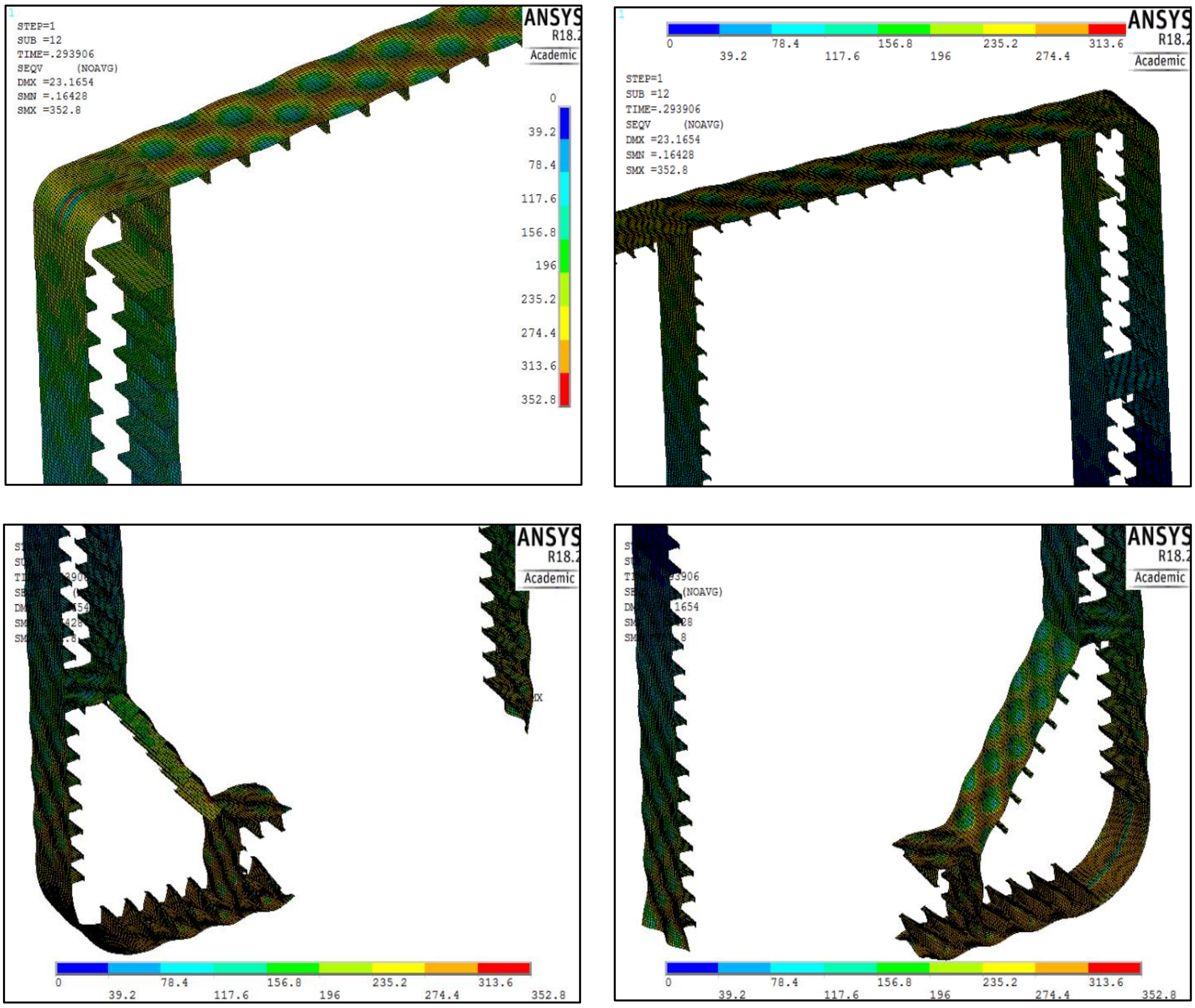


*Figure 4.30: von Mises stress distribution for vertical bending load case in damaged condition under hogging (point 1)*

This collapse behaviour (simultaneous yielding and buckling in this particular case) is as a result of the upward shift of the neutral axis due to the damage. As the applied curvature is gradually increased to point 2, complete plastic deformation of the central deck region occurs. Also, localized yielding of the gunwales, part of the longitudinal bulkheads and other parts of the deck takes place. Concurrently, the bottom part of the structure buckles. This extends to parts of the longitudinal bulkheads and double bottom tank (figure 4.31).

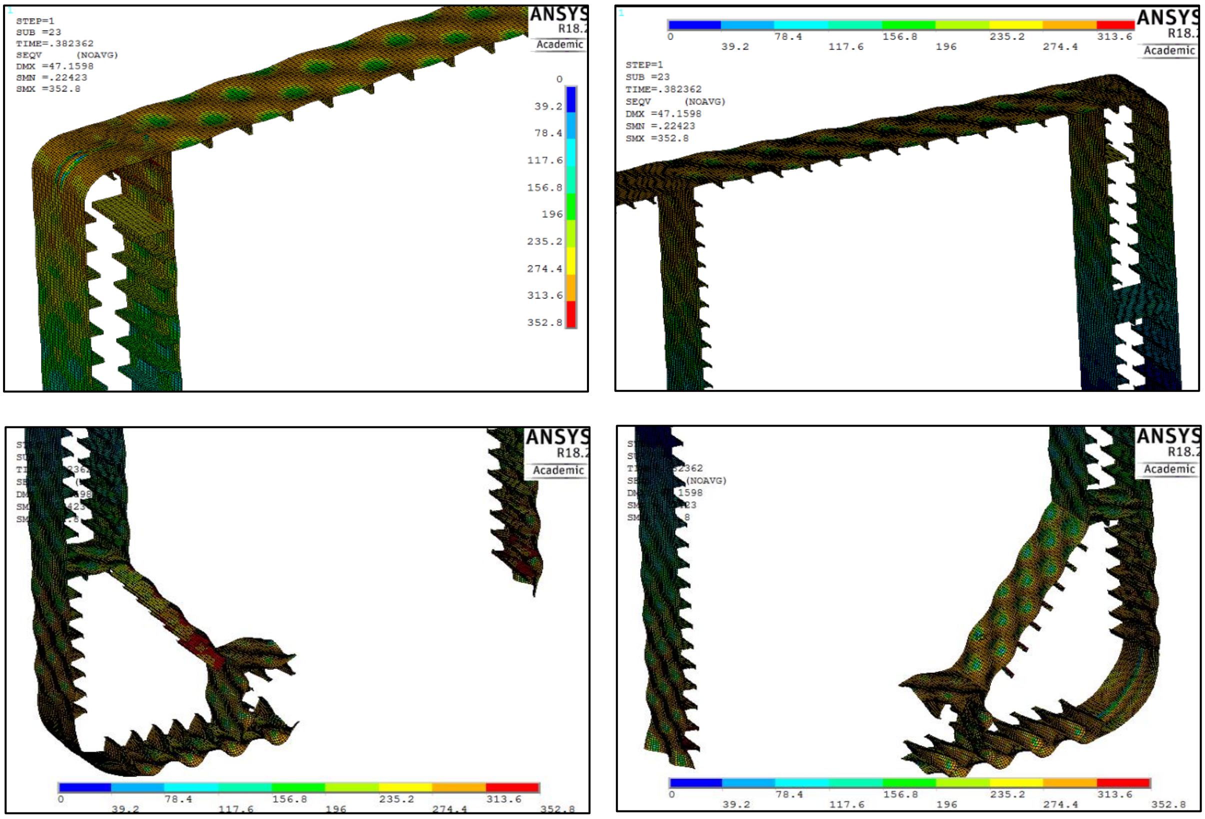


*Figure 4.31: von Mises stress distribution for vertical bending load case in damaged condition under hogging (point 2)*

Finally at point 3, the maximum bending capacity is attained. At this point, the whole deck region becomes plastically deformed including the parts of the longitudinal bulkheads close to the deck and the side shell region close to the gunwales (figure 4.32). Also, the remaining parts of the double bottom collapses completely due to compressive instability (figure 4.33). the double bottom tank buckles completely at this point. Also, the parts of the longitudinal bulkheads close to the damaged region buckles as well.

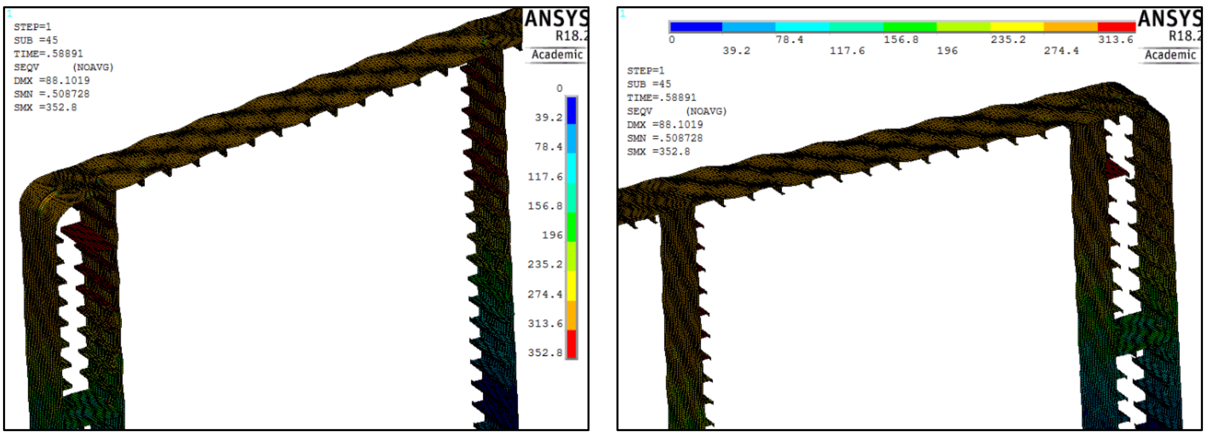


*Figure 4.32: von Mises stress distribution of the deck region for vertical bending load case in damaged condition under hogging (point 3)*

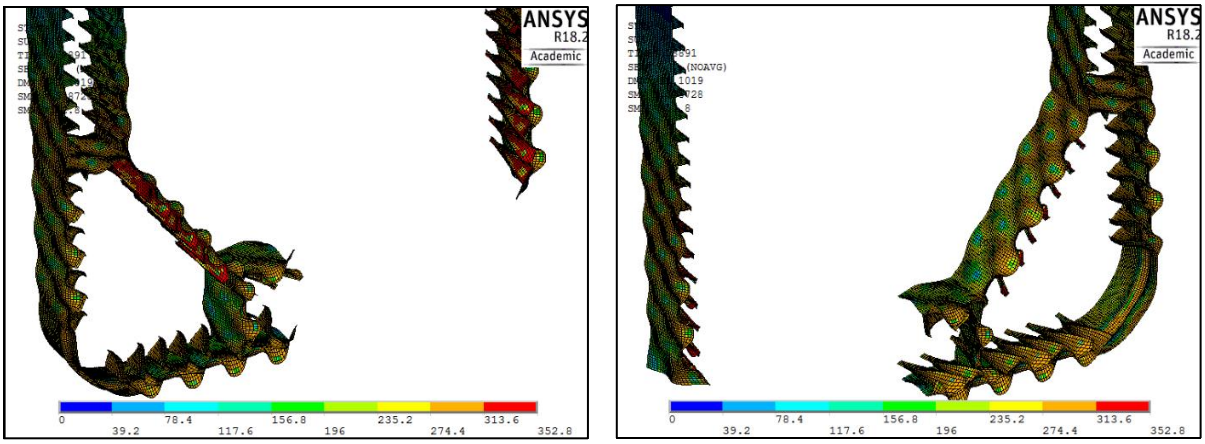


*Figure 4.33: von Mises stress distribution of the bottom region for vertical bending load case in damaged condition under hogging (point 3)*

Under the sagging condition, at point a, localized yielding of the deck in compression begins and this spreads to the gunwales. At the same time, the remaining part of the outer bottom and some parts of the double bottom tank deforms plastically in tension as shown in figure 4.34. This concurrent collapse behaviour is attributed to the upward shift of the neutral axis due to the damage region.

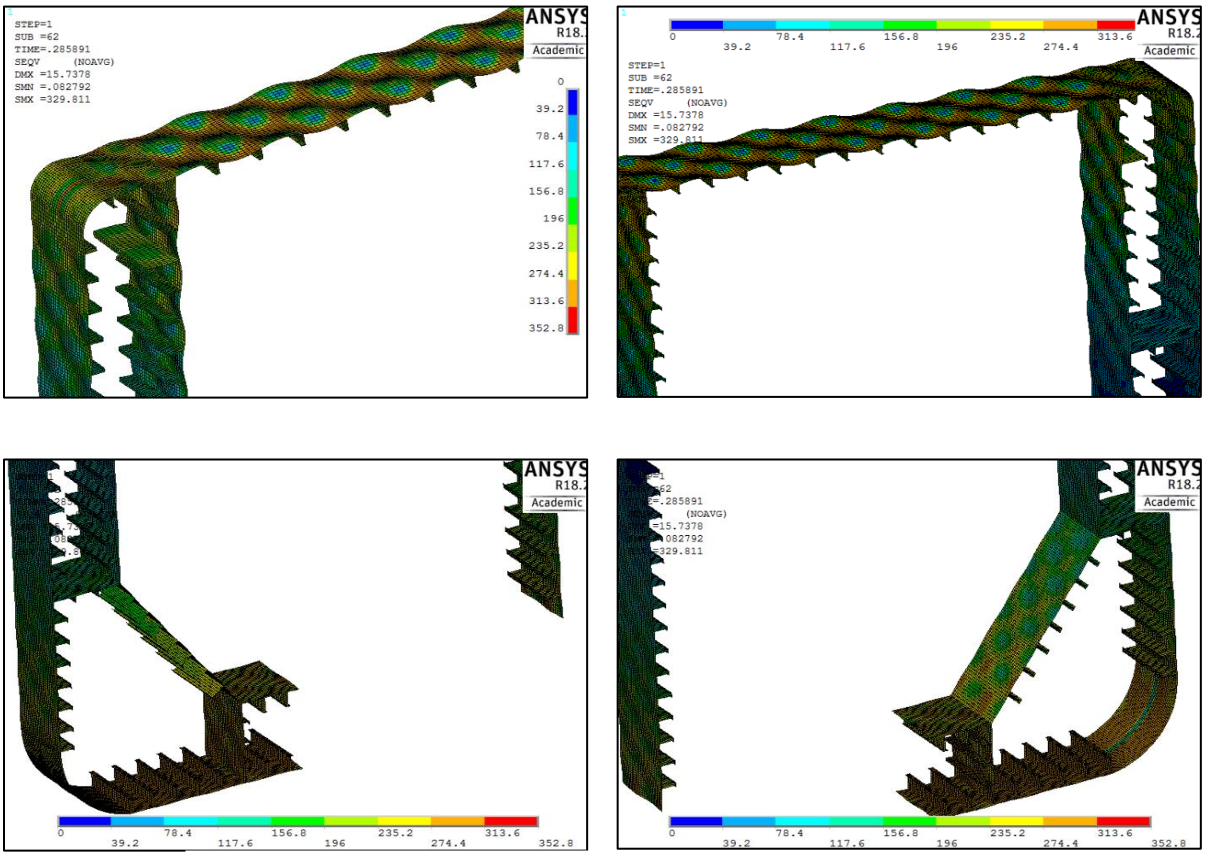


*Figure 4.34: von Mises stress distribution for vertical bending load case in damaged condition under sagging (point 1)*

As the applied load is gradually increased to point b, the deck starts to buckle in compression, the gunwales deforms plastically and the parts of the longitudinal bulkheads and side shells close to the deck begins to buckle in compression. Concurrently, the double bottom yields in tension and this extends to a large portion of the double bottom tanks. Also, the longitudinal bulkheads close to the bottom yields as shown in figure 4.35.

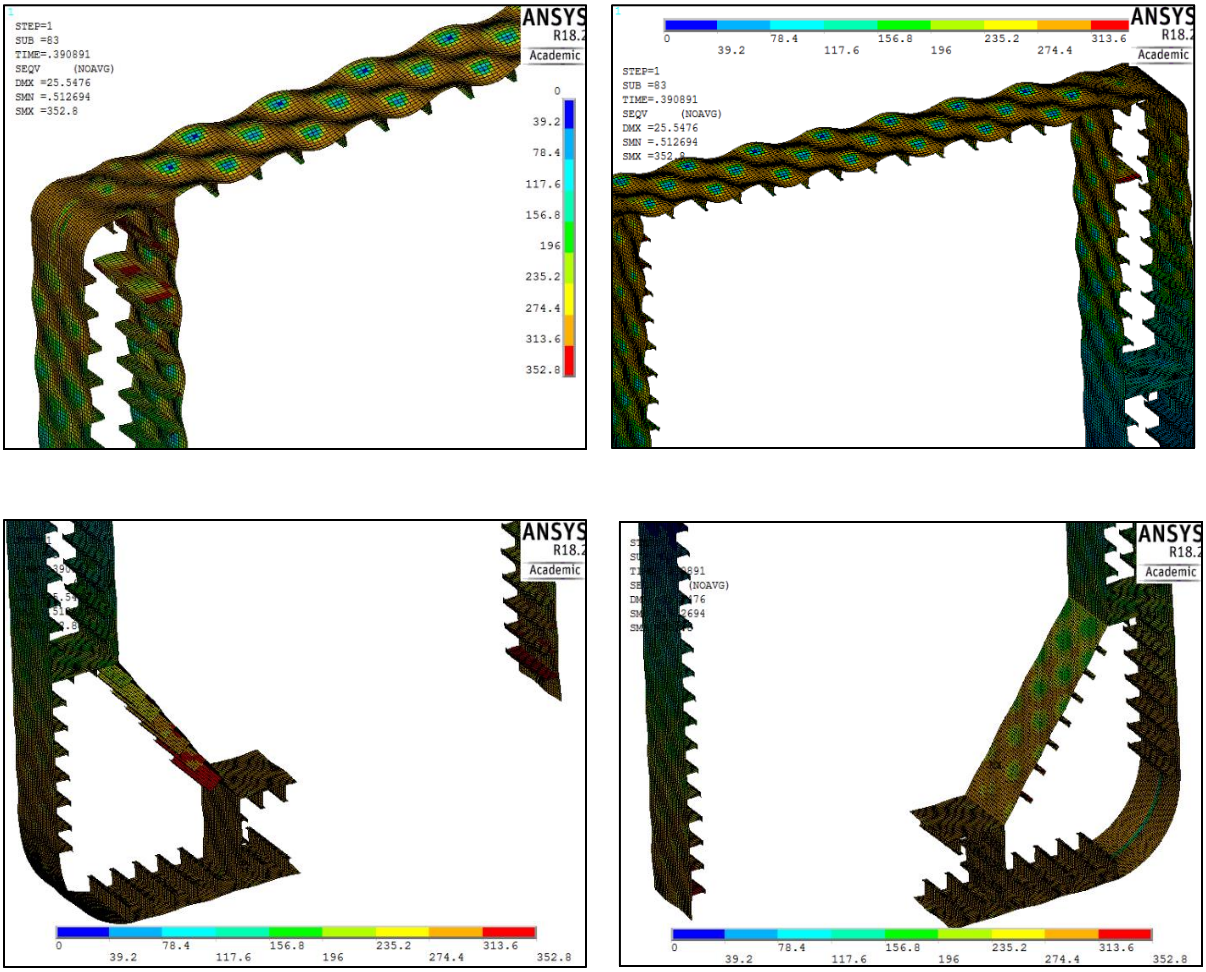


*Figure 4.35: von Mises stress distribution for vertical bending load case in damaged condition under sagging (point 2)*

Lastly, at point c, the maximum bending capacity is attained. At this point, the deck collapses completely in compression. This then extends to the side shells and longitudinal bulkheads close to the deck region. Also, the remaining part of the double bottom, the double bottom tanks and the part of the longitudinal bulkheads close to the bottom completely yield in tension as shown in figure 4.36.

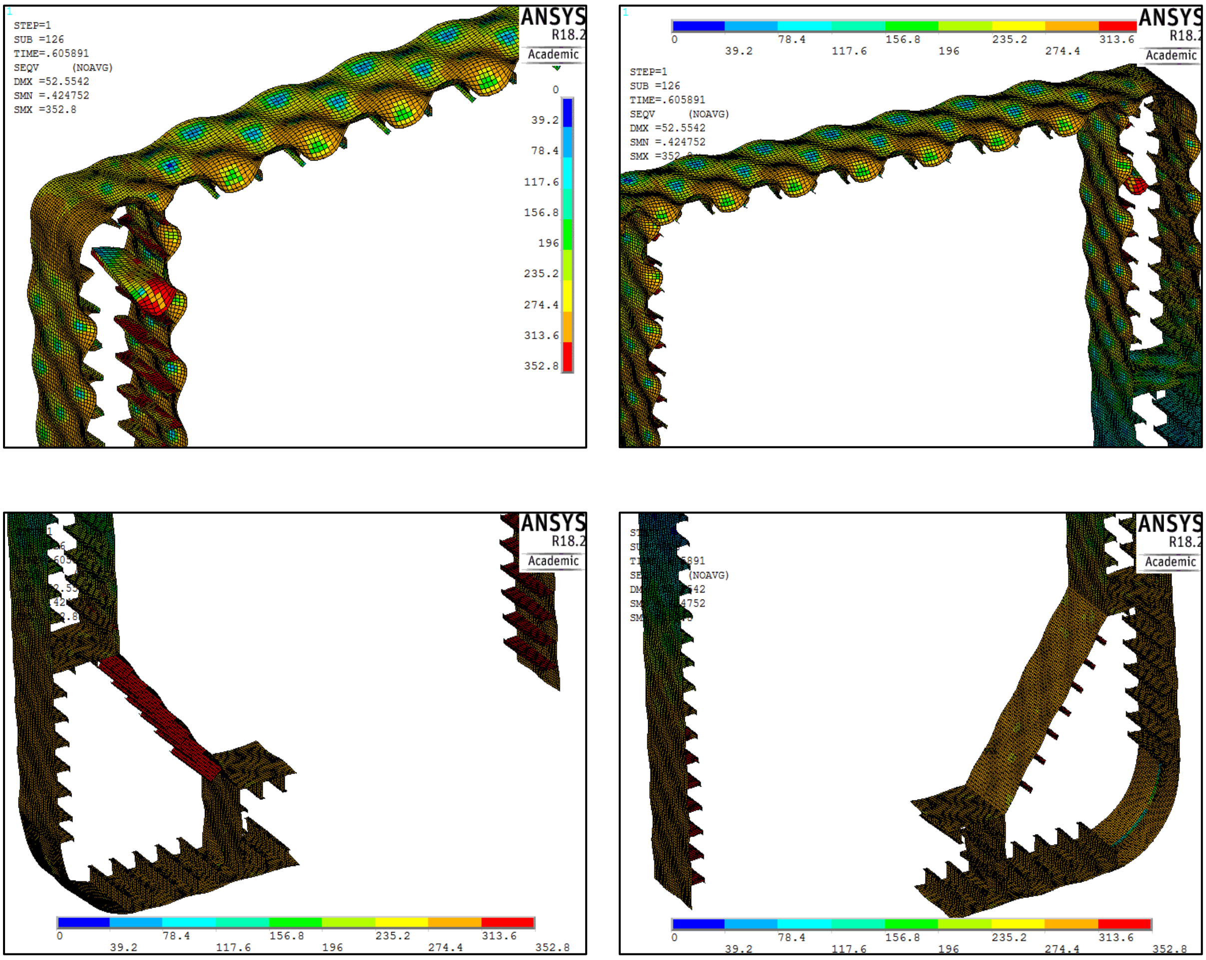


*Figure 4.36: von Mises stress distribution for vertical bending load case in damaged condition under sagging (point 3)*

### *4.4.2 Horizontal Bending Load Case*

The boundary conditions, coupling equations and load application routines adopted in this case are similar to those of the intact condition (see section 3.4.1).

- Hogging and sagging conditions

The results of the residual strength for the different damage configurations considered in this work are shown in figure 4.37. As can be seen from the figure, the values obtained for the residual strength of 'dam1' and 'dam2' configurations are very close to the ultimate strength in intact condition. This is because the damage extent is relatively small. Thus, the load carrying capacity of the double hull VLCC is not significantly affected. However, as the extent of the damage increases, the ultimate strength of the structure reduces.

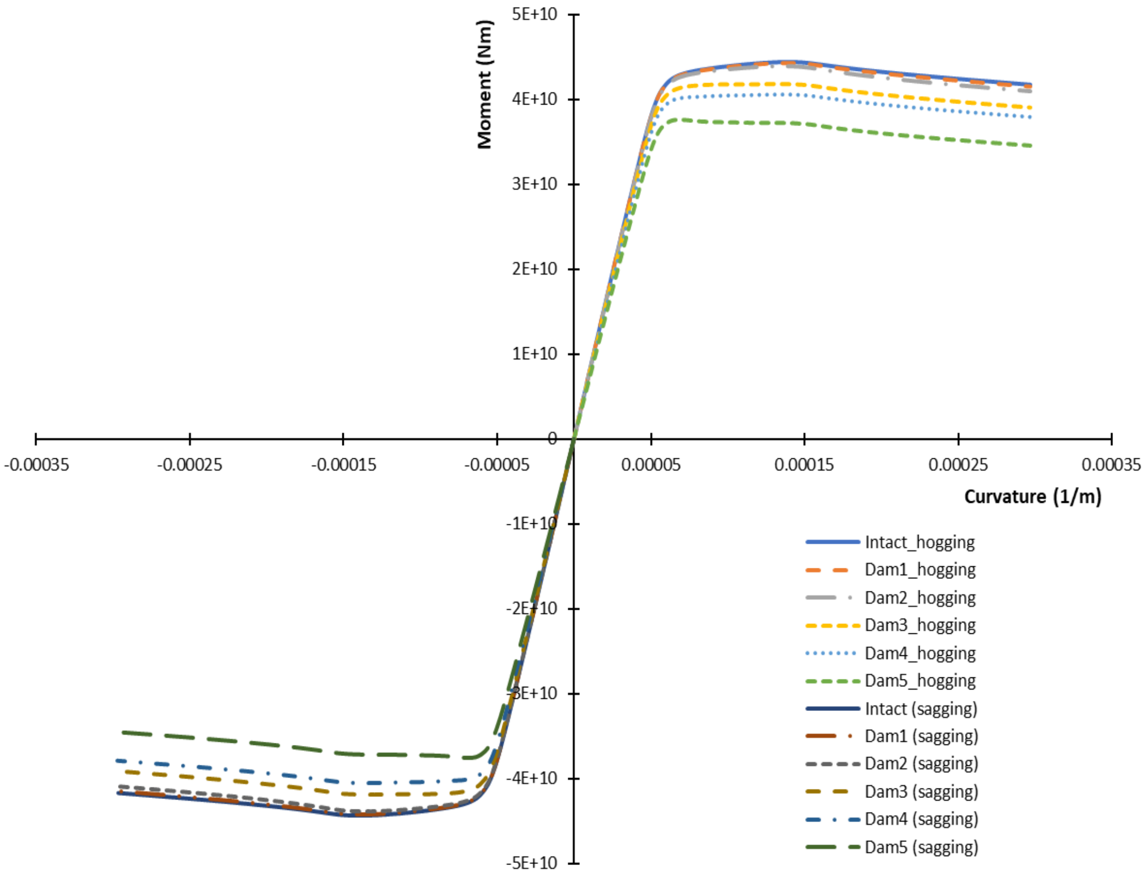


*Figure 4.37: Results of US in intact and damaged conditions for horizontal bending load case*

A summary of the results for the residual strength of the damage cases considered is presented in table 4.11.

*Table 4.11: Summary of results for horizontal bending load case in damage condition*

| Model | Ultimate strength (GNm) | |
|---|---|---|
| | Hogging | Sagging |
| Intact | 44.38 | 44.38 |
| Dam1 | 44.29 | 44.29 |
| Dam2 | 43.91 | 43.91 |
| Dam3 | 41.86 | 41.86 |
| Dam4 | 40.57 | 40.57 |
| Dam5 | 37.62 | 37.62 |

An investigation of the structural behaviour of the double hull VLCC in the worst damage case (Dam5) is done at two points (figure 4.38). The points correspond with the end of the linear elastic region and the maximum bending capacity of the structure. Due to symmetry with the centre plane, only hogging condition is analyzed for this damage condition.

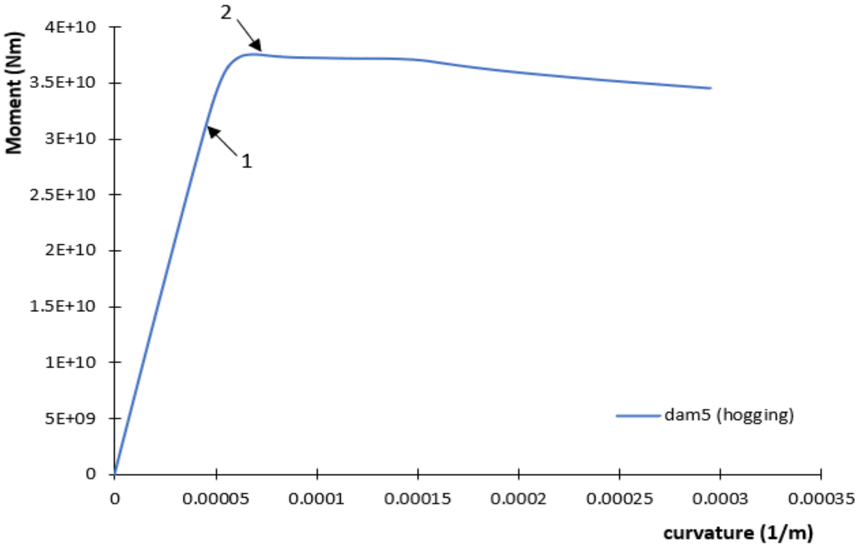


*Figure 4.38: moment curvature curve for horizontal bending load case of 'dam5' in hogging*

At point 1, where the applied load is 32.81GNm, some localized yielding in tension starts to propagate at the starboard side of the structure and at the same time, buckling collapse commences at the port side which happens to be in compression. These failure modes extend to the deck and double bottom of the VLCC (see figure 4.39 and figure 4.40).

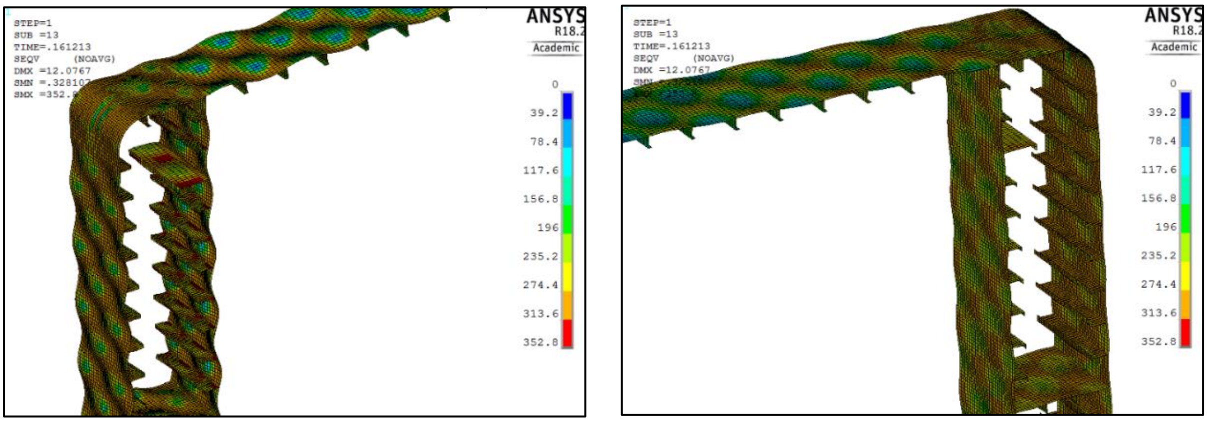


*Figure 4.39: von Mises stress distribution of the deck region for horizontal load case in damaged condition under hogging (point 1)*

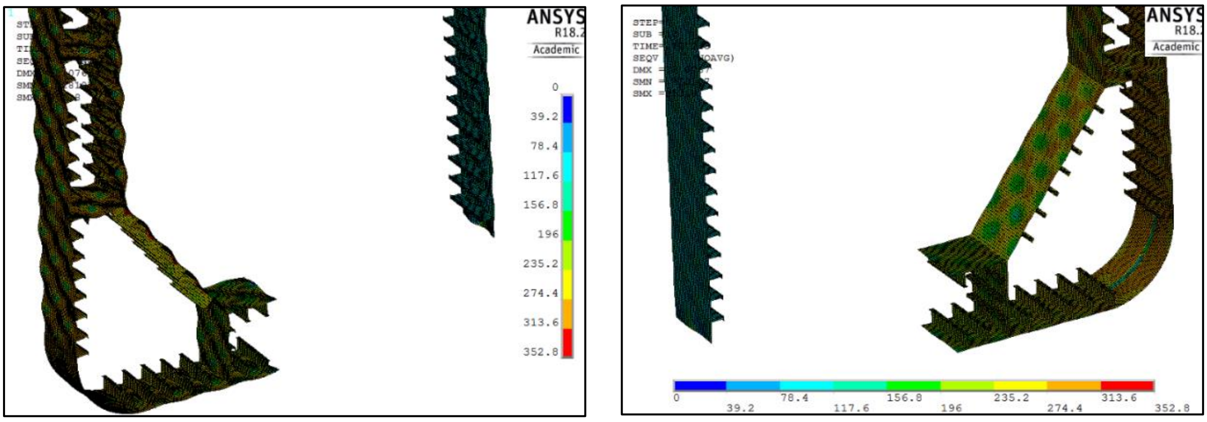


*Figure 4.40: von Mises stress distribution of the bottom region for horizontal load case in damaged condition under hogging (point 1)*

As the applied curvature is increased to point 2, the maximum bending capacity is attained. At this point, the starboard side shell yields completely in tension and spreads to the deck and double bottom. Simultaneously, the port side shell buckles in compression and extends to the deck and double bottom (figure 4.41).

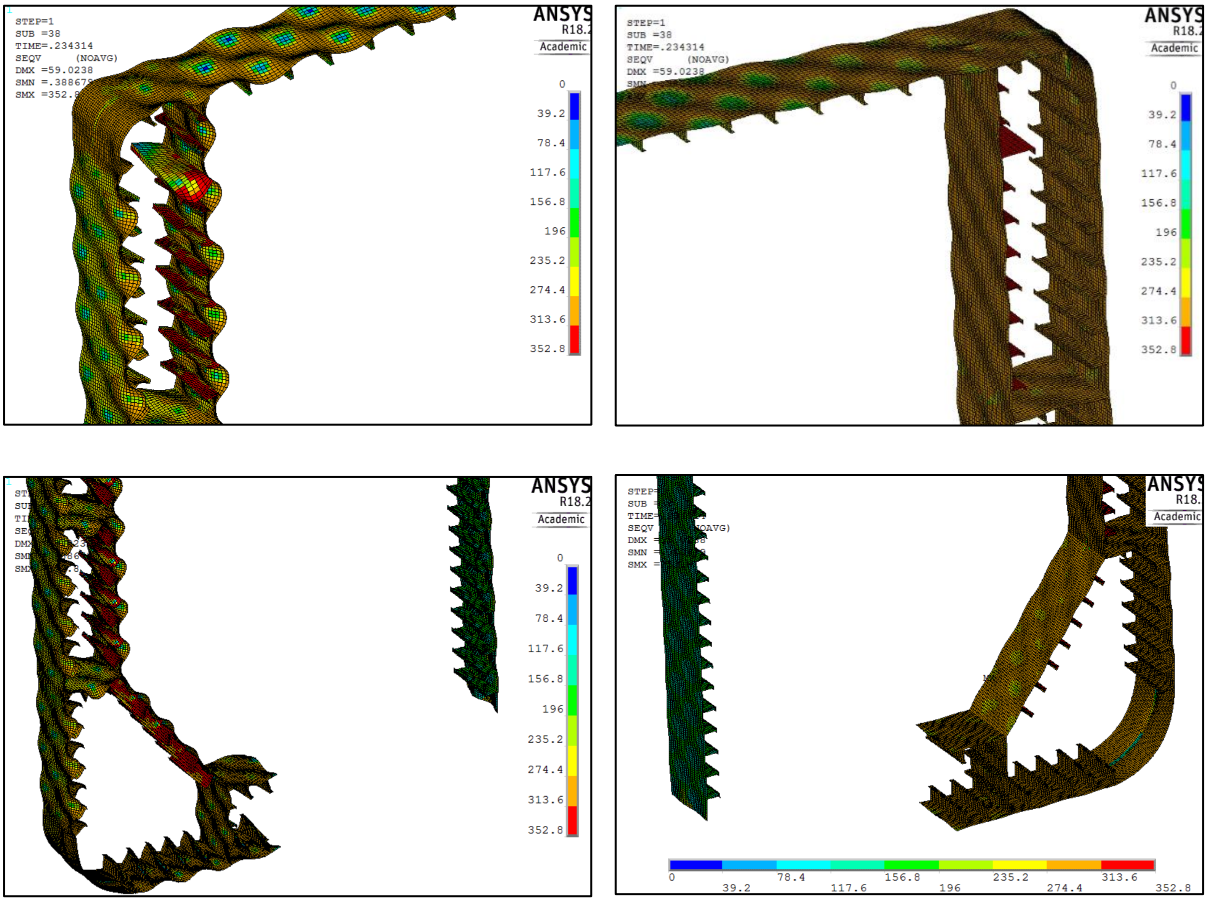


*Figure 4.41: von Mises stress distribution for horizontal load case in damaged condition under hogging (point 2)*

It can be observed that the collapse behaviour in the intact and damaged conditions in this study are similar except for the fact that the maximum bending capacity is reduced in the damaged case.

### *4.4.3 Biaxial Bending Load Case*

The boundary conditions, coupling equations and load application routines adopted in this case are similar to those of the intact condition (see section 3.4.1). For brevity, only 'dam3 and dam5' damage conditions are considered for this load case.

- Hogging and sagging conditions

Figure 4.42 shows the results of the residual strength for the considered damage cases in comparison with the intact condition. The dash curves represent the damage cases while the solid curves represent the intact condition. As can be seen, the curves representing the interaction relationship between vertical and horizontal bending get smaller as the extent of the damage increases.

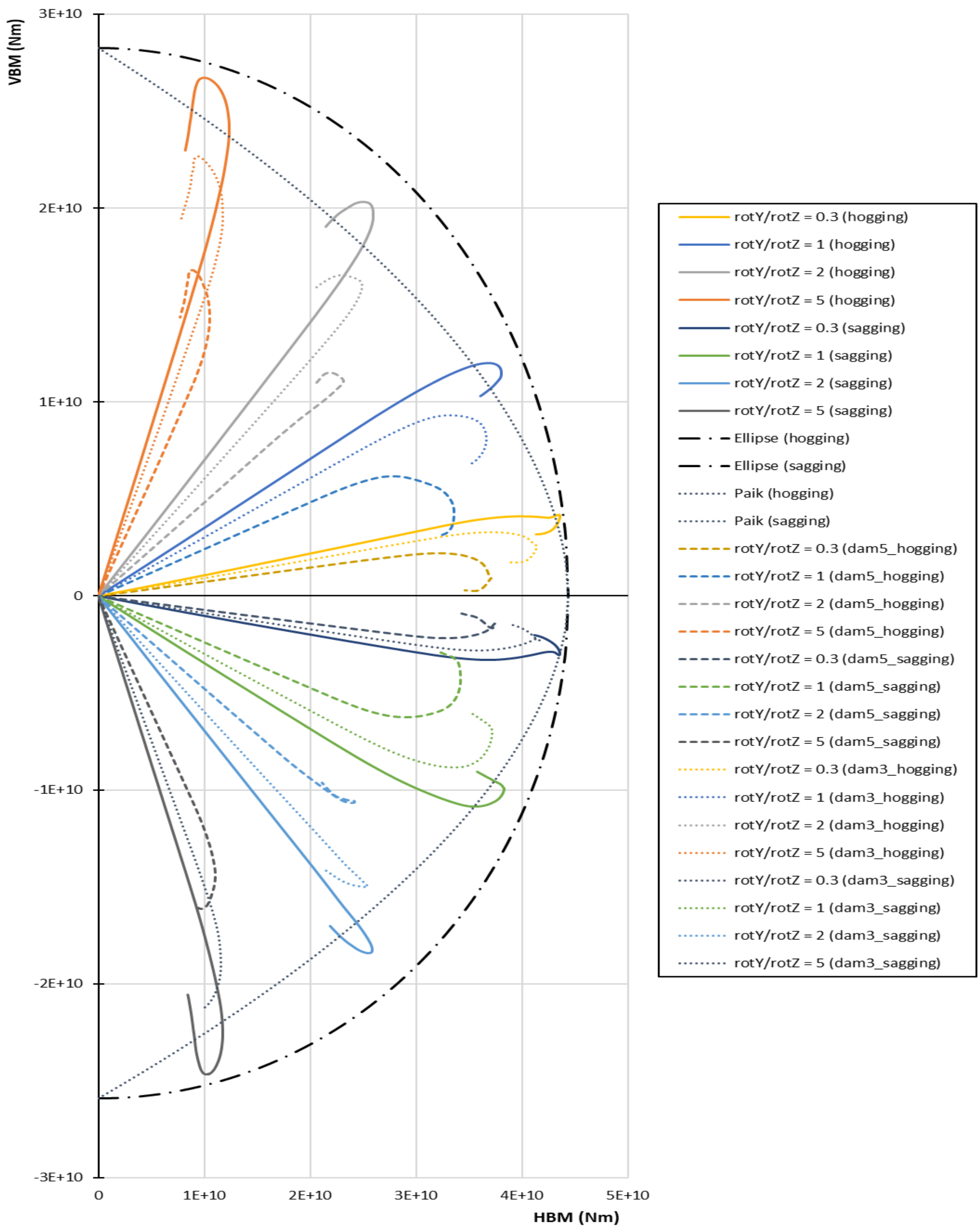


*Figure 4.42: biaxial interaction relationship curves for intact and damage conditions (dam3 and dam5)*

A curvature ratio of unity is used to analyze the collapse behaviour of 'dam5' (worst damage condition) configuration under biaxial load case. Three important points are considered for each condition of hogging and sagging. The three considered points coincide with the end of the linear elastic region, maximum vertical bending capacity and maximum horizontal bending capacity (Figure 4.43).

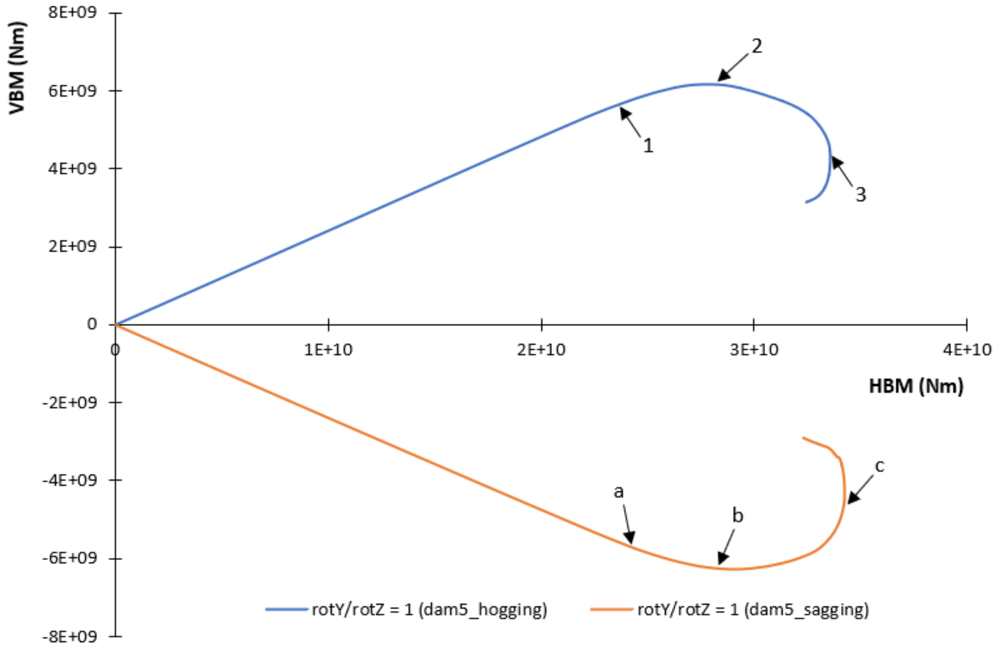


*Figure 4.43: interaction curve for curvature ratio of unity for biaxial bending load case of 'dam5' in hogging and sagging*

Under the hogging condition, at point 1, initial plastic deformation begins at the right gunwale and concurrently, compressive instability commences at the left double bottom tank and extends to the side shell and double bottom as shown in figure 4.44 and figure 4.45. It can also be seen that some localized yielding occurs at the deck and also part of the side shell close to the right gunwale.

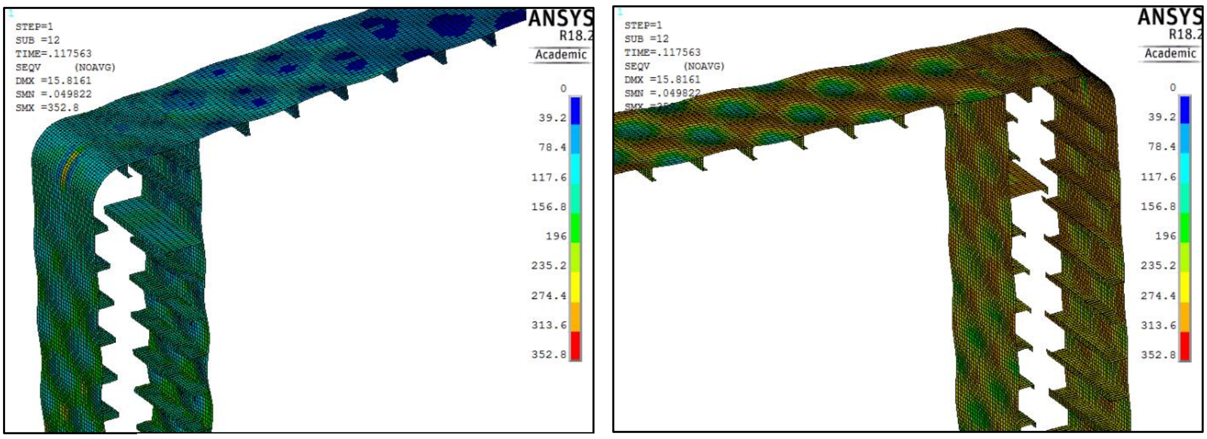


*Figure 4.44: von Mises stress distribution of the deck region for biaxial load case in damage condition under hogging (point 1)*

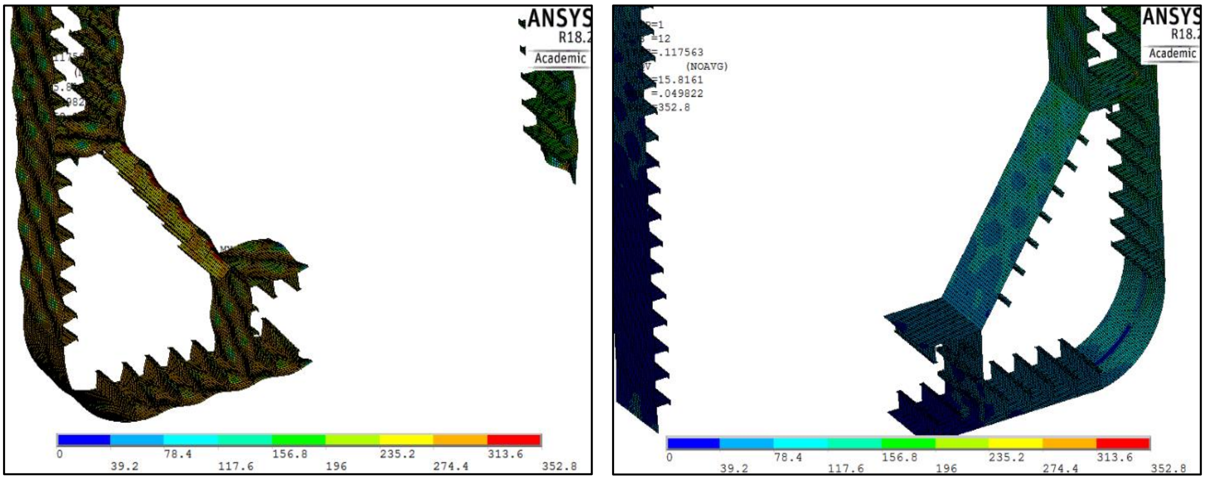


*Figure 4.45: von Mises stress distribution of the bottom region for biaxial load case in damage condition under hogging (point 1)*

As the applied load is further increased to point 2 where the maximum vertical bending capacity is attained, the region surrounding the right gunwale becomes more plastically deformed in tension and the buckling collapse of the left double bottom tank increases (Figure 4.46).

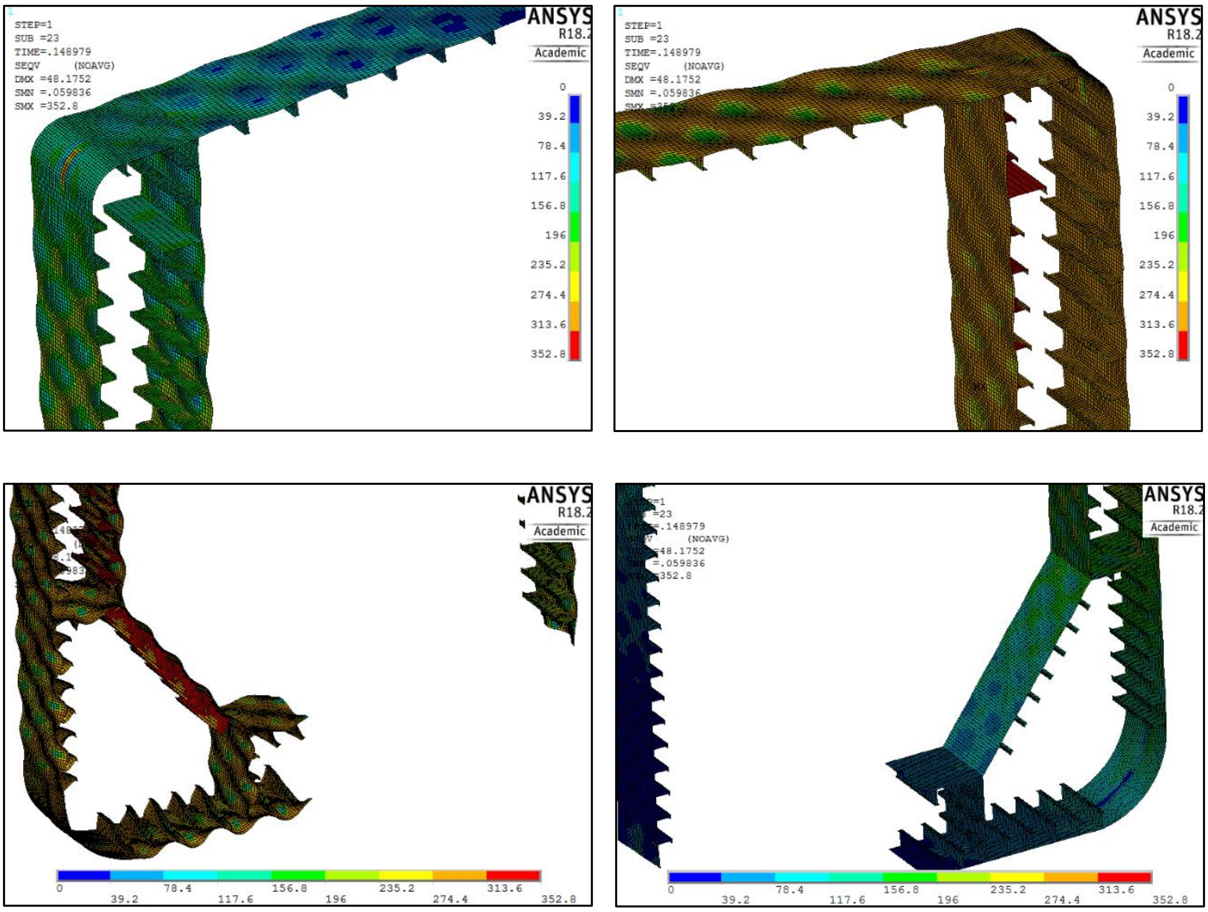


*Figure 4.46: von Mises stress distribution for biaxial load case in damage condition under hogging (point 2)*

Finally at point 3 where the maximum horizontal bending capacity is attained, the right gunwale becomes fully yielded and this spreads through the deck and the side shell as shown in figure 4.47. Simultaneously, the port side double bottom tank buckles completely. This then spreads through the side shell up to the deck. It can also be observed that the plates of the longitudinal bulkhead close to the right gunwale also yields in tension while those close to the left double bottom tank buckles in compression.

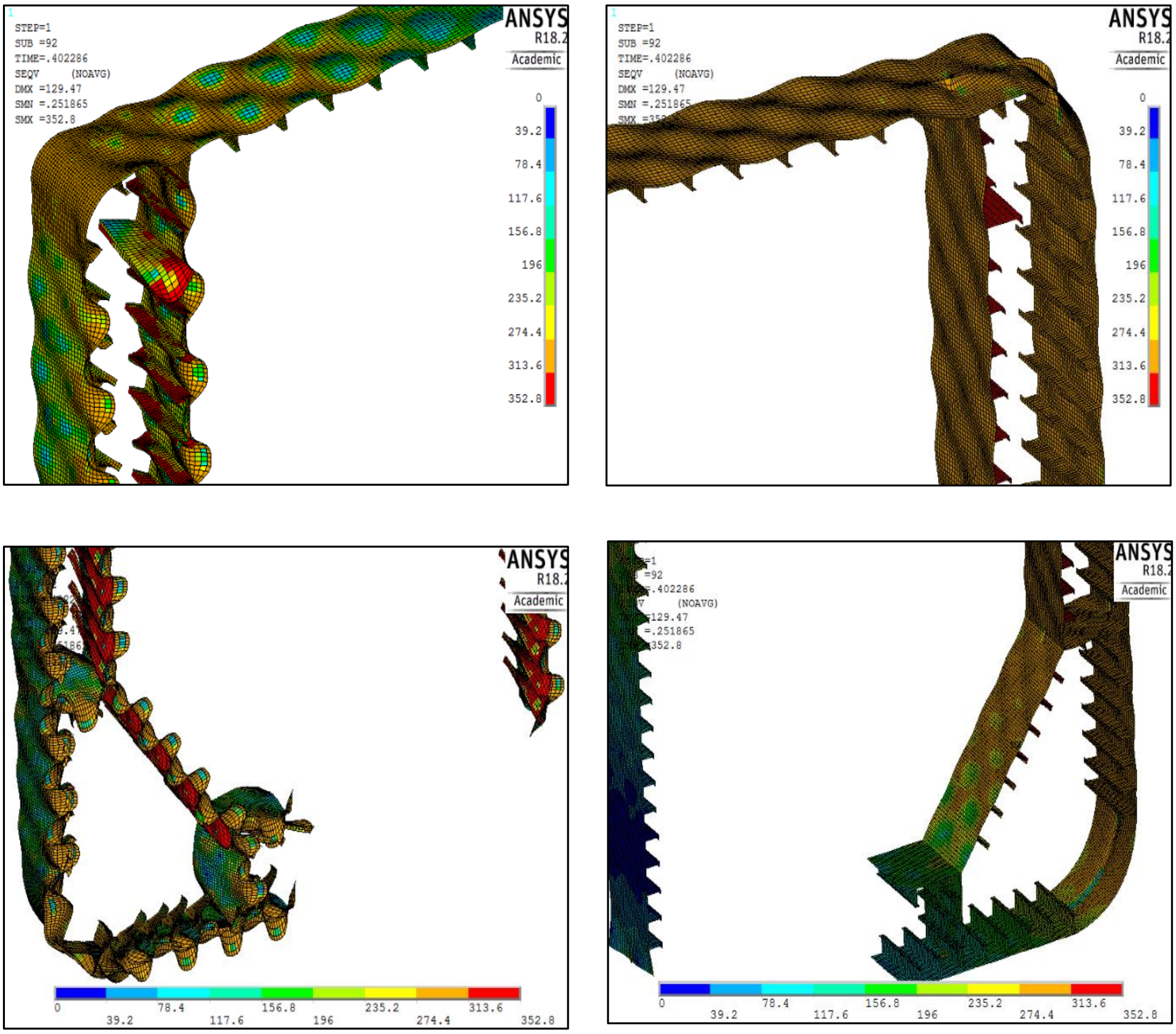


*Figure 4.47: von Mises stress distribution for biaxial load case in damage condition under hogging (point 3)*

Under the sagging condition, at point a, initial collapse starts at the right gunwale and left bilge simultaneously. The right gunwale starts to collapse in compression while the left bilge region begins to yield in tension at this point. There are also some localized plate and stiffener collapse around the right gunwale and the left bilge regions (see Figure 4.48). This localized collapse spreads through the deck and side shell (in the case of collapse of the right gunwale). The localized collapse also extends through the remaining part of the double bottom and side shell (in the case of yielding of the left bilge).

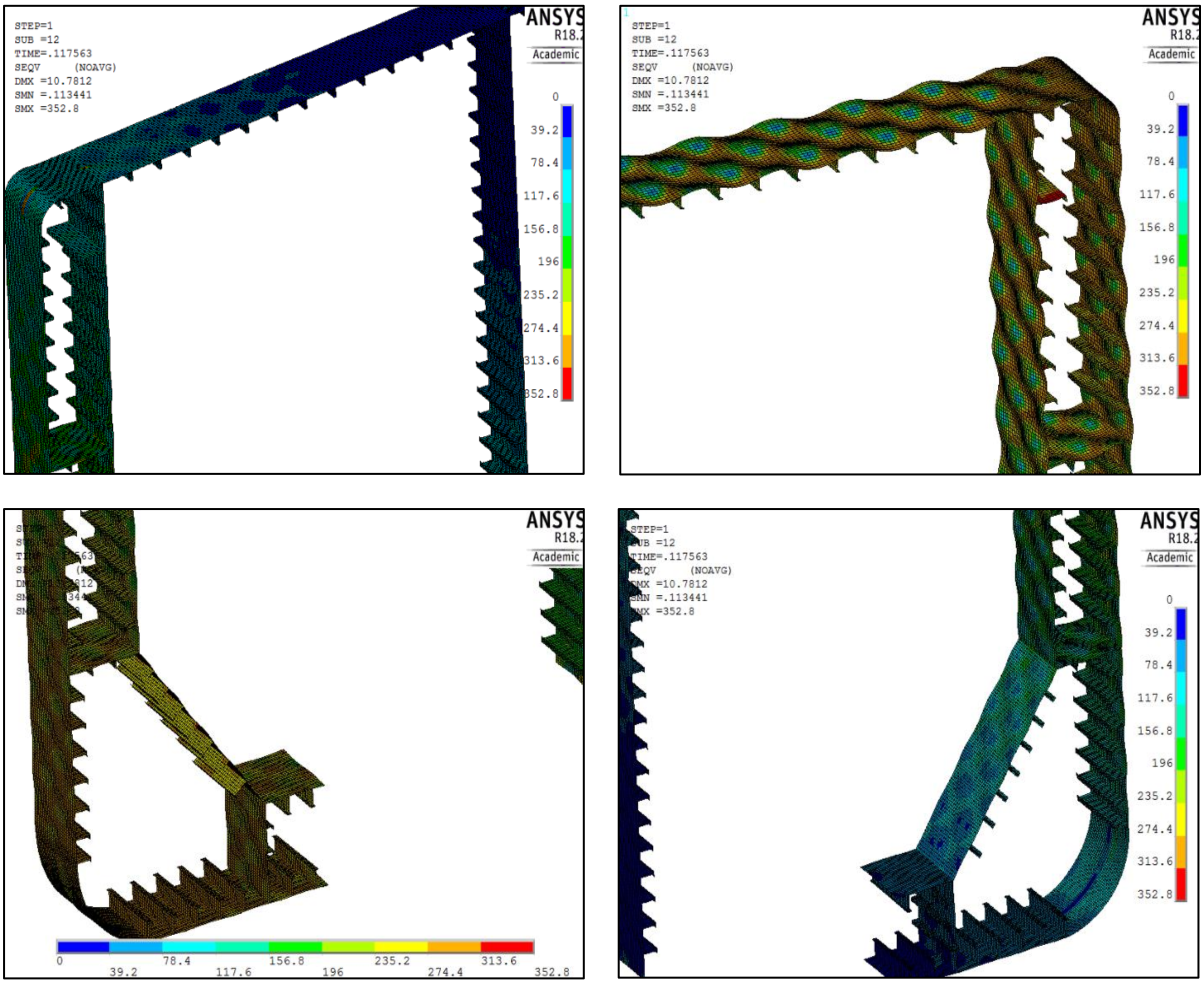


*Figure 4.48: von Mises stress distribution for biaxial load case in damage condition under sagging (point a)*

As the applied curvature is further increased to point b, the right gunwale buckles and this spreads to the surrounding deck and side shell. Concurrently, plastic deformation occurs at the left double bottom tank and spreads through the side shell and the remaining part of the double bottom as shown in Figure 4.49.

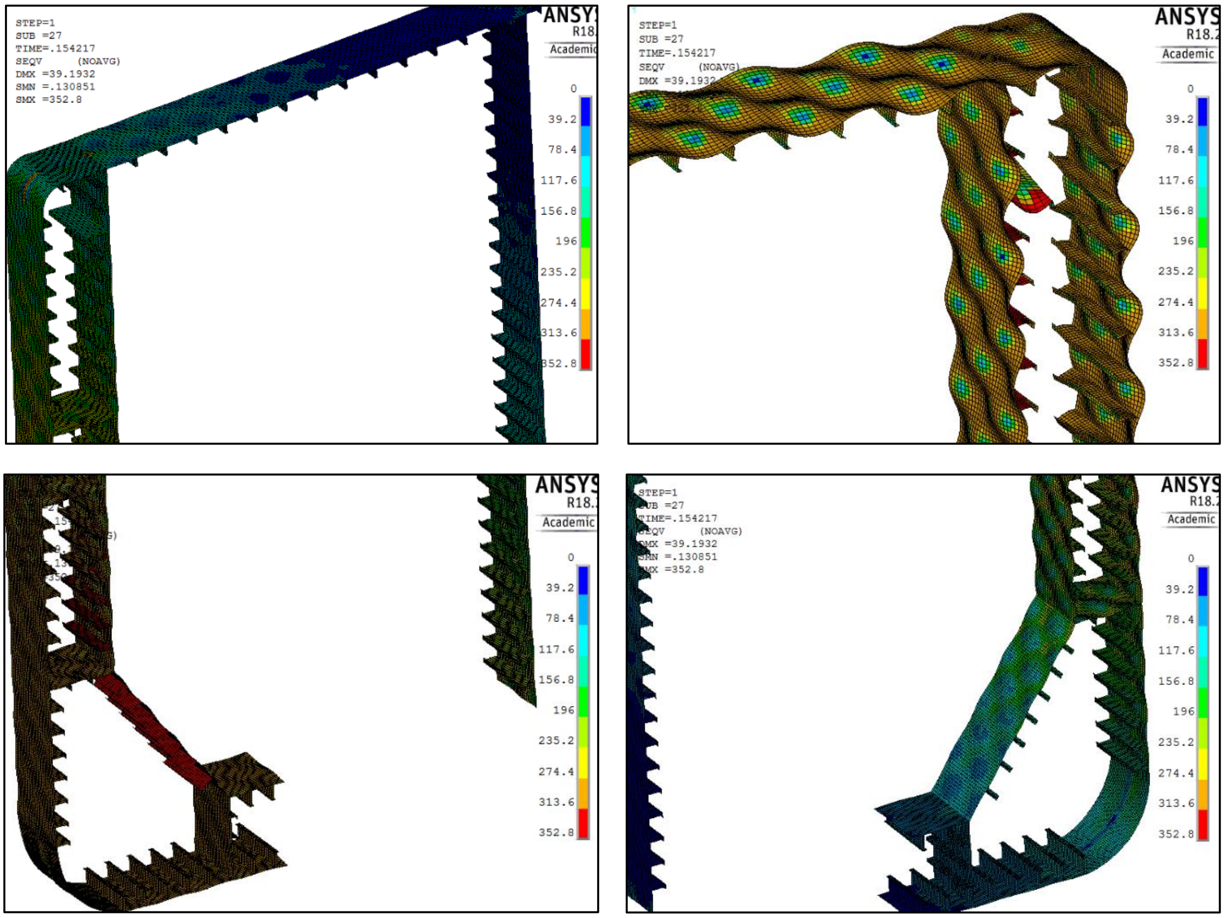


*Figure 4.49: von Mises stress distribution for biaxial load case in damage condition under sagging (point b)*

Ultimately, at point c, the right gunwale buckles completely and the buckling extends to the double bottom tank and the deck. It also extends to the longitudinal bulkhead close to the starboard side. At the same time, the left double bottom tank completely deforms plastically and spread through the side shell up to the left gunwale. Plastic deformation is also observed in the lower part of the left longitudinal bulkhead (Figure 4.50).

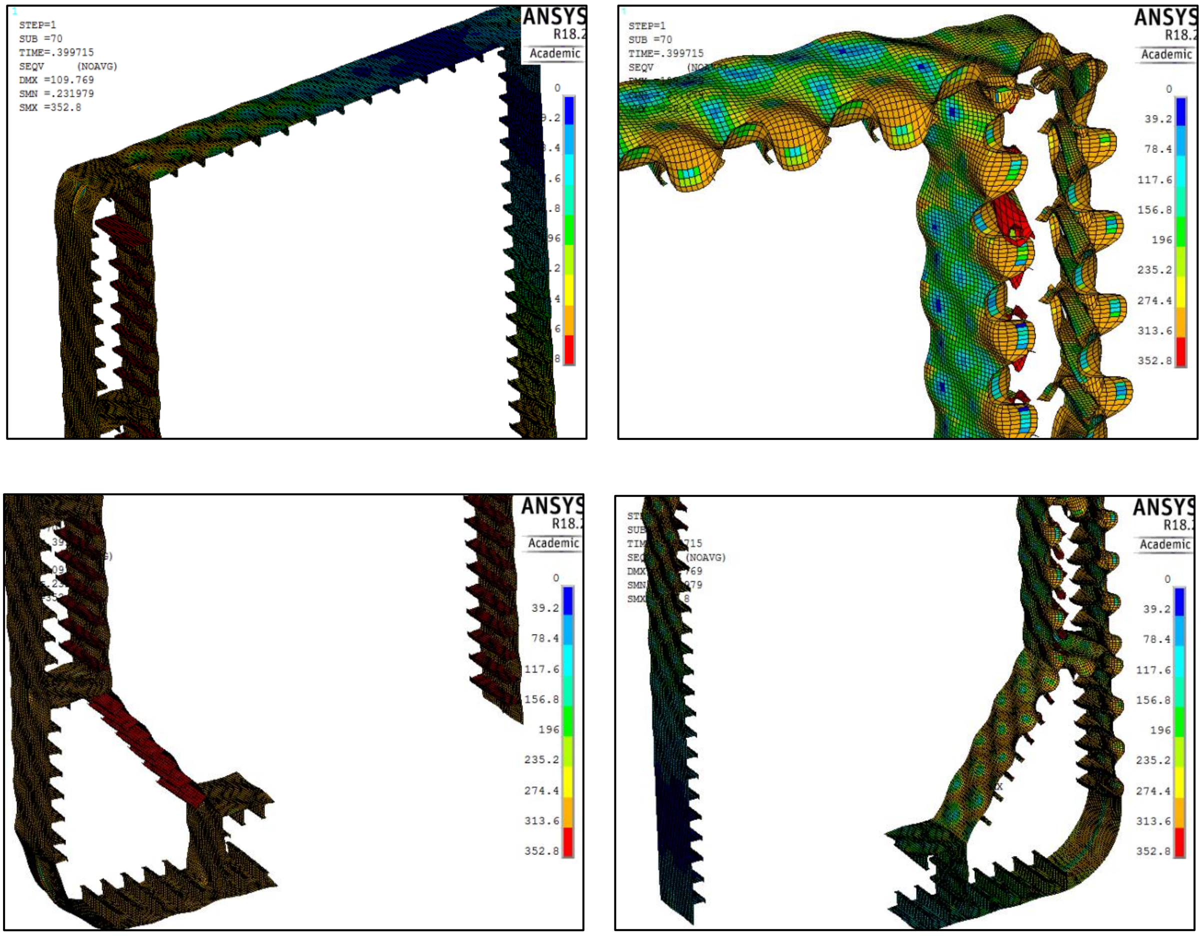


*Figure 4.50: von Mises stress distribution for biaxial load case in damage condition under sagging (point c)*

# 5. CONCLUSION AND RECOMMENDATIONS

## 5.1 Conclusion

Ultimate strength is a very good basis for structural design and safety assessment. Hence, it is imperative that the ultimate strength of structures is calculated accurately and efficiently. The ultimate strength of a double hull VLCC under combined loads has been determined in this project by performing progressive collapse analysis using nonlinear finite element method. These analyses have been performed using APDL. The residual strength of the double hull VLCC has also been determined in this work.

It has been shown in this work that despite the advances in ultimate strength analysis procedures, the results obtained can still be influenced or affected by uncertainties. Thus, these uncertainties must first be ascertained and estimated/idealized. It has been found in this study that displacement-controlled calculation using the Newton-Raphson iterative scheme shows better convergence than force-controlled analysis using Arc-length iterative scheme. Also, it has been shown in this work that the force-controlled analysis using Newton-Raphson iterative scheme does not exceed the ultimate limit state.

In this work, the ultimate strength of the double hull VLCC has been determined for the cases of vertical, horizontal and combined vertical and horizontal bending in hogging and sagging conditions. The results obtained have been validated against ISSC2000 report, ISSC2012 report and other publications. The results of this study tend to be in good correlation with those obtained in the ISSC reports and other publications. In the vertical bending load case, it has been shown that, as a result of the double bottom, the ultimate strength under hogging condition is higher than the ultimate strength under sagging condition. In the horizontal bending load case, it has been shown that the ultimate strength under hogging and sagging conditions are almost similar. This is due to the symmetry of the structure about the centre plane. In the biaxial case, the interaction relationship between vertical and horizontal bending for different curvature ratios has been presented in hogging and sagging conditions. It has been demonstrated that as the curvature ratio increases, vertical bending dominates and the collapse behaviour of the structure tends towards the case of pure vertical bending and vice versa.

The influence of different material models on the ultimate strength of the VLCC has also been investigated. It has been shown that the bilinear elastic plastic material models give higher values of ultimate strength when compared with the ideal elastic plastic material model. Also, the influence of welding residual stresses on the ultimate strength of the structure has been examined. It has been proven that welding residual stresses have negligible effects on the ultimate strength of the structure.

Furthermore, the residual strength of the double hull VLCC due to symmetric grounding damage has been evaluated. Expectedly, it has been demonstrated that ultimate strength decreases as the extent of the damage increases. Also, it has been shown that the collapse behaviour for the considered damage cases is similar to that of the intact condition.

## 5.2 Recommendations for Future Work

Further works could be carried out on this thesis. The effects of hydrostatic pressure and dynamic lateral loads could possibly be investigated to evaluate their influence on the ultimate strength of the structure. Also, the impact of ageing and in-service damage effects like corrosion, fraction and fatigue cracks on the ultimate strength of the structure could be evaluated. Furthermore, the scripts (codes) developed in this thesis could be extended to care about neutral axis changes as the structure collapses. In addition, other hull girder (sectional) load components like shear and torsional moment could be studied.

In the aspect of residual strength, the results obtained could be validated using one of the progressive collapses analysis methods. Also, the case of collision damage and unsymmetric grounding could be investigated.

In addition, the influence of the model extent on the results obtained could be investigated by increasing the extent of the model.

Lastly, the progressive collapse behaviour of composite ship structures could be analyzed.

## REFERENCES


ANSYS, Inc.. Element Reference.

Bathe, K.-J., 2006. *Finite Element Procedures.* 1st ed. New Jersey: Prentice-Hall.

Bathe, K. J. & Dvorkin, E. N., 1983. On the Automatic Solution of Nonlinear Finite Element Equations. *Computers & Structures,* Volume 17, pp. 871-879.

Bronsart, R., 2017. *Ship safety - Damage stability and roll motion in waves.* Rostock: New edition.

Caldwell, J. B., 1965. Ultimate Longitudinal Strength of Ships. *Transactions RINA,* Volume 98, pp. 411-430.

Carlsen, C. A., 1980. A Parametric Study of Collapse of Stiffened Plates in Compression. *Journal of the Structural Engineer,* Volume 58B, pp. 33-40.

Chaithanya, P. P., Das, P. K., Crow, A. & Hunt, S., 2010. The effect of distortion on the buckling strength of stiffened panels. *Ships and Offshore Structures,* Volume 5, pp. 141-153.

Cook, R. D., Malkus, D. S., Plesha, M. E. & Witt, R. J., 2002. *Concepts and applications of finite element analysis.* New York: Wiley.

Crisfield, M. A., 1981. A Fast Incremental/Iterative Solution Procedure That Handles Snap-Through. *Computers & Structures,* Volume 13, pp. 55-62.

Faulkner, D., 1975. A review of Effective Plating for Use in the Analysis of Stiffened Plating in Bending and Compression. *Journal of Ship Research,* Volume 19, pp. 1-17.

Fujikubo, M. & Yao, T., 1999. Elastic Local Buckling Strength of Stiffened Plate Considering Plate/Stiffener Interaction and Welding Residual Stress. *Marine Structures,* Volume 12, pp. 543-564.

Gordo, J. M. & Guedes, S. C., 1997. Interaction Equation for the Collapse of Tankers and Container Ships under Combined Vertical and Horizontal Bending Moments. *Journal of Ship Research,* Volume 41, pp. 230-240.

Grondin, G. Y., Elwi, A. E. & Cheng, J. J., 1999. Buckling of Stiffened Steel Plates: A Parametric Study. *Journal of Constructional Steel Research,* Volume 50, pp. 151-175.

Hallquist, J., 1998. *LS-DYNA theoretical manual.* California: Livermore Software Technology Corporation.

Hughes, O. F. & Paik, J. K., 2010. *Ship Structural Analysis and Design.* Jersey City, New Jersey: The Society of Naval Architects and Marine Engineers.

Hu, Y., Zhang, A. & Sun, J., 2001. Analysis on The Ultimate Longitudinal Strength of a Bulk Carrier by using a Simplified Method. *Marine Structures,* Volume 14, pp. 311-330.

IACS, 2020. *Common Structural Rules for Bulk Carriers and Oil Tankers.* s.l.:International Association of Classification Societies.

ISSC, 2000. Ultimate Hull Girder Strength (Committe VI.2). *Proceedings of the 14th International Ship and offshore Structures Congress,* Volume 2, pp. 321-391.

ISSC, 2012. Ultimate Strength (Committee III.1). *Proceedings of The 18th International Ship and Offshore Structures Congress,* Volume 1, pp. 285-363.

ISSC, 2015. Ultimate Strength (Committee III.1). *Proceedings of the 19th International Ship and Offshore Structure Congress,* pp. 279-350.

Ivanov, L. D., 2009. Challenges and possible solutions of the time-variant reliability of ship's hull girder. *Ships and Offshore Structures,* Volume 4, pp. 215-228.

Jiao, J., Ren, H., Adenya, C. A. & Chen, C., 2017. Development of a Shipboard Remote Control and Telemetry Experimental System for Large-Scale Model's Motions and Loads Measurement in Realistic Sea Waves. *Sensors,* Volume 17, pp. 1-26.

Khedmati, M., Rastani, M. & Ghavami, K., 2009. Ultimate strength and ductility characteristics of intermittently welded stiffened plates. *Journal of Constructional Steel Research,* Volume 65, pp. 599-610.

Kim, N.-H., 2015. *Introduction to Nonlinear Finite Element Analysis.* 1st ed. New York, NY: Springer.

Madenci, E. & Guven, I., 2015. *The Finite Element Method and Applications in Engineering Using ANSYS.* 2nd ed. New York: Springer.

Maestro, M. & Marino, A., 1989. An Assessment of the structural capacity of damaged ships: The Plastic Approach in Longitudinal Unsymmetrical Bending and The Influence of Buckling. *International Shipbuilding Progress,* Volume 36:408, pp. 255-265.

Mansour, A. E., Lin, Y. H. & Paik, J. K., 1998. Ultimate Strength of Ships under Combined Vertical and Horizontal Moments. *PRADS'95,* Volume 2, pp. 844-851.

Mao, F., n.d. Longitudinal Ultimate Bending Strength Analysis of Ship Structure for Emergency Response. Thesis (MSc). *Delft University of Technology.*

Misirlis, K., Downes, J. & Dow, R., 2010. *Assessment of the ultimate compressive strength for FRP plates with geometrical imperfections.* Rio de Janeiro, Brazil, s.n., pp. 1102-1113.

Muehmer, M., 2020. Nonlinear Finite Element Analyses for Ultimate Strength Investigations of a Tanker. Thesis (MSc). *University of Rostock.*

Nishihara, S., 1983. Analysis of Ultimate Strength of Stiffened Rectangular Plate (4th Report) - on the Ultimate bending moment of ship hull girder. *Journal of the Japan Society of Naval Architects and Ocean Engineers,* Volume 154, pp. 367-375.

Ozguc, O., Das, P. K. & Barltrop, N. D., 2007. Rational Interaction Design Equations for The Ultimate Longitudinal Strength of Tankers, Bulk Carriers, General Cargo and Container Ships Under Coupled Bending Moment. *Journal of Ship Research.*

Ozguc, O., Samuelides, M. & Das, P. K., 2005. *A Comparative Study of the Collision Resistance of Single and Double Side Skin Bulk Carriers.* Lisbon, Portugal, s.n., pp. 26-30.

Paik, J. K., 2018. *Ultimate Limit State and Design of Plated Structures.* Second ed. Hoboken, NJ: John Wiley & Sons.

Paik, J. K., Thayamballi, A. K. & Che, J. S., 1996. Ultimate strength of ship hulls under combined vertical bending, horizontal bending and shearing forces. *Trans. SNAME,* Volume Vol 104, pp. 31-59.

Rabiul, I. M. & Sumi, Y., 2011. *Geometrical effects on strength and deformability of corroded steel plates.* Hamburg, Germany, s.n.

Reddy, J. N., 2004. *An Introduction to Nonlinear Finite Element Analysis.* New York: Oxford University Press Inc.

Rigo, P. & Rizzuto, E., 2010. *Analysis and design of ship structures.* Liege: T Lamb, SNAME.

Rizzuto, E., Teixeira, A. & Guedes, S. C., 2010. *Reliability assessment of a tanker in damage conditions.* Rio de Janeiro, Brazil, s.n.

safety4sea, 2018. *SAFETY4SEA.* [Online]
Available at: https://safety4sea.com/cm-learn-from-the-past-prestige-sinking-one-of-the-worst-oil-spills-in-europe/?__cf_chl_jschl_tk__=pmd_c95e681a09266f9ed29cedea6f9d2f2f8b3d2438-1627710877-0-gqNtZGzNAjijcnBszQii
[Accessed 05 06 2021].

Shama, M., 2013. *Hull Girder Loading,* s.l.: Springer, Berlin, Heidelberg.

Smith, C. et al., 1992. Strength of Stiffened Plating Under Combined Compression and Lateral Pressure. *Transactions of the Royal Institution of Naval Architects,* Volume 134, pp. 131-147.

Sumi, Y. & et al., 1997. *Calculation Procedures. In Quasi-static Response.* s.l., Elsevier Science, pp. 128-138.

Trust, P., 2013. *The Indian Express.* [Online]
Available at: https://indianexpress.com/article/india/latest-news/merchant-vessel-mol-comfort-splits-into-two-off-mumbai-coast-crew-rescued/
[Accessed 05 06 2021].

Valsgard, S., Jorgensen, L., Boe, A. & Thorkildsen, H., 1991. *Ultimate Hull Girder Strength Margins and Present Class Requirements.* Arlington, USA, s.n., pp. B.1-19.

Viner, A. C., 1986. *Development of Ship Strength Formulations.* London, New York, Elsevier, pp. 152-173.

Wang, G. et al., 2008. A statistical investigation of time-variant hull girder strength of ageing ships and coating life. *Marine Structures,* Volume 21, pp. 240-256.

Yao, T., 2000. *Ultimate Hull Girder Strength (Committe VI.2).* Japan, Elsevier, pp. 321-391.

Yao, T. & Fujikubo, M., 2016. *Buckling and Ultimate Strength of Ships and Ship-like Structures.* s.l.:Elsevier.

Yao, T., Fujikubo, M., Kondo, K. & Nagahama, S.-i., 1994. *Progressive Collapse Behaviour of Double Hull Tanker Under Longitudinal Bending.* Osaka, Japan, The International Society of Offshore and Polar Engineers, pp. 570-577.

Yao, T., Nagahama, S. & Fujikubo, M., 1993. Ultimate Longitudinal Strength of Double Hull Tanker. *Trans West Jpn Soc Naval Arch,* Volume 86, pp. 183-198 [in japanese].

Zhu, Z., Ren, H., Li, C. & Zhou, X., 2020. Ultimate Limit State Function and Its Fitting Method of Damaged Ship under Combined Loads. *Journal of Marine Science and Engineering,* Volume 8.

# APPENDICES

## A1: Parametric Model Showing Damage Case (dam_1)

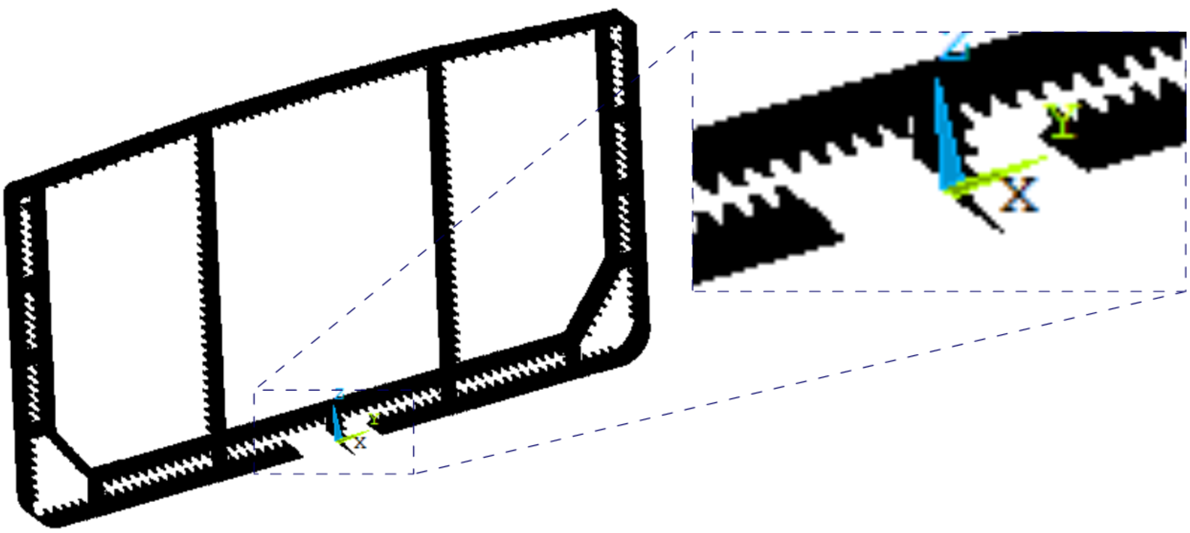

## A2: Stiffener Types, Properties and Dimensions

| Stiffener ID | Dimensions (mm) | Type | Yield Stress (MPa) | Stiffener ID | Dimensions (mm) | Type | Yield Stress (MPa) |
|---|---|---|---|---|---|---|---|
| 1 | 300 × 90 × 13/17 IA | Angle Bar | 313.6 | 25 | 250 × 90 × 12/16 IA | Angle bar | 313.6 |
| 2 | 350 × 100 × 12/17 IA | Angle Bar | 313.6 | 26 | 450 × 11 + 150 × 22 | T-bar | 352.8 |
| 3 | 400 × 100 × 11.5/17 IA | Angle bar | 313.6 | 27 | 450 × 11 + 150 × 19 | T-bar | 352.8 |
| 4 | 400 × 11 + 150 × 12 | T-bar | 313.6 | 28 | 450 × 11 + 150 × 16 | T-bar | 352.8 |
| 5 | 400 × 11 + 150 × 14 | T-bar | 313.6 | 29 | 450 × 11 + 150 × 14 | T-bar | 352.8 |
| 6 | 450 × 11 + 150 × 12 | T-bar | 313.6 | 30 | 450 × 11 + 150 × 12 | T-bar | 352.8 |
| 7 | 400 × 11 + 150 × 14 | T-bar | 313.6 | 31 | 450 × 11 + 150 × 14 | T-bar | 352.8 |
| 8 | 450 × 11 + 150 × 16 | T-bar | 313.6 | 32 | 400 × 100 × 11.5/16 IA | Angle bar | 352.8 |
| 9 | 450 × 11 + 150 × 19 | T-bar | 313.6 | 33 | 350 × 100 × 12/17 IA | Angle bar | 352.8 |
| 10 | 450 × 11 + 150 × 22 | T-bar | 313.6 | 34 | 300 × 90 × 13/17 IA | Angle bar | 352.8 |
| 11 | 450 × 11 + 150 × 25 | T-bar | 313.6 | 35 | 850 × 17 + 150 × 19 | Angle bar | 352.8 |
| 12 | 500 × 11 + 150 × 28 | T-bar | 313.6 | 36 | 250 × 90 × 12/16 IA | Angle bar | 352.8 |
| 13 | 500 × 11 + 150 × 30 | T-bar | 313.6 | 37 | 300 × 90 × 12/16 IA | Angle bar | 352.8 |
| 14 | 500 × 11 + 150 × 32 | T-bar | 313.6 | 38 | 400 × 11 + 150 × 14 | T-bar | 352.8 |
| 15 | 500 × 11 + 150 × 34 | T-bar | 313.6 | 39 | 450 × 11 + 150 × 12 | T-bar | 352.8 |
| 16 | 550 × 12 + 150 × 30 | T-bar | 313.6 | 40 | 450 × 11 + 150 × 14 | T-bar | 352.8 |
| 17 | 550 × 12 + 150 × 25 | T-bar | 313.6 | 41 | 450 × 11 + 150 × 16 | T-bar | 352.8 |
| 18 | 350 × 100 × 12/17 IA | Angle bar | 313.6 | 42 | 450 × 11 + 150 × 19 | T-bar | 352.8 |
| 19 | 550 × 12.5 + 150 × 32 | T-bar | 352.8 | 43 | 450 × 11 + 150 × 22 | T-bar | 352.8 |
| 20 | 500 × 11.5 + 150 × 30 | T-bar | 352.8 | 44 | 450 × 11 + 150 × 25 | T-bar | 352.8 |
| 21 | 500 × 11.5 + 150 × 28 | T-bar | 352.8 | 45 | 450 × 11 + 150 × 28 | T-bar | 352.8 |
| 22 | 500 × 11 + 150 × 25 | T-bar | 352.8 | 46 | 500 × 11 + 150 × 25 | T-bar | 352.8 |
| 23 | 450 × 11 + 150 × 28 | T-bar | 352.8 | 47 | 500 × 11 + 150 × 28 | T-bar | 352.8 |
| 24 | 250 × 12.5 | Flat bar | 313.6 | 48 | 230 × 12.5 | Flat bar | 313.6 |

## A3: Average Values of Amplitudes

| Area | a | b | k | t | $Re_H$ | E | $\boldsymbol{\beta}$ | $A_0$ | $A_{0(average)}$ | $B_0 = C_0$ |
|---|---|---|---|---|---|---|---|---|---|---|
| | [mm] | [mm] | [-] | [mm] | [N/mm$^2$] | [N/mm$^2$] | [-] | [mm] | [mm] | [mm] |
| Double bottom | 2490 | 830 | 3.00 | 22.5 | 313.6 | 206000 | 1.44 | 4.66 | 4.89 | 3.735 |
| | 2490 | 830 | 3.00 | 20.5 | 313.6 | 206000 | 1.58 | 5.12 | | 3.735 |
| | 2490 | 830 | 3.00 | 18.5 | 313.6 | 206000 | 1.75 | 5.67 | 5.27 | 3.735 |
| | 2490 | 830 | 3.00 | 21.5 | 313.6 | 206000 | 1.51 | 4.88 | | 3.735 |
| | 2490 | 750 | 3.32 | 16.5 | 313.6 | 206000 | 1.77 | 5.19 | 5.19 | 3.735 |
| Longitudinal Bulkhead | 2490 | 830 | 3.00 | 16.5 | 313.6 | 206000 | 1.96 | 6.36 | 6.66 | 3.735 |
| | 2490 | 830 | 3.00 | 16 | 313.6 | 206000 | 2.02 | 6.55 | | 3.735 |
| | 2490 | 830 | 3.00 | 15.5 | 313.6 | 206000 | 2.09 | 6.77 | | 3.735 |
| | 2490 | 830 | 3.00 | 15 | 313.6 | 206000 | 2.16 | 6.99 | | 3.735 |
| | 2490 | 830 | 3.00 | 14 | 313.6 | 206000 | 2.31 | 7.49 | | 3.735 |
| | 2490 | 830 | 3.00 | 18 | 313.6 | 206000 | 1.80 | 5.83 | | 3.735 |
| Deck | 2490 | 770 | 3.23 | 20 | 313.6 | 206000 | 1.50 | 4.51 | 4.51 | 3.735 |
| | 2490 | 1130 | 2.2 | 20 | 313.6 | 206000 | 2.20 | 9.72 | 9.72 | 3.735 |